Encapsulating of humic acid in hydrogel matrix for the complexation of heavy metals in aqueous solutions

UNIVERSITY *of the*
WESTERN CAPE

By

Rabelani Leonard Sithi

This thesis is submitted in fulfillment of the requirements for the degree of Masters in science to the department of chemistry, SensorLab University of the Western Cape

Supervised: Prof Priscilla Baker

Co-supervised: Dr Francis Muya

I. Keywords

Hydrogels (HGL)

Humic acid (HA)

Polysulfone (PSF)

Glutaraldehyde (GA)

Polyvinyl alcohol (PVA)

Cyclic voltammetry (CV)

Atomic force microscopy (AFM)

Square wave voltammetry (SWV)

Fourier transform infrared (FTIR)

Differential pulse voltammetry (DPV)

Scanning electron microscopy (SEM)

II. Abstract

Rapid industrialization growth without appropriate emission standards for discharging environmental pollutants had exposed the ecosystem to detrimental effect. Due to their bioaccumulation propensity in organisms, toxicity and non-biodegradable aspect, heavy metal spoliation is currently a significant ecological obligation. Owing to their natural abundance and extensive use, cadmium (Cd) and lead (Pb), among different heavy metals, are the predominant toxic metals. The intrusion of Cd and Pb metal ions into the ecosystem is accomplished by widely accepted methods such as anticorrosive coating of steel, electronic circuit and batteries.

Cu is essential for the maintenance of body metabolism but Cd and Pb are not required. So, exposure of these metal ions to very low amounts can cause serious health hazards such as lung cancer, kidney problems, neurological impairment and hypertension. The recommendations for the concentrations of Cu, Cd and Pb in potable water by the World Health Organization (WHO) are 2 mgL^{-1}, 0.003 mgL^{-1} and 0.01 mgL^{-1} respectively, but most typical reservoirs have much higher levels. Therefore, new technologies for a robust and ultra-trace measurement of Cd^{2+} and Pb^{2+} need to be developed immediately in order to satisfy wellbeing and environmental preservation requirements.

The adsorption of heavy metals by organic compounds such as humic acid is also an interesting aspect of research. Humic substances (HS) are small organic particles that are ubiquitous in soil, water and organic matter. The prevailing HS mass fractions are fulvic acid (FA) and humic acid (HA), they are differentiated on the grounds of their solubility in acid and alkaline solutions. The humic acid (HA), is soluble in alkali but insoluble in acid, while the fulvic acid (FA), is soluble in both alkali and acid solutions. HS particles have a completely open framework and comprise of various functional groups that are mainly anions in aqueous solutions owing to proton dissociation and can interrelate with other positively charged ions, like metal ions. Metal ion bioavailability and toxicity in the environment are therefore affected by HS. HS comprises two main functional groups, carboxylic and phenolic, that are especially important for the binding of metal ions.

Humic acid and polysulfone hydrogel are both materials with clearly defined electrochemistry and can be readily processed in the development of different sensor formats. In this investigation we present both hydrogel (HGL) working electrode and hydrogel-humic acid (HGL/HA) working electrode which were prepared for electrochemical complexation of heavy metals (copper, cadmium and lead) in aqueous solutions. The Ag / AgCl pair was used as the reference electrode and the counter electrode was used as a platinum wire. Polysulfone hydrogel was successfully synthesized and characterized by scanning electron microscopy (SEM) and atomic force microscopy (AFM) to analyze structural and topographic properties, cyclic voltammetry (CV) to study the electrochemical behavior of the hydrogel and Fourier transform infrared spectroscopy (FTIR) to confirm chemical make up by studying chemical bonds and composition of the hydrogel. The first electrode (AuE/HGL) was prepared by electrochemical deposition of the synthesized hydrogel (0.05 mol/L) onto AuE electrode using 10 cycles from 0 V and 1 V at 50 mV/s. The AuE/HGL/HA sensor was prepared by soaking the hydrogel thin film in humic acid for 30 minutes for impregnation. The measurements of heavy metals were performed in triplicates and LOD was determined for each detection. Average LOD values were calculated for comparison purposes. The complexation ability of AuE/HGL electrochemical sensor toward Cu, Cd and Pb was compared to that of AuE/HGL/HA sensor. For Cu studies, the AuE/HGL sensor achieved an LOD of 6.67 µM and the AuE/HGL/HA sensor offered an LOD of 6.24 µM. For cadmium studies, the AuE/HGL sensor achieved an LOD of 3.00 µM and the AuE/HGL/HA sensor offered an LOD of 2.61 µM. Lastly, for Pb studies, the AuE/HGL sensor achieved an LOD of 5.03 µM and the AuE/HGL/HA offered an LOD of 4.85 µM. The sensitivity of AuE/HGL/HA sensor was higher than that of AuE/HGL sensor.

III. Declaration of own work

I, Rabelani L Sithi, by reason of comprehending the plagiarism policy of the University hereby confirm that this is my own original work, apart from where denoted by referencing, and that I have obeyed the good academic practices, proclaim that all origins have been precisely reported and acknowledged, and that this thesis has not been submitted, as a whole, at any higher Education Institution for credit.

Rabelani Leonard Sithi May 2020

Signed…… Date…….

IV. Acknowledgements

I would like to take this time to communicate my heartfelt appreciation to the following entities, people and institutions for their much-needed assistance in my academic pursuits. Without a shadow of a doubt, I would not have made it this far if it was not for their unwavering support.

- I return all the glory to God the Father, the Son and the Holy Ghost for the gift of life, health and vitality and hence I could to do this work.
- Thank you to the department of chemistry for the opportunity to use the equipment.
- To National Research Foundation, thank you so much for financial assistance.
- To my supervisors Prof P.G.L. Baker and Dr F.N. Muya, I cannot thank you enough for your contribution to my work and personal life. I couldn't have asked for better supervisors, so I sincerely thank God for the privilege of being supervised by you.
- I am thankful also to Dr X. Ngema for helping me with suggestions in my experimental work and during thesis-writing period.
- I am grateful also to all my friends and colleagues at Sensorlab, especially Kelechi Nwambaekwe, Andisiwe Ngwekazi, Clementine Louw, Dhielnawaaz Abrahams and Kevin Tambwe for the good times we have shared and for the much-needed assistance that you gave me.
- Thank you so much to all my other friends, especially Sinazo Nqeketo and Sazi Thwala for the inspirational conversations we had.
- My thank you also goes to the Voice of Faith Mission Church members in Limpopo and Christ Worship Church members in Cape Town, especially my brothers and sisters at the campus for your spiritual support.
- To the entire research team at SensorLab, University of the Western Cape, you guys are wonderful human beings, not to mention colleagues.
- To my parents, Aaron Sithi and Mpho Sithi, thank you for sacrificially holding the ladder for me to climb up in life. Your care and support will forever be appreciated.
- Last but not least, I want to thank my sister, Rerani Sithi, for all her much-needed assistance.

V. Dedication

This project is dedicated

To

God the Father, the Son and the Holy Ghost.

And all my family members, especially:

My Parents

Mr. Livhuhani Aaron Sithi and Mrs. Mpho Joyce Sithi.

And my sister

Rerani Success Sithi

VI. Table of contents

VII. List of tables

List of schemes

VIII. List of figures

IX. List of abbreviations

PSF:	Polysulfone
GA:	Glutaraldehyde
PVA:	Polyvinyl alcohol
DMAc:	N,N-dimethyl acetamide
HCl:	Hydrochloric acid
Cu:	Copper
Cd:	Cadmium
Pb:	Lead
HA:	Humic acid
KBr:	Potassium bromide
CV:	Cyclic voltammetry
SWV:	Square wave voltammetry
SPCE:	Screen printed carbon electrode
DPASV:	Differential pulse anodic stripping voltammetry
Pt:	Platinum electrode
AFM:	Atomic force microscopy
FTIR:	Fourier transform infrared
SEM:	Scanning electron microscopy
TEM:	Transmission electron microscopy
Sa:	Surface roughness
Ra:	Area roughness
De:	diffusion coefficient
E^o:	Formal potential
Rpm:	Revolution per minute
LOD:	Limit of detection
LOQ:	Limit of quantitation

X. List of units

amu:	molecular weight
M:	molarity
µM:	micromolar
mL:	milliliter
µL:	microliter
A:	ampere
mA:	milliampere
nm:	nanometer
$cm^2\ s^{-1}$:	centimeter square per second

Chapter 1

1.1. Background

Metal contamination in South Africa is largely due to the use of water for irrigation, mining, afforestation, power generation, and industrial and domestic purposes. Metals, particularly in sediments, are persistent and have a propensity for building up in the environment. The rationale for the toxicity of all metals at some high levels are attributed to their chemical properties [1].

Main routes of human exposure to reported carcinogens such as heavy metals in sub-Saharan Africa (SSA) are poor waste management, increasing urbanization, and mining activities. The World Health Organization (WHO) approximates that 40 per cent of all cancers can be prevented because it is possible to avoid exposure to their causes. Cancer causes include exposure to heavy metals in large quantities. As per the WHO, 70 per cent of the 7.6 million deaths from cancer (about 13 per cent of all deaths) took place in low-and middle-income countries, including SSA in 2008 [2]. According to an extensive investigation by the WHO on the environmental burden of disease, environmental risk factors contribute a quarter of the overall disease burden and 2,97 million human lives are lost in Africa each year [3]. The classification of human carcinogenic metals is summarized in Table 1 [2]. The use of momentary dust, leaded gasoline, unidentified toxic waste, including cadmium-based batteries, as a consequence of deficient contamination regulations, has aggravated heavy metal contamination on the continent [4]. In most African countries, there are financial constraints for environmental sustainability, as most of the development projects concentrate on economic growth and industrialisation [5]. As a result, industrial development and greater exploitation of natural resources have led to a widespread heavy metal contamination [6]. Since heavy metals comprise severe health hazards, the degree of heavy metal contamination of the environment has attracted great interest. Despite advancements in analytical methods, such as adsorption, for removal of heavy metals from aqueous solutions, literature on the current status of more efficient sensor materials is scarce and hence the aim of this investigation was to construct a hydrogel sensor functionalized with humic acid for complexation of heavy metals of biological significance in aqueous solutions.

Table 1: Classification of heavy metal human carcinogens, updated in 2012

Metal reference	Class	Class* IARC, monograph
Cadmium and cadmium compounds	1	58, 100C
Chromium III compounds	3	49
Lead	2B	23, supp 7
Lead compounds, inorganic	2A	87
Lead compounds, organic	3	23, supp 7
Potassium bromate	2B	73
Selenium and selenium compounds	3	9, supp 7

Group 1: Carcinogenic to humans.

Group 2A: Probably carcinogenic to humans:

Group 2B: Group 3: Not yet classifiable as to its carcinogenicity to humans.

Group 4: Probably not carcinogenic to humans [2].

1.2. Metals

In general, heavy metals are known to be those with a density above 5 g/cm^3. This classification includes a huge number of elements. Although arsenic is actually a semi-metal it is generally considered a dangerous heavy metal [7]. In the environment, heavy metals are non-degradable, which ensures that they cannot be depleted. Heavy metals are primarily associated with anthropic activities such as smelting, mining, or various types of wastes. It is worthy of note that although some of the heavy metals are essential for life (iron, selenium, cobalt, copper, manganese, molybdenum, zinc), several others are poisonous [8].

Metal contamination of the marine ecosystem is also a major difficulty of growing severity which has become a matter of concern because the majority of heavy metals are carried into the marine environment and build up along the food chain without degradation. Addition of toxic substances into the marine ecosystem leads to detrimental consequences, including harm to living organisms and human health [9].

Heavy metals bioaccumulation can have an adverse effect on growth and development and is also linked to causing organ damage, cancer, damage to the nervous system, and death in extreme cases. Exposure to certain heavy metals can also lead to autoimmune disease wherein individual's immune system attacks their own cells and this tends to result in diseases of kidneys, nervous system, circulatory system, and joint disorders, such as rheumatoid arthritis [7].

Through industrialization, all kinds of waste disposed from industrial manufacturing are disposed and pollute our environment severely. Harmful heavy metals as well as other toxins pollute the soil. Intake of food is one of the major routes of reaching the human body, meaning there could be risks to the plants and animal foods that have been heavy metal-polluted in contaminated farmland [10]. Since huge quantities of metal-polluted wastewater are discharged, industries bearing heavy metals such as Cu, Ni, As, Zn, Cd, Cr, and Pb are the most toxic among chemical-intensive industries. Heavy metals can be absorbed by living organisms because of their high solubility in marine ecosystem [7]. There are several analytical techniques used in the determination of metals such as X-ray fluorescence spectroscopy [11], [12], [13], atomic absorption spectroscopy [14], inductively coupled plasma (ICP) spectroscopy [15], [16], and electrochemical methods (amperometry, impedimetry and voltammetry) [17], [18], [19]. Recently, stripping voltammetry (SV) with differential pulse [20], and square wave [21] were preferentially reported for detection of trace elements [22].

1.3. Problem statement

Heavy metals are important in sustaining different biochemical and physiological processes in organisms at quite low levels, but then when they surpass certain threshold level, they become harmful. Heavy metal ingestion in many regions of the world is continuing and growing even though it is known that heavy metals have several negative health consequences and last for a considerable period of time. Obviously, heavy metals occur in the ecosystem as trace elements in rocks and soils, but they are often discharged into the ecosystem due to human practices such as mining, automotive pollution, chemical plant operations, chemical wastewater, residential drainage, waste discharges, bug or disease prevention chemicals administered to plants as well as other activities. Heavy metals represent substantial contaminants to the ecosystem, and their toxic effects is a concern of growing importance for environmental, physiological, nutritional reasons. Copper, nickel, zinc, cadmium, chromium, lead, and arsenic have been the most commonly encountered heavy metals in wastewater, all of which poses threats to people and the environment. Even though these metals play essential biological roles in animals and plants, they have also been given an additional advantage by their chemical chelation and oxidation-reduction characteristics so they can avoid regulatory mechanisms like transportation, compartmentalization, transportation, and binding to the appropriate cell components. These metals trigger cell defect, which in turn causes toxicity, by attaching to protein sites which are not formed for them and replacing the initial metals from their normal binding sites. Their numerous agricultural, domestic, technological, pharmaceutical, and industrial implementations have contributed to their widespread distribution throughout the ecosystem, raising fears regarding their impact on human health and the environment. A broad spectrum of treatment methods, such as chemical precipitation, membrane filtration, coagulation–flocculation, ion exchange, and flotation have been invented for the elimination of heavy metals from water systems in order to comply with more and more strict environmental legislation. Chemical precipitation is inefficient once the level of metal ions is low and can generate large quantities of effluent to be treated with limited success. Membrane filtration method has problems such as significant costs and membrane fouling. Coagulation–flocculation treatment method involves chemical usage and increased volume of effluent production. Ion exchange, however, is costly and cannot be used on a broad scale. The drawbacks of the flotation method include high maintenance and operating expenses. Electrochemical techniques for heavy metal wastewater treatment are considered to be fast and

very well-controlled, necessitating far less chemicals, offering good reduction output, generating less effluent, appropriate for field testing, and handheld, making it suitable for the detection of heavy metals. Nevertheless, electrochemical methods involving large initial capital investment and costly electricity supply are continuing to limit its development. To address this challenge, we aim to construct a hydrogel-humic acid based, economical and highly sensitive electrochemical sensor for the determination of the heavy metals (Cu, Cd, and Pb). Acute toxicity of lead, cadmium, arsenic, mercury, and chromium makes them some of the most critical metals of public health importance.

1.4. Aims and objectives of the studies

1.4.1. Aim

The aim of this study is to develop a hydrogel electrode modified with humic acid as a complexing agent for metal cation detection.

1.4.2. Objectives

The main objectives of this investigation were as follows;

I. Prepare the hydrogel material for the production of stable chemically crosslinked hydrogel.

II. Characterize the synthesized hydrogels by:
   - Examining the electrochemical behavior of the hydrogel by cyclic voltammetry (CV).
   - Analysis of structural and topographic properties using electron scanning microscopy (SEM), atomic force microscopic (AFM).
   - Confirming the chemical make up by studying chemical bonds and composition of the hydrogel using FTIR.

III. Study the redox behavior of metals such as copper (Cu), cadmium (Cd) and lead (Pb) at the hydrogel-modified gold electrode.

IV. Impregnate the hydrogel material with humic acid to produce a hydrogel -humic acid sensor for detection and complexation of Cu, Cd and Pb metal ions from aqueous solutions.

1.5. Motivation

It is essential, as suggested by the World Health Organization, to assess water quality. The main purpose of the guidelines on water quality is to protect public health and to support the development and execution of risk management policies to ensure water safety by managing harmful water components [23]. Our contribution in this project will focus on developing a humic acid sensor for complexation of heavy metals from aqueous solutions by impregnating polysulfone hydrogel thin film with humic acid. The complexation ability of humic acid on its own towards heavy metals has been reported in literature but only limited publications address humic acid in the matrix of a polymer, which is the focus of the current work. The metal-detection capability of humic acid on a hydrogel platform will be studied electrochemically and compared to that of a hydrogel on its own. The successful immobilization of the hydrogel onto commercially available gold disc electrodes and the subsequent functionalization with humic acid are some of the highlights reported in this thesis.

1.6. Thesis scope

- The aims and objectives of this work may be divided into the following sections, which provides relevant information on the development, characterization and application of synthesized hydrogels.
- ***Chapter1:***

  This chapter provides a general introduction to the challenge of metal pollution in Africa which results in chronic diseases and deaths through human exposure to high concentrations of metals.
- ***Chapter 2:***

  In this chapter a critical literature review on the hydrogels as possible adsorbents for heavy metal removal from aqueous solutions.
- ***Chapter 3:***

  This section describes how PSF-PVA hydrogels are prepared and synthesized and the concepts of various analytical techniques and instruments used in these studies.
- ***Chapter 4:***

  The results achieved by characterization methods such as spectroscopy microscopy, and electrochemistry are exhibited.
- ***Chapter 5:***

  This chapter provides details of the determination of three heavy metals based on square wave voltammetry.
- ***Chapter 6:***

  This chapter offers general conclusions and recommendations on complexation of other heavy metals and organic pollutants by the hydrogel and humic acid.

Chapter 2

Literature review

2.1. Adsorption

Several methods could be used to extract heavy metals from aqueous solutions. Some of the most broadly performed techniques include membrane filtration, chemical precipitation, ion exchange, advanced coagulation and adsorption. There is a need for inexpensive alternative technologies or adsorbents for metal removal [24]. Several strategies for developing faster and more effective innovations have been investigated, both to reduce the amount of water produced and to enhance the quality of the treated effluent. Adsorption has surfaced as one of the alternative solutions, and the quest for inexpensive adsorbents with metal-chelating capabilities has risen significantly. Adsorbents that derive from zeolites, biological or organic sources, industrial by-products, minerals, biomass and polymeric substances [7]. Adsorption is usually preferred, with the advantages of high performance, ease of application and availability of specific adsorbents. Researchers are looking for economical adsorbents. Among different absorbents, starch has been known to be one of the best choices to prepare affordable absorbents and could be used to isolate pollutants from waste water, but the hydrophilic aspect of starch is a disadvantage that constrains the production of starch-based materials [25].

A number of physical and chemical techniques are currently being developed to recover metals from water, but most of these techniques need sophisticated equipment, controlled environments, sludge problems and high costs, and are therefore not desirable for selective detection of metal ions. Adsorption has emerged as one of the few viable alternatives to remove low heavy metal levels and widely accepted in environmental treatment applications globally [26]. Adsorption is considered to be one of the most effective wastewater treatment approaches used by factories to minimize the concentrations of heavy metals in effluents by offering flexibility in design and operation, remedying effluents containing low and high concentrations of heavy metals [27]. Numerous studies have focused on developing new, simple, selective, sensitive, and inexpensive analytical methods for measuring ultra-trace amounts of heavy metals in environmental waters. Whereas spectroscopic methods are most commonly used, some of them

suffer from methodological challenges such as interference or memory effects [28]. Conventional treatment methods were mostly restricted by technological inevitabilities and are typically difficult to implement, particularly when metals are dissolved in large amounts of water, but adsorption has emerged as one of the highly effective alternative treatment methods for the recovery of heavy metals because the interface between two processes, that is, the solid surface and the adjacent solution, accumulates a certain component or material during adsorption [29].

Over the last few years, enormous progress in the synthesizing of conducting polymers has been followed by the development of a wide range of potential applications for such materials, including the removal of pollutants and the construction of sensors. The properties of these materials are well known to make them particularly attractive for adsorption processes. In order to enhance selectivity and develop a better interaction, these materials must be chemically modified with organo-functional groups, making conducting polymers more suitable for adsorption applications compared to their unmodified counterparts [28].

2.2. Hydrogels

A hydrogel is a water-swollen, crosslinked polymeric network formed by one or more monomers in a single reaction [30]. It can also be described as a polymeric substance capable of swelling and retaining a significant fraction of water or biological fluid inside its matrix, but does not dissolve [31]. In the polymeric network there are hydrophilic groups which hydrate in aqueous media producing hydrogel structure. The hydrogel's cross-links keep the polymer chains from dissolving before use [32]. Hydrogels' physicochemical characteristics rely on the selection of starting polymers and the method of synthesis since there are various methods to produce hydrogels [33], and they are made from materials such as polysaccharides, gelatin, polyelectrolyte complexes, polyacrylamide cross-linked polymers, and methacrylate esters polymers or copolymers [34].

Based on the application requirement, the functional properties of the suitable hydrogel material may include the highest absorption capacity in saline and the maximal absorption rate (preferred particle size and permeability) [30]. The polar hydrophilic groups are the first to be hydrated after contact with water, resulting in primary bound water being formed. As a result, the network swells and reveals the hydrophobic groups that also interact with the molecules of water. It leads to the production of hydrophobically-bound water. Owing to the osmotic driving force of the network chains towards infinite dilution, additional water must be absorbed by the network and the

hydrogel will therefore attain an equilibrium degree of swelling [35]. The extent of gel swelling is determined by the degree of cross-linking and the extent to which the gel likes water [36]. Unstable cross-links can be broken down by hydrolysis under physiological conditions, whether enzymatically or chemically [37]. It is presumed that the relatively large fraction of water in certain hydrogel materials is related directly to their high bio-compatibility. In addition, the higher the water content of the gel, the lower the mechanical properties of the gel [38].

In the last two decades, natural hydrogels have been progressively replaced by synthetic hydrogels with a long lifetime, high absorption capability and high gel strength. Fortunately, synthetic polymers typically have well-defined structural characteristics that can be adjusted to improve their degradability and usability. Hydrogels can be produced using simple synthetic materials. This is also stable under conditions of rapid and high temperature variations [30].

2.2.1. Physically cross-linked gels

Reversible/physical gels are referred to as 'reversible' or 'solid' gels when molecular attachments connect networks together and/or secondary forces such as hydrogen, ionic bonding or hydrophobic interactions. Disintegration is averted by physical interactions between various polymer chains in physically cross-linked gels. All such interactions are reversible and could be disarranged by variations in physical conditions or stress [35], [39]. Increased interest in physically interconnected hydrogels in the current era is attributable to a shortage of cross-linkers used for synthesis [32], and major characteristics such as self-healing and reversibility of hydrogels are becoming important features for the construction of new biomedical materials [40]. One of the hydrogel crosslinking methods for the fabrication of hydrogels is metal coordination between metal ions and functional groups in polymer chains. For instance, hydrogels produced from side-chain bipyridyl-functionalized poly(2-oxazoline) could be crosslinked to Co(III), Fe(II), Ni(II) or Ru(II). At room temperature metal-ligand interactions between Co(III) and Fe(II) are comparatively stable, however the interactions decompose once temperatures exceed 30 °C [41].

2.2.2. Chemically cross-linked gels

Permanent or chemical gels are referred to when they are covalently cross-linked, by the substitution of the hydrogen bonds with stronger and stable covalent bonds. Polymer chains are

bound by covalent bonds in chemical gels. They reach an equilibrium swelling state depending on the polymer-water interaction parameter and the crosslink density [35], [42]. The production of chemical hydrogels entail the use of a cross-linking agent, usually a bifunctional molecule of low molecular weight [43]. Growing interest in chemically interconnected hydrogels in the current age is due to the good mechanical strength of chemically crosslinked hydrogels [32]. One of the most appealing methods is enzymatic crosslinking. It provides the prospect of kinetic exploitation of gel formation in situ by regulating the amount of the enzyme. Strong covalent bonding and swift gelling under physiological conditions are some of the advantages of enzymatic crosslink. For example, transglutaminase (TG) and calcium ions as cofactors can facilitate formation of amide linkages between amine groups and carboxamide [41].

2.3. Application of hydrogels

Hydrogels are commonly used in several technical fields, including contact lenses and protein separation materials, dies for cell encapsulation and instruments for controlled release of proteins and drugs [32]. Hydrogels have become outstanding delivery agents for drugs and bioactive macromolecules in their swollen state of equilibrium or as progressively swelling systems [39]. Therefore, in applications such as tissue engineering, wound healing and drug delivery, biocompatible hydrogels containing labile bonds are advantageous [35]. Apparently, polymers have found their way into every aspect of our everyday life. From smart devices in our pockets and the automobiles we drive to the artificial heart valves required to keep some people alive-polymers are omnipresent [44]. Hydrogels are progressively being investigated as tissue engineering matrices. Hydrogels designed for use as tissue-based scaffolds may contain pores that are large enough to accommodate living cells, or they may be designed to degrade, releasing growth factors and creating pores into which living cells infiltrate and proliferate [45].

2.4. Hydrogels as adsorbents for removal of metals from wastewater

Water is a vital resource for life, and for our activities only 0.03 per cent of the maximum water available on earth can be used. Rapid urbanization and industrial development have raised water requirements, but water supply remains constant. Furthermore, lack of sufficient industrial wastewater remediation has limited the supply of safe water [46]. With the exponential growth of

modern industrial production, water pollution by heavy metals has become a serious worldwide environmental issue. At high concentrations, heavy metals are highly toxic and can accumulate in organisms, leading to various diseases and disorders. It is therefore all-important to minimize or eradicate the amount of heavy metals in industrial wastewater discarded into the environment [47]. Adsorption has recently become one of the alternative treatment methods for heavy metal-contaminated water. In an adsorption process, a mass of a substance is transferred from the solution to a solid's surface and becomes bound through chemical or physical interactions. Different affordable adsorbents made from farm waste, industrial by-products and organic substances have been lately produced and used to extract heavy metals from metal-polluted wastewater [48].

Increased attention has been paid to polymer adsorbents in recent years due to their high performance at low concentration sewage, comparatively straightforward process and recyclability. Most researchers prefer inexpensive natural polysaccharide materials such as starch, chitosan, and cellulose among the adsorbents used to extract a variety of heavy metals. Adsorption method is typically preferred over other heavy metal treatment methods due to its high performance, range of various adsorbents, ease of operation and low cost through the use of inexpensive adsorbents such as starch and cellulose [49], [47], [50].

Starch is an organic raw material that is plentiful, inexpensive, renewable and completely biodegradable. Modified starch uses for remediation of metal-laden wastewater have received considerable attention in recent years due to their environmental friendliness, ease of operation and accessibility [51], [52].

Functional materials based on cellulose are usually used in the field of separation, especially in wastewater detoxification. Natural polymers, including lignin, chitosan-based nanofibers, chitin, and cellulose offer good adsorption capacity for heavy metal ions in aqueous solutions [53], [54], [55].

Gum-polysaccharide-based graft copolymers have demonstrated their ability to adsorb various contaminants from wastewater. The key benefit of the use of such materials is their biodegradability, affordability and the capability to customize the material to the intended application. Polysaccharide-based crosslinked hydrogels are advantageous since they produce no secondary contaminants, in fact, they can be reused for adsorption [46]. Also, chitosan-based adsorbents have recently been tested and demonstrated the high capacity for water remediation due to their high contents of amino and hydroxyl functional groups and affordability [56].

One of the most important features of the hydrogel and other adsorbent materials is swelling behavior. The formation of a permeable structure results in high swelling ratio of the hydrogel. As per Flory's theory, the swelling of the gel varies depending on the ionic osmotic strain, crosslinking density, and affinity of the gel for water [57]. Several findings have shown that the pH value of the solution, among other variables, has a direct effect on the swelling behavior of the hydrogel with regard to the change in the swelling proportion [58], [59]. The functional groups (carboxylic and amine groups) are protonated when pH is below pKa, resulting in a decline in swelling ratios but the functional groups are deprotonated when pH is above pKa, which increases the number of ionized groups, which in turn induces electrostatic repulsion forces between the neighboring ionized groups of the polymer matrix. It results in a network-like swelling of the hydrogels, which will in turn increase the swelling ratio [58], [60]. There is a direct correlation between the swelling ratio of hydrogels and their adsorption capability, that is, the higher swelling potential indicates the greater number of ionic groups in hydrogels [57], and this can promote the adsorption of metal ions because as soon as functional groups on the hydrogel networks are exposed they are readily available for adsorption [61]. The deprotonated functional groups on the surface of the hydrogels attract metals ions, among other positively charged pollutants. The carboxylic group has been used as a functional group for the adsorption of contaminants by electrostatic interactions in the majority of studies in literature [62].

2.5. Hydrogels for sensor construction

A sensor is an instrument that is capable of receiving and responding to environmental signals and stimuli. A physical sensor is an instrument that offers information on a system's physical property and a chemical sensor is an instrument which converts chemical information, ranging from the amount of a particular sample element to a general component analysis, into an analytically helpful signal [63]. In general, the two major components of all hydrogel sensors are the transducer and a hydrogel. The transducer transforms the hydrogel's swelling signal into the optical or electrical domain. Various hydrogels have been used as the sensing part, including pH-sensitive hydrogels, glucose-sensitive hydrogels and ion-sensitive hydrogels, among others [64]. Hydrogels could be synthesized in aqueous solutions using radical polymerization, UV and addition reaction, among

others. These methods could be executed in many specialized techniques for the synthesis of special hydrogel structures that are applicable to sensing [63].

Hydrogels that are sensitive to stimulation may serve as effective sensing material. These gels are responsive to slight environmental changes and offer the reaction to chemical stimuli (such as pH and ions), physical stimuli (such as pressure, temperature, ionic force, among others) or biological stimuli (such as enzyme and glucose) through volume changes. The response rate depends on the composition, shape and molecular weight of the hydrogel and can be enhanced by many suggested methods such as increasing ionic group content and pore size, and decreasing the size of cross-linking density [65].

The hydrogels derived from poly(2-hydroxyethyl methacrylate) (pHEMA) have shown a low swelling ratio and high durability for pharmaceutical and biomedical uses. They can potentially give firm swelling and good mechanical features due to a strong configurational hydrophilic and lipophilic balance. Because of these features, pHEMA can be utilized as a covering material for biosensor tips and as a matrix for redox mediator immobilization due to its hydrophilic and excellent biocompatible characteristics [66].

Functional materials derived from cellulose have new applications as sensing materials in line with the trend of artificial intelligence in science and technology development. Hundreds of self-designed gold arrays on cellulose membranes are used to assemble paper-based gold electrode arrays using low-cost inkjet printer. The resultant materials have many special features as thin-film sensor platforms, such as excellent conductivity, good durability, and affordability [67].

These are comparatively hydrophilic and thus compatible with most biomolecules. Sensor construction [68], [69] as a function of these attributes, is now one of the most common areas in the broad context of hydrogel use. Conductive hydrogels, for instance, have been used efficiently to monitor glucose [70], [71] and hydrogels that are responsive to changes in the external environment are also used as photonic sensors [72].

2.6. Humic acid

Humic compounds are a major part of organic material and some of the most common materials on earth. They are formed during the decay of plant and animal biomass in ecological systems and typically contain skeletons of alkyl and aromatic monomers with functional groups such as carboxylic acid, quinine and phenolic hydroxyl groups connected to them [73]. Complexation

capability is an important characteristic of humic acids that affects the bioavailability and mobility of both nutrients and pollutants in the environment [74]. Humic substances manage the behavior of contaminants in the environment; their interactions are dependent on the humic material, pH metal and metal-ions [75].

Lately, humic materials have been incorporated into polymeric hydrogels to improve their water absorbencies [73]. As far as copper(II) binding on humic substances is concerned, different sorbent composition determines the complexed amounts and adsorption coefficient [74]. Complexation reactions of humic acids and metal ions have a complicated character given by their polydispersive, heterogeneous, polyelectrolyte identity. Humic acids can bind metal ions in various ways, including electrostatically, interaction of a cationic charge of a metal and the net anionic charge on the humic acid backbone in the formation of chelates and complexes with functional groups [76]. Humic materials constitute several various types of functional groups and can be used as multifunctional ligands, scheme 1. The most prevalent functional groups are the oxygen-containing ones and hence the most essential for metal binding. The participation of other groups cannot be dismissed, nonetheless [75].

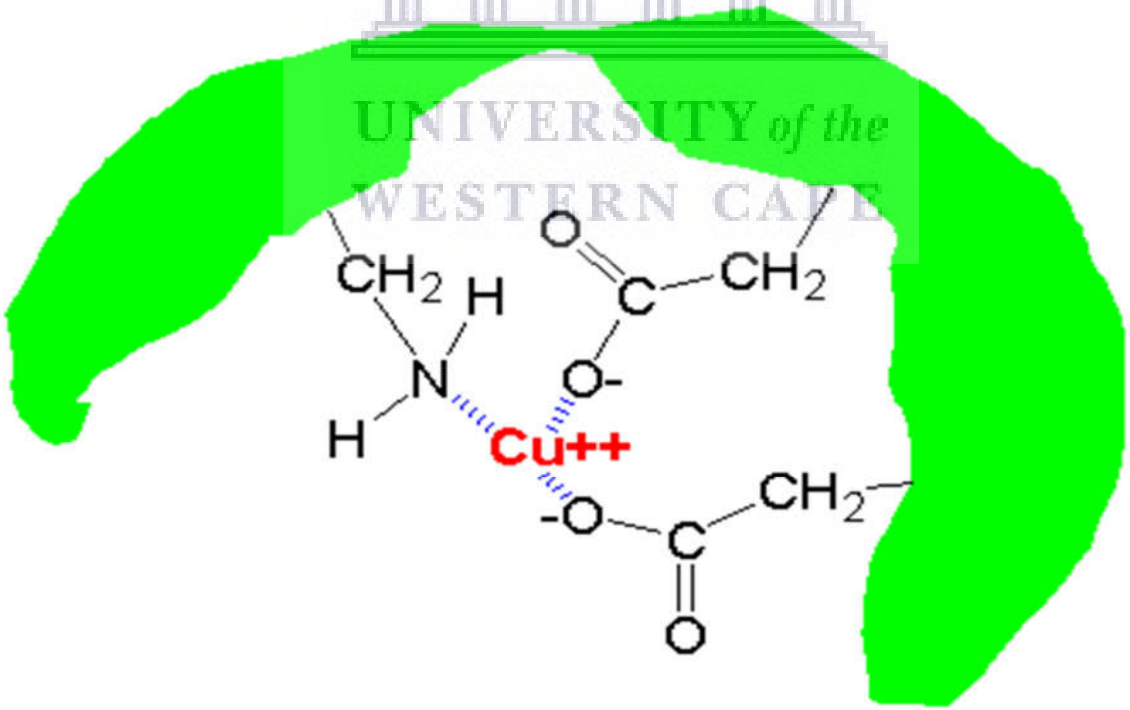

Scheme 1: Complexation of a metal ion (shown in red) by a naturally occurring humic acid (shown in green) [77]

2.7. Functionalization of hydrogels with humic acid

Hydrogels are effectual for the absorption of huge quantities of water and organic solutions and have the potential to be used in sanitary products, agricultural technology, medical applications and wastewater treatment [78]. New biomedical applications have been opened up by functional modifications in the porous surface of macroporous polymeric materials with different biological and chemical functional groups. In addition to altering or enhancing the constraints related to physical characteristics of the hydrogels, functionalization would also provide functionality in the hydrogels for biological activities [79], [80]. Although there are many ways in which a functional group can be added on the backbone of polymers, in the context of polymeric hydrogels, copolymerization a functional group is a feasible option but it may become unreachable after polymerization due to entrapment inside the porous network [81]. Physical and chemical interactions are alternative methods for combining functional groups of macroporous hydrogels [82]. Physical interactions, that is, noncovalent connections between biomolecules and polymeric hydrogels, are fragile in nature, including electrostatic interactions, hydrophobic and metal-mediated coordination [83]. It is possible to use a simple functionalization method that leaves no organic fraction other than the trapped humic molecules. To be effective, the trapping method should not alter the properties of the humic molecules, the gel matrix should interact minimally with the pollutant and the trapped humic molecules should be reachable through the pore to the exterior pollutant [84].

2.8. Analytes

2.8.1. Copper (II) ions

Copper (Cu (II)) is a vital and useful microelement for several plants and animals in trace amounts but it is toxic to aquatic plants at high concentrations (from 5.3 mg/L for humans [85] and 20 nM for plants [86]) due to its connection with cell membranes, inhibiting transport through the cell wall [26]. It is considered vital at particular levels (0.6 mg/day for women and 0.7 mg/day for men), nevertheless, at high concentrations, it induces toxicity and can lead to bleeding, hepatitis, and brain inflammation. Copper (II) is one of the biologically significant component various organs such as nerves, blood and bones and its imbalance may cause anemia, skin pigmentation,

and Wilson's disease, among other disorders in animals [29], [87], [88]. Copper could be found in plants and animals, and in mussels and oysters at high levels and is also present in a variety of amounts in many foods and drinks that we consume, including potable water. Substances of copper are most widely used in farming for the prevention of plant pests and as preservatives for wood, leather and textiles [88]. Copper (II) is extremely toxic to drinking water, and mercury may be the only element that is more hazardous than copper. Thus, the overall permissible level in drinking water is not to exceed 0.05 mg / L. The development of innovative methods for the simultaneous study and complexation of low concentrations of copper in environmental waters is of great significance [26].

2.8.2. Cadmium (II) ions

Pure cadmium (Cd) is a silver-white metal that is delicate and not normally present as a pure metal in the environment but as a mineral combined with other elements [89], and it is an environmental contaminant that is always-present and worldwide. Environmental exposure levels to Cd, which are considerably beyond the average, exist in places of current or historic industrial contamination [90]. Cd enters aquatic environments from factory and user waste. It contaminates the aquatic ecosystem and builds up in vertebrates throughout the food chain, destroying aquatic animals' physiological tissues even at levels way below the hazardous level. Cadmium has many adverse effects on habitats, animal and human wellbeing. It is embryotoxic, provoking different types of mammal and reptile abnormalities [91]. The likelihood of cadmium affecting your wellbeing depends on the present state of cadmium, the amounts taken into your blood, and whether you are consuming or breathing cadmium. Inhaling air with very high cadmium quantities can cause serious damage to the lungs and even death [89]. Based on the particle size, 10 to 50 per cent of the inhaled cadmium dust is absorbed. Roughly, five to ten percent of Cd ingested is absorbed, depending on particle size too. Intestinal absorption of Cd is greater for people with calcium, zinc, or iron shortage. Cigarette smoking is considered the greatest cause of human vulnerability to cadmium [92].

2.8.3. Lead (II) ions

Lead is a blue-grey metal that occurs naturally and is found in small amounts in the earth's crust. Metallic lead does not dissolve in water and does not melt. Some natural and manufactured chemicals contain lead, but they do not look the same as lead in its metallic state [93]. Special lead characteristics such as tensile strength, smoothness, low melting point and corrosion resistance have caused extensive application in various industries such as automotive plastics, coatings, ceramics, among others. That, in effect, resulted in a significant increase in the occurrence of free lead in ecological systems and in the sterile environment [94]. The widespread use of lead is in the production of certain types of batteries, the manufacturing of weapons, certain types of metal goods and ceramic glazes. Several lead-containing substances are used in painting [93]. Lead exposure by occupational routes can trigger lead poisoning. In particular, in developing countries, lead is present in particulate form in the air and can be inhaled along with other heavy metals [95]. The primary target for lead toxicity is the nervous system. Long-term exposure of adults to lead at work has resulted in decreased performance in some tests that assess the role of the nervous system. Lead exposure can also induce anemia, which is a low number of blood cells, and it can also severely damage the brain and kidneys in adults or children at high levels of exposure [93].

Chapter 3

Methodology and characterization techniques

3. Introduction

This chapter lays out the preparation steps for hydrogel synthesis, solvent preparation and instrumental characterization methods utilized to evaluate hydrogels. Different characterization methods have been utilized to study the attributes of polysulfone hydrogels as thin film membranes, prepared on a conductive electrode surface. These shall include:

- Electrochemical techniques such as cyclic voltammetry and square wave voltammetry
- Spectroscopic techniques used for membrane structure understanding at its molecular level (Fourier transform infrared spectroscopy (FTIR))
- Microscopic techniques such as (Scanning electron microscopy (SEM), and atomic force microscopy (AFM)) to evaluate the morphological and topographic features

3.1. Methodology and experimental procedures

3.1.1. Instrumentation

3.1.1.1. Potentiostat set-up

All electrochemical experiments were performed and recorded with a computer interfaced to a PalmSens electrochemical biosensor with PalmSens software, ((Palm Instruments BV, Netherlands), using either cyclic voltammetry (CV), or square wave voltammetry (OSWV). A conventional three-electrode system was utilized. The working electrode was a gold disc electrode (Bioanalytical Systems, Lafayette, IN, USA). Silver/silver chloride (Ag/AgCl – 3 M NaCl type) was used as the reference electrode and a platinum wire was used as auxiliary electrode [96], [97].

3.1.1.2. Electrode surface preparation

Before use, the gold working electrode was cleaned by sonication in 0.1 M HCl for about 30 minutes, rinsed with deionized water and then polished using aqueous slurries of 1 µm, 0.3 µm and 0.05 µm alumina powder. The electrode was then rinsed with huge amounts of deionized water. The platinum (Pt) counter and glassy carbon reference electrode was frequently cleaned before, after and in between analysis [98].

3.2. Materials and reagents

Polyvinyl alcohol: PVA of 89,000-98,000 molecular weights, 99+ % hydrolyzed was supplied by Sigma-Aldrich, South Africa, Cape Town, with lot number MKBL028IV, Product code 10001444119. this product was used as received from the supplier without any modification and was stored at room temperature.

Polysulfone: Polysulfone (MW = 35.000, 0.2%w/v in CH_3Cl_3 25ºC) was supplied by Sigma-Aldrich, South Africa, Cape Town, with lot number MKBS2962V and product code 1001845122. This product was used as received from the supplier without any modification and stored at room temperature.

Glutaraldehyde: The cross-linker glutaraldehyde (GA), Grade I, 25% in water, total impurities ≤ 0, 05% free of carboxylic acid (lot number SLBS4196) was supplied by Sigma Aldrich, South Africa, Cape Town. GA was stored in the freezer at a temperature of below -25°C

N, N- dimethylacetamide (DMAc): DMAc of a molecular formula C_4H_9NO, lot number BCBL2233V, purity ≥ 99.5% (GC) was supplied by Sigma-Aldrich South Africa, Cape Town.

Hydrochloric acid: 37% HCl product was supplied by Sigma-Aldrich, with lot number STBH1214 and product code 101947915 in which 2M HCl was prepared out of the 37% by dilution using the following formula.

$$C_1 \times V_1 = C_2 \times V_2 \qquad (1)$$ [99]

The concentration of the 37% could be calculated from the following

$$C = \frac{\text{Purity (or density)} \times 10}{\text{Mw}} \qquad (2) \qquad [100]$$

3.3. Synthesis and preparation of polysulfone-polyvinyl alcohol hydrogels

3.3.1. PSF-PVA synthesis

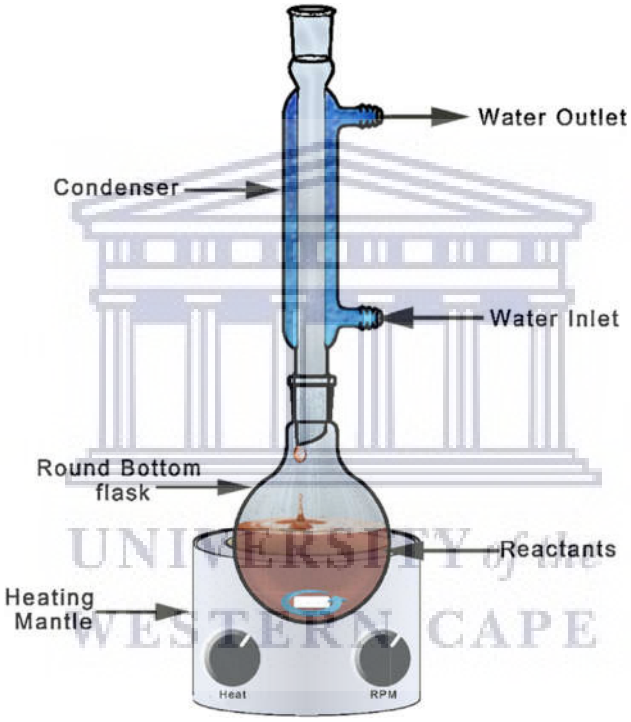

Figure 1: Reflux reaction set up

A reflux system (figure 1) makes for the boiling and condensing of liquid, with the condensate going back to the reaction mixture. The application of heat speeds up the reaction but high volatility of most organic compounds makes them susceptible to loss through evaporation, which is averted by heating the reaction mixture under reflux. The reaction vapours condense, as a result of the circulating water in the condenser, and return to the round bottom flask and this increases product yield. The reflux equipment was coupled to a temperature control device for temperature moderation. The purpose for attaching the controller device was to prevent reaching the boiling point of polyvinyl alcohol. The PSF-PVA hydrogels were synthesized by dissolving 0,4421g of

polysulfone crystal into 50 mL of N, N-dimethylacetamide (DMAc) to yield 0.0554 M PSF-solution after 1 hour of sonication. 5 mL of this solution was transferred to a round bottom flask, to which 2,5895g of PVA was added. To the mixture 1 mL glutaraldehyde crosslinker solution was added followed by the catalyst in order to speed up the reaction during the crosslinking process. An excess of acid was required for protonation and reduction of the aldehyde to produce alcohol. 1 mL of 2 M HCl catalyst was introduced to the reflux mixture and the mixture was allowed to react for 3 hours at 75ºC with uniform stirring. After three hours the mixture was stored at room temperature for 10 days in order to ensure completeness of cross-linking reaction.

3.3.2. Hydrogel thin films prepared by drop coating method

PSF-PVA hydrogels were physically adsorbed onto the screen-printed gold electrode by drop coating 10 µl of the hydrogels onto the gold electrode. For each experiment the same amount of 10 µl of the hydrogels was drop coated and dried at room temperature for 24 hours to allow the interaction between the hydrogels and the surface of the electrode for a good conductivity.

3.3.3. Cyclic voltammetry analysis of hydrogels

In a three-electrode system (figure 2) all electrodes (working, reference and counter) are set in the self-same electrolyte solution. During the experiment, movement of charge mainly happens between the working and counter electrodes, whereas the potential of the working electrode is determined in respect to the reference electrode. Cyclic voltammetry (CV) was performed at a normal scan rate of 100 $mV.s^{-1}$ to study the redox behavior of hydrogels by applying potential scan between -1200 mV and + 1400 mV (vs. Ag/AgCl). Cyclic voltammograms were obtained in the absence of any other analyte.

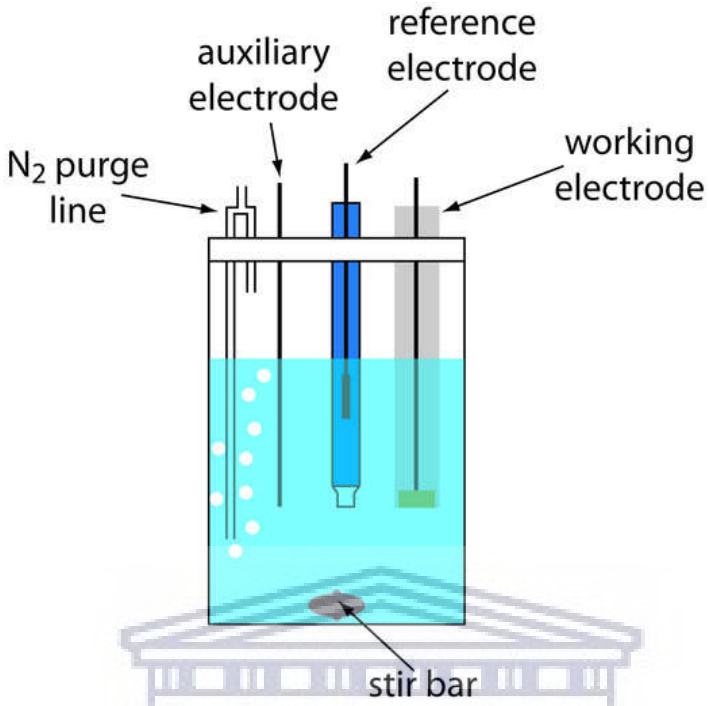

Figure 2: Three-electrode electrochemical cell

3.4. Theoretical principles

3.4.1. PSF-PVA hydrogel composite mechanism of formation

This segment of the work shows the suggested pathways of polysulfone hydrogels. The possible mechanism involves three steps, first, alcoholic oxygen protonation, second, aldehyde reduction into primary alcohol followed by crosslinking via the incorporation of oxygen.

The mechanism's detailed steps can be summarized as follows (scheme 2):

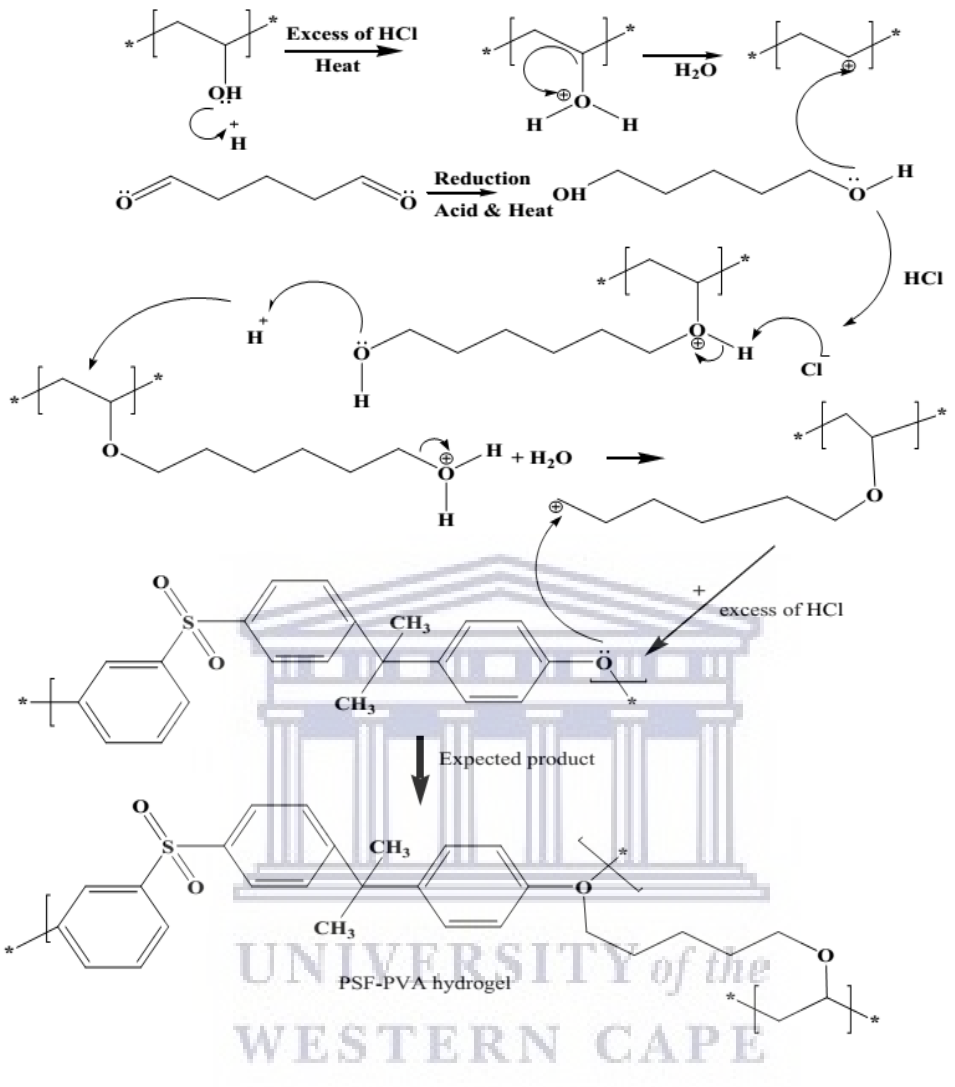

Scheme 2: Mechanism of PSF-PVA hydrogel [101]

Protonation of an alcoholic oxygen in PVA makes it a better group to leave. This is a really fast and reversible step [102]. The lone pairs of electrons on the oxygen render it a base for Lewis. Cleavage of the C-O bond makes it easier to lose the good leaving group as a neutral water molecule, leaving behind a very reactive primary intermediate carbonation. This step is the rate determining step (bond breaking endothermic). Generally, the reduction of an aldehyde yields a primary alcohol [102]. Reduction of glutaraldehyde mainly involves the introduction of a hydrogen atom to either end of the carbon-oxygen double bond to produce an alcohol (1, 5 pentanol). This will further undergo protonation of alcoholic oxygen to yield a primary carbocation. Attack of the

primary carbocation to an available oxygen site (ester or sulfone oxygen) occurs to yield PSF-PVA hydrogels. The line across the bond of the ether oxygen indicates that the polymer chain could be extended through polymerization.

3.4.2. Electrochemical characterization

Chemists and physicists have been using various methods to study conducting polymers. Transient electrochemical techniques such as chronoamperometry (CA), chronocoulometry (CC) and cyclic voltammetry (CV) are major tools used to monitor the formation and deposition of polymers and to follow the kinetics of their charge transport processes. Electrochemical impedance spectroscopy (EIS) has emerged as the most effective technique used to acquire parameters such as the double layer capacity, the resistance, the rate of charge transfer, the pseudocapacitance of the polymer film, as well as diffusion coefficients. CV supplies fundamental information about the oxidation ability of the monomers, about the redox behavior of the polymer, as well as about the surface concentration. Deductions can also be made from the cyclic voltammograms about the rate of charge transfer and the interactions that take place in the polymer segments [103].

The electrochemical workstation analysis tool is a system which helps to conduct all the techniques of electrochemical characterization, such as CV, CA, EIS, chronopotentiometry (CP), galvanostatic charging discharge (GCD), and other techniques. It can be used for various applications such as research of sensors, batteries and capacitors. The measurement of potential, charge or current is often used in electrochemical characterization to assess the amount of an analyte or to characterize the reaction kinetics of an analyte. The potential, load, and current are the profound electrochemical indicators that act as analytical indicators. For all the electrochemical characterization methods, these indicators establish the key experimental models.

There are three kinds of electrode systems available in an electrochemical cell, the system of two electrodes, the system of three electrodes, and four electrodes. Electrochemical characterizations can be carried out using any of these electrode systems. The electrochemical cell comprises a working electrode and a counter-electrode. The working electrode's potential is responsive to the amount of the analyte. The loop is closed by the counter electrode. The working electrode's potential in relation to the counter electrode should be measured as it acts as a reference potential. The counter electrode's potential should therefore remain constant. If the counter electrode's

potential is not constant, two electrodes must replace the counter electrode, a reference electrode whose potential remains constant and an auxiliary electrode to complete the electrical circuit.

The electrochemical system also makes it possible to measure all electrochemical characteristics in varying reaction conditions such as stirring, heating, purging of air, and introducing substances during actual-time measurement. In addition, it is also possible to detect and correct in situ pH and temperature while characterizing the cell. Hence, the in situ electrochemical evaluation of electrode material utilizing electrochemical characterization methods would therefore be possible in an electrochemical unit. Electrochemical output can be enhanced by expanding the porosity and surface area of the electrode, as this will give a good large number of active sites together with ease in the ion diffusion route for optimal charging storage. The lower scan is preferable over the higher one because at higher scan rates the charges are unable to adequately reach the active surface area of the electrodes because of the inadequate time [104].

The redox reactions that happen in the cell form the basis for generating the current that passes between the electrodes. When the reaction is balanced, zero current (open circuit) is produced. The initial current is huge given the high concentration gradient. As time progresses, there is a reduction in the concentration gradient and an increase in the diffusion layer (when the other modes of mass transport are absent), which ultimately causes reduction in the value of the current (close to zero) and the equilibrium is attained. This can also be performed in another way where the current is supplied and the potential is controlled. This is the principle on which electrochemical techniques like CA (chronoamperometry) and CP (chronopotentiometry) work. In amperometry [105], the excitation signal applied to the working electrode (WE) is a constant potential. It is selected such that all the electroactive substance (the analyte) at the electrode surface is instantly electrolyzed (oxidized or reduced) and the electron transfer is not the rate-limiting step of the electrode process. The current flowing in the cell as a consequence of the electron transfer is monitored as a function of time and constitutes the analytical signal. In chronopotentiometry stripping analysis [106], after the pre-concentration of analyte at the electrode, a fixed current is applied to oxidise (or reduce) the accumulated species, and the E–t curve is recorded. During the stripping process, the potential remains close to a constant value, during a time known as the transition time, τ, which is directly proportional to the concentration of analyte in solution.

3.4.2.1. Cyclic voltammetry

CV is the basic electrochemical material test. In this, the current is detected by sweeping the potential back backwards and forwards (from positive to negative and from negative to positive) between the chosen limits. Information collected from CV can be used to learn about the electrochemical activity of the material. The graphical analysis of the cyclic voltammogram shows redox peaks (figure 3), which are reduction and oxidation peaks of the material, predicting the capacitive behavior of the electrode. Therefore, the potential to oxidize and reduce the material can be found. Figure 3 displays a conventional potential-excitation signal (a) wherein the potential is first scanned to more positive values, to oxidize material R to O, and then reduce material O back to R by changing directions to scan to more negative potentials. Since cyclic voltammetry is performed in an unstirred electrolyte, the resultant cyclic voltammogram (b) shows distinct peaks for the oxidation reaction and reduction reaction, marked by a peak potential and a peak current respectively.

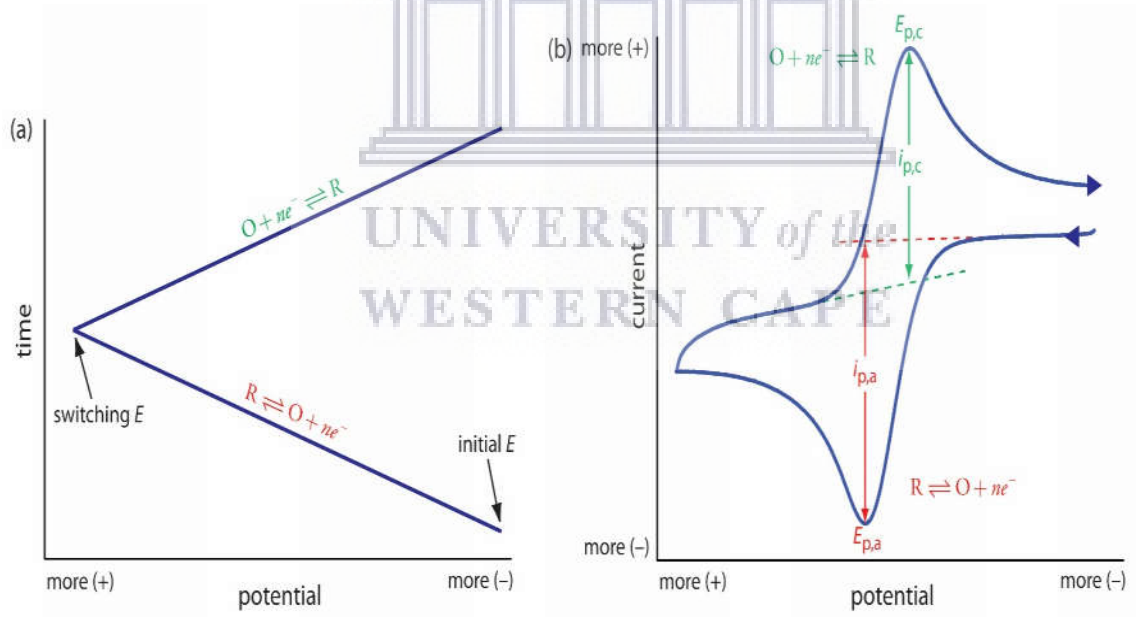

Figure 3: Schematic diagram of cyclic voltammetry

As a feedback to the CV, a ramp signal is obtained. A positive ramp (neutral slope) signal is produced for the forward scan, while the voltage is reversed after the first half cycle, preceded by a negative ramp, which inverts the cyclic voltammogram structure for the second (next) half cycle.

With the aid of redox reactions, the process aims to achieve the state of equilibrium. It obeys a cyclic trend in which the trend gives information on the transitions the system has experienced. Through examining the curve of CV appropriately, one can draw many significant conclusions about the material and its characteristics (such as capacitive nature) along with the behavior of the system (reversible, irreversible, or quasi-reversible).

The CV experiment can be carried out with one cycle or multiple potential cycles. The slope of the ramp signal expressed in volts per unit time is termed as the scan rate. The range of this scan rate can be from a few fractions of millivolts per second to several hundreds of volts per second. The scan rate of the system can be varied to get a clear idea of the electrochemistry of the cell. Hence, the scan rate plays a crucial role in the voltammetric behavior of the sample to be tested. Based on the scan rate, one can expect some changes in the oxidation and reduction peak currents along with peak potentials. Also, if the peak current (faradaic current) is increasing with the increasing scan rate, then it represents a good rate capability along with better pseudo capacitive behavior of the electrode material. Higher scan rate results in a higher number of redox reactions due to the presence of the electroactive species at the electrode's (working electrode) surface.

For a slower scan rate, however, there is the possibility of missing the peak (either forward or reverse scan peak) owing to the sufficient time available for the products from the reduction or oxidation to participate in a chemical reaction whose products may not be electroactive. This peak current in the CV can be computed using the Randles-Sevcik equation:

$$i_p = 0446\ 3\left(\frac{F^3}{RT}\right)^{1/2} An^{3/2} D^{1/2} C_o v^{1/2} \quad (3)$$

where I_p is the peak current, C represents the concentration of the electroactive species at the electrode, n represents the number of electrons in the redox reaction, A represents the area of the working electrode, D represents the diffusion coefficient of the electroactive species, and n is the scan rate. All of these factors have a vital role to play in deciding the CV maximum current. CV makes it easier to find the coefficient of electron transfer (the number of electrons transferred), the limiting factor (the factor controlling the speed of the reaction) and the rate constant of the reaction. The difference between the CV's two peak potentials provides insight into the impact of analyte diffusion levels. In contrast, the system's reversible, irreversible, and quasi-reversible existence can be observed using the anodic and cathodic maximum currents ratio [104]. For a reversible electrochemical reaction, the CV recorded has certain well-defined characteristics. These are:

1. The voltage separation between the current peaks is given as:

$$\left|E_{p-}E_{1/2}\right| = \frac{285}{n}mV \qquad (4)$$

2. The positions of peak voltage do not alter as a function of voltage scan rate.
3. The ratio of the peak currents is equal to one.

The CV for cases where the electron transfer is not reversible shows considerably different behaviour from their reversible counterparts. For quasi-reversible or irreversible electrochemical reaction the recorded CV has following characteristics.

1. The voltage separation between the current peaks differs from that given in equation 4.
2. The peak currents are a function of the applied potential.
3. The positions of peak potential are a linear function of the logarithm of sweep rate.

By analysing the variation of peak position as a function of a scan rate, it is possible to gain an estimate for the electron transfer rate constants. Adsorption processes on electrode surface can be distinguished from charge transfer processes, as in former case cyclic voltammogram is symmetrical around potential axes [107].

The formal potential (E^o) is represented by the following equation and is obtained from the average values of the peak potentials:

$$E^o = \frac{(E_{pa} + E_{pc})}{2} \qquad (5) \qquad [108].$$

3.4.2.2. Square wave and stripping voltammetry

Square wave voltammetry (SWV) was developed by G.C. Barker and Jenkins in 1952 but it had a constrained scope of application due to the available equipment at that time. Now that appropriate potentiostat electronics are accessible, it is the preferred technique in several analyses on the basis of its sensitivity. The SWV waveform is a square wave which is overlaid on a potential stairway. The square wave is defined by a staircase height, ΔE_s, pulse length, tp, cycle time, t_s, and square wave amplitude, ΔEp. Alternatively, the pulse time can be expressed as a square wave frequency,

f = 1/2 t_p. The stairway shifts by ΔEs at the beginning of each cycle so that the scanning rate is as shown in figure 4 [108].

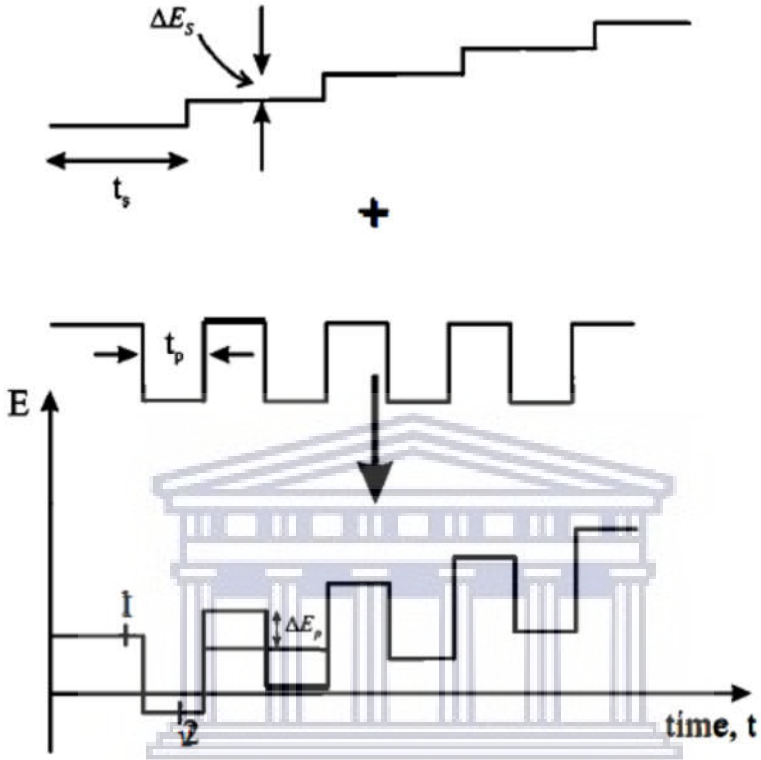

Figure 4: Waveform and measurement scheme for SWV. It shows the sum of a staircase and a square wave [108]

Stripping voltammetry (ASV) is an extremely sensitive technique for the electroanalytical sensing of a broad range of metals and organic material offering low detection limits that can reach 10^{-10} M in advantageous cases. The procedure is categorized into three parts: anodic, cathodic or adsorptive stripping voltammetry, ASV, CSV or AdSV. In every case the first is 'pre-concentration' step:

ASV: M^{n+} (aq) + ne^- —⟶ M(electrode).
CSV: M + L^m⟶ $ML^{(n-m)-}$ (ads) + ne^-,
Ad S V: M(aq) + L(aq) ⟶ ML(ads)y,

Succeeded after an appropriate accumulation by a stripping step in which the potential from the working electrode is swept to Faradaic degradation of the built-up material from the electrode:

ASV: M(electrode) → M^{n+} (aq) + ne^-,

CSV: $ML^{(n-m)-}$ (ads) + n^{e-} → M + L^m

AdSV: *A(ads)* ± *ne*$^-$ → *B(aq)*

In ASV, the stripping step, generated by scanning the working electrode towards positive potentials compared to that used for pre-concentration step, produces a characteristic peak that allows the target trace ion to be quantified. The use of SWV to enhance sensitivity and the potential at which the stripping peak comes about at various potentials for various metals.

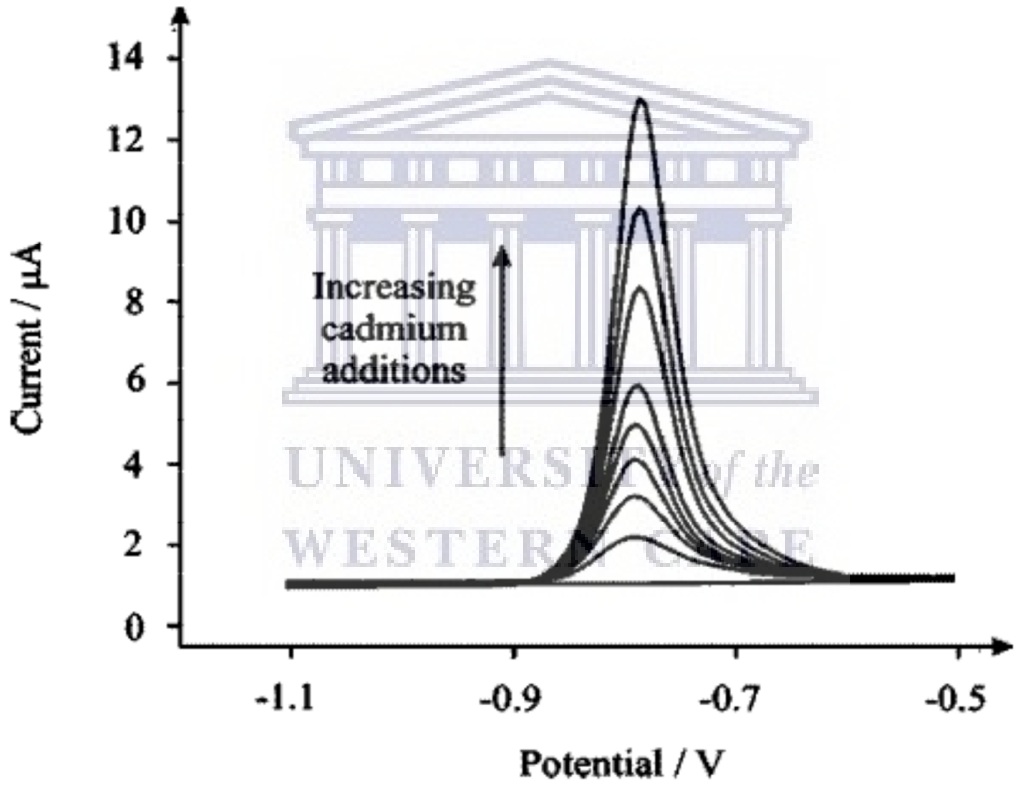

Figure 5: Illustration of Square-wave anodic stripping voltammetry in 0.5 M acetate buffer for increasing additions of cadmium (II) [108]

Figure 5 shows well-defined square wave anodic stripping signatures with a detection limit of 2.5 x 10^{-8} M easily achievable.

The following is an example of stripping voltammetry.

(A) The detection of As(III) in some drinking water supplies using a gold electrode and ASV:

Pre-concentration: $As(III)(aq) + 3e^- \rightarrow As(electrode)$

Stripping: $As(electrode) \rightarrow As(III)(aq) + 3e^-$.

In this case after pre-concentration at a suitable reducing voltage, the working electrode is swept to positive potential and the resultant peak is used to measure low concentrations of As(III) [108].

3.4.3. Spectroscopic characterization techniques

Spectroscopy is essentially an experimental topic of interest and concerns the absorption, emission or dispersion by atoms or molecules of electromagnetic radiation. Electromagnetic radiation covers a broad range of wavelengths, from radio waves to g ɣ-rays, and atoms or molecules may be adsorbed on a solid surface in the gas, liquid or solid phase, or of great importance in surface chemistry [109].

Electromagnetic radiation is usually classified as radio waves, microwaves, infrared, visible and ultraviolet light waves, X-rays, and gamma rays. Electromagnetic waves are transverse waves that move at light speed and involve electrical and magnetic fields that oscillate at perpendicular to each other. Usually, spectrochemical techniques measure the generated electromagnetic radiation (emitted) or are absorbed by molecular or atomic species of species of interest. By introducing energy in the form of heat, light, or chemical reactions, the material to be characterized is triggered in this technique. The energy tends to result in the excitation of molecules held at ground level (low-energy state) to the excited state (high-energy state). Each species of molecules can absorb its own typical frequency. Each molecular species can absorb its own characteristic electromagnetic radiation frequencies and this process transfers energy to the molecule and tends to lead to a decrease in electromagnetic radiation intensity [104]. In spectrochemical analysis there are four main types of analysis:

1. Atomic spectrochemical evaluation measures the fundamental makeup of a sample by atomic or ionic emissions and absorption spectra.
2. Molecular spectrochemical evaluation by molecular absorption, luminescence, and Raman spectra measures the molecular makeup of materials.

3. Evaluation of the emission spectrum utilizes the spectra of atomic, ionic or molecular emissions produced by various sources of electromagnetic radiation in the range from gamma rays to microwaves.

4. Absorption spectrum evaluation makes use of the absorption spectra of the material being evaluated; these spectra can be generated by a material's atoms, molecules or ions in different aggregation states [104].

In our research FTIR will be utilized to corroborate the formation of the cross links between polyvinyl alcohol and polysulfone as starting materials to yield the desired hydrogel materials. The FTIR of polysulfone starting material and the PSF-PVA product will be compared to find data concerning the crosslinking chemistry.

3.4.3.1 Fourier transform infrared (FTIR) spectroscopy

FTIR stands for Fourier transform infrared, the preferable method of infrared (IR) spectroscopy. In IR spectroscopy, IR radiation is passed through a sample. Some of the IR radiation is absorbed by the sample and some of it is passed through (transmitted). The resulting spectrum represents the molecular absorption and transmission, creating a molecular fingerprint of the sample. As two fingerprints never match, similarly no two unique molecular structures produce the same IR spectrum. This makes IR spectroscopy useful for several types of analysis. IR spectroscopy has been a workhorse technique for materials analysis in the laboratory for over 70 years. An IR spectrum represents the fingerprint of a sample, with absorption peaks that correspond to the frequencies of vibrations between the bonds of the atoms making up the material [104]. Infrared Spectroscopy is the evaluation of the interaction of infrared light with matter. Analysis of infrared spectra can reveal what molecules are present in a sample and at what amounts; this is why infrared spectroscopy is useful [110].

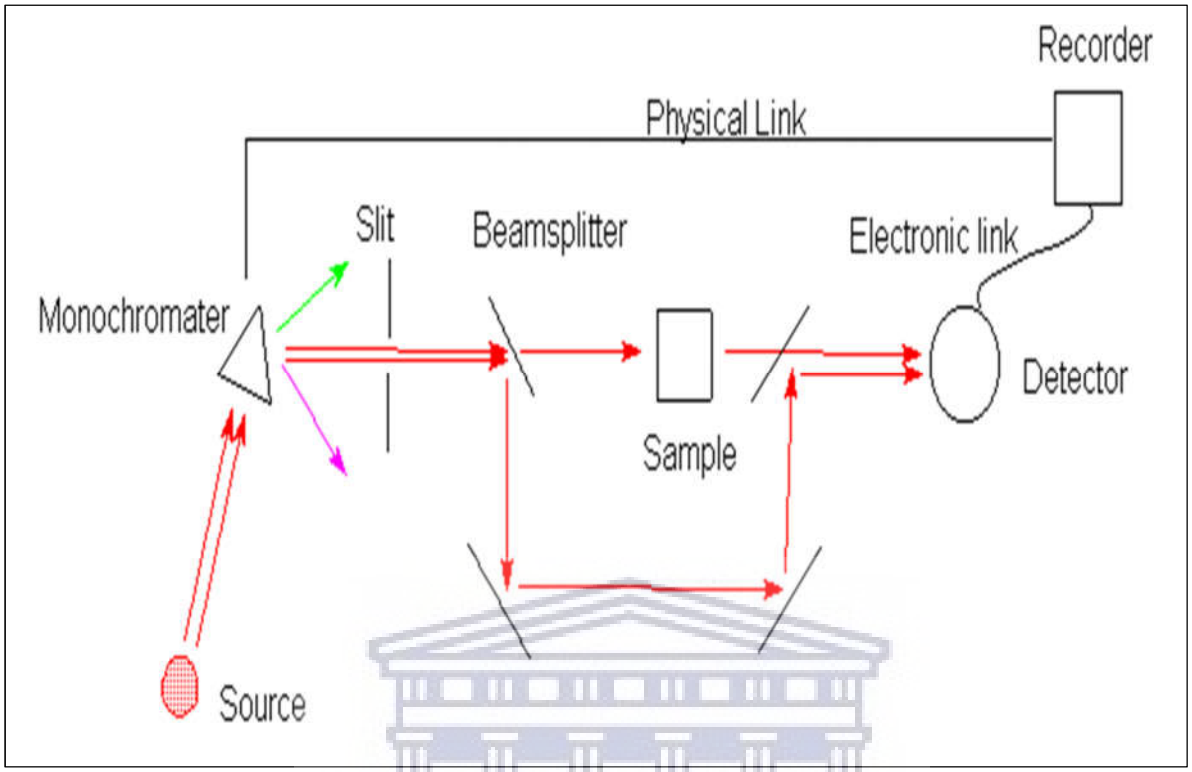

Figure 6: Scheme showing the working principle of Fourier Transform Infrared Spectroscopy

In Figure 6 a beam of monochromatic radiation is passed into a beamsplitter, fifty percent of the incident radiation is reflected to one of the mirrors and fifty percent will be transmitted through the beamsplitter and the sample. The two beams then recombine and interfere at the interferometer. The path difference of the two beams interfere destructively in the case of the transmitted beam and constructively in the case of the reflected beam. The beam that emerges from the mirror at 90° to the input beam is called the transmitted beam, which is the beam detected in FTIR spectroscopy. The recorder then records the IR spectrum [111].

The principle of infrared spectroscopy is that a molecule absorbs infrared light under some conditions when irradiated with it. The energy h_v of the absorbed infrared light is equal to an energy disparity between a certain energy level of vibration of the molecule (having an energy E_m) and another energy level of vibration of the molecule (having an energy E_n). In the form of an equation,

$$H_v = E_n - E_m \qquad (6)$$

In other words, absorption of infrared light happens principally based on a transition between energy levels of molecular vibration. This is why an infrared absorption spectrum is a vibrational spectrum of a molecule [112].

3.4.4. Microscopic characterization

Microscopy involves the study of objects that are too small to be examined by the unaided eye. In the SI (metric) system of units, the sizes of these objects are expressed in terms of sub-multiples of the meter, such as the micrometer (1 Pm = 10^{-6} m, also called a micron) and also the nanometer (1 nm = 10^{-9} m). To describe the wavelength of fast-moving electrons or their behavior inside an atom, even smaller units are needed [113].

3.4.4.1. Scanning electron microscopy (SEM)

Scanning electron microscopy (SEM) today is a versatile technique used for research and development in many industrial labs. SEM is often used in materials science, including polymer science, to elucidate the microscopic structure or to distinguish several phases from each other due to its high lateral resolution, its high focus depth and its X-ray microanalysis facility [114].

There is no question that the scanning electron microscope (SEM) is the most commonly used of all instruments with electron beams. The SEM's success can be attributed to many factors: the flexibility of its different imaging modes, the excellent spatial resolution that can now be achieved, the very modest required sample preparation and condition, the relatively straightforward analysis of the acquired image., accessibility of related techniques of spectroscopy and diffraction. And most of all, its user-friendliness, high levels of automation, and high performance make it accessible to most researchers. With the recent generation of SEM equipment, high-quality images can be obtained with an image magnification that is as low as approximately 5 and as high as > 1 M ×; A wide range of image magnifications extends our visualization capacity from naked eyes to measurements of nanometers. Image resolution of approximately 0.5 nm can now be obtained in the current generation field emission gun SEM (FEGSEM), clearly surpassing that of a transmission electron microscope (TEM); nevertheless, the sample size may be as high as silicon wafers on a production scale [115].

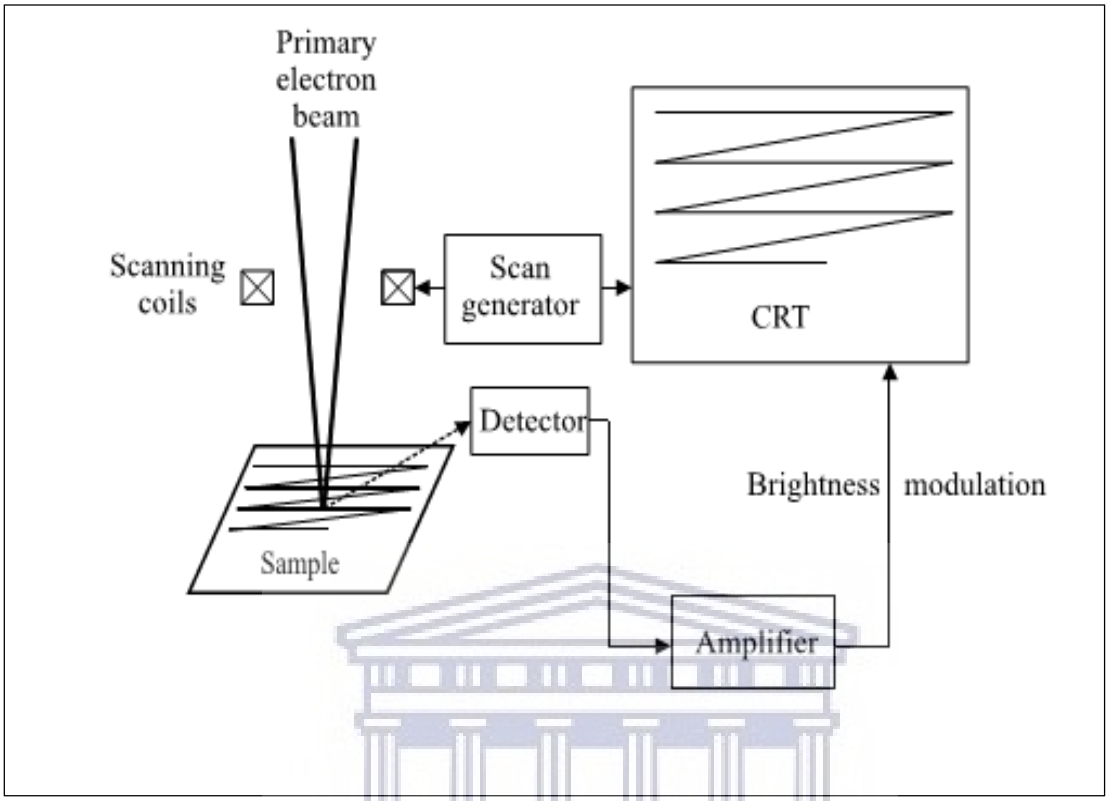

Figure 7: Scheme showing the principle of scanning electron microscope (SEM)

The basic principle of the SEM is founded on the experiment of Knoll and the concept of von Ardenne for a microscope for the transmission of a scanning sample. In a similar approach to scanning the electron beam in a cathode ray tube (CRT), the focused electron beam scans the surface of the specimen in the evacuated microscope column line by line and forms signals based on the encounters between the beam and the specimen. The response signal was originally displayed as a modulation of brightness on a CRT where the electron beam is simultaneously driven to the column beam as shown in Figure 7. The conventional CRTs have now been substituted by digital computer techniques. Since the area of the displayed image remains unchanged, the magnification of the image is determined by the dimension of the scanned sample area. Generally, the resolution of the SEM image is determined both by the diameter of the electron probe focused on the sample surface and the interaction of the primary electrons (PE) with the sample [114].

3.4.4.2 Atomic force microscopy (AFM)

Since its advent, atomic force microscopy (AFM) has become a well-established tool for the characterization of soft materials. The strong interest in AFM studies arises from the fact that this technique complements or even replaces other microscopy or diffraction techniques commonly used for studying the structure and morphology of polymeric systems. AFM, initially introduced for high-resolution surface profiling, does not require for this purpose any special sample preparation and allows real-space visualization of the surface structures under study. Therefore, a great flexibility exists that also allows operation under different conditions, for example, in a controlled atmosphere, in liquids, or at elevated temperatures. The continuously growing popularity of AFM can be explained by the fast development of AFM instrumentation that has significantly extended its capabilities to include measurements of local mechanical, adhesive, magnetic, electric, and thermal properties [116].

One can easily distinguish between two general modes of operation of the atomic force microscope (AFM) depending on absence or presence in the instrumentation of an additional device that forces the cantilever to oscillate in the proximity of its resonant frequency. The first case is usually called static mode, or DC mode, because it records the static deflection of the cantilever, whereas the second takes a variety of names (some patented) among which we may point out the resonant or AC mode. In this case, the feedback loop will try to keep at a set value not the deflection but the amplitude of the oscillation of the cantilever while scanning the surface. To do this, additional electronics are necessary in the detection circuit, such as a lock-in or a phase-locked loop amplifier, and also in the cantilever holder to induce the oscillatory excitation. From a physical point of view, one can make a distinction between the two modes depending on the sign of the forces involved in the interaction between tip and sample, that is, by whether the forces there are attractive or repulsive [117].

3.4.4.2.1. DC mode

3.4.4.2.1.1. Contact mode

Also called constant force mode, the contact mode is the most direct AFM mode, where the tip is brought in contact with the surface and the cantilever deflection is kept constant during scanning

by the feedback loop. Image contrast depends on the applied force, which again depends on the cantilever spring constant. Softer cantilevers are used for softer samples. It can be used easily also in liquids, allowing a considerable reduction of capillary forces between tip and sample and, hence, damage to the surface. Because the tip is permanently in contact with the surface while scanning, a considerable shear force can be generated, causing damage to the sample, especially on very soft specimens like biomolecules or living cells.

3.4.4.2.2. AC mode

3.4.4.2.2.1. Intermittent contact mode

The general scheme is comparable to that of the non-contact mode, however in this case, during the oscillation, the tip is put into contact with the sample surface so that the dampening of the cantilever oscillation amplitude is caused by the same repulsive forces found in the contact mode. The oscillation amplitude of the cantilever is typically larger in intermittent contact than that used for noncontact. The vertical resolution is very good together with lateral resolution, there is less interaction with the sample compared with contact mode (especially lateral forces are greatly reduced), and it can be used in liquid environment [117].

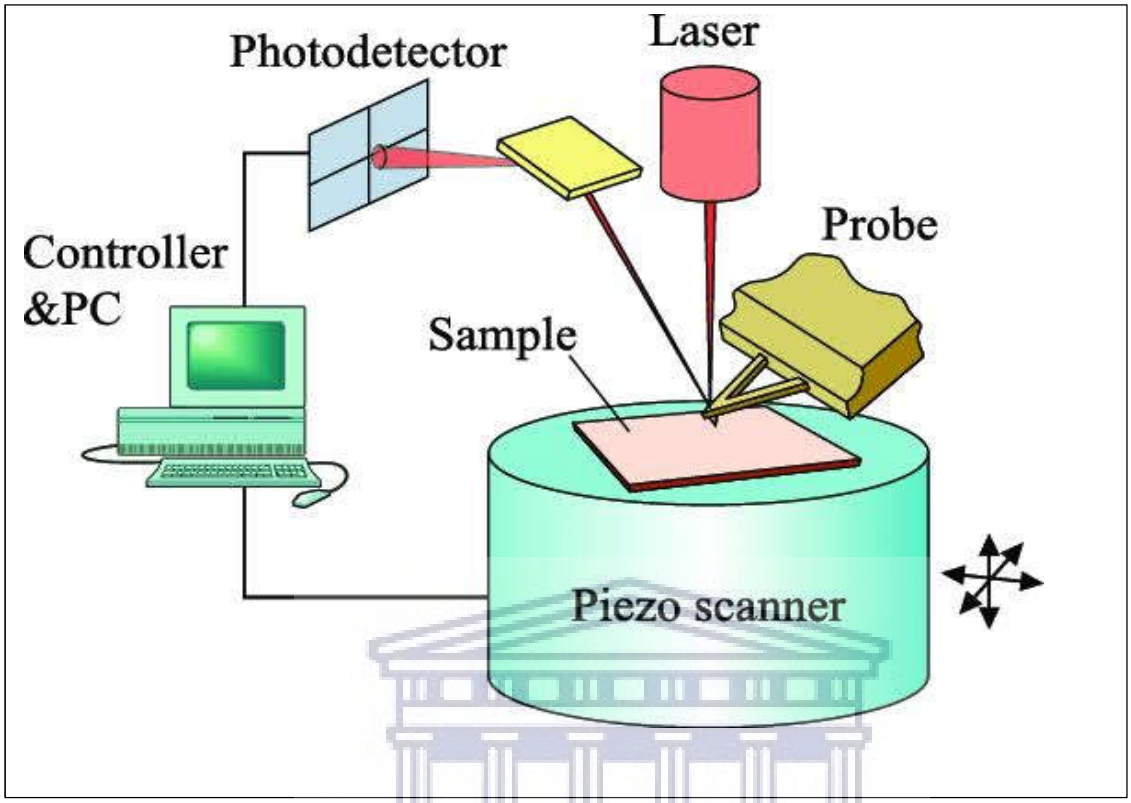

Figure 8: Scheme showing the principle of atomic force microscope (AFM)

Chapter 4

Results and discussion

The emphasis of this chapter is on interpreting the results obtained on the synthesized polysulfone hydrogels by different characterization techniques. The various techniques help to examine the different features of these hydrogels.

4. Part I: Synthesis and characterization

4.1. Electrochemical deposition of PSF-PVA hydrogel

Polysulfone-polyvinyl alcohol hydrogels was synthesized as explained in chapter 3 and prepared as thin films on a gold electrode by electrodeposition. That is, about 1 mL of the hydrogel solution was injected into 5 mL of 1 M HCl with a syringe and electrodeposition was carried out by cycling the potential ten times from 0 to 1 V at the scan rate of 50 mV/s.

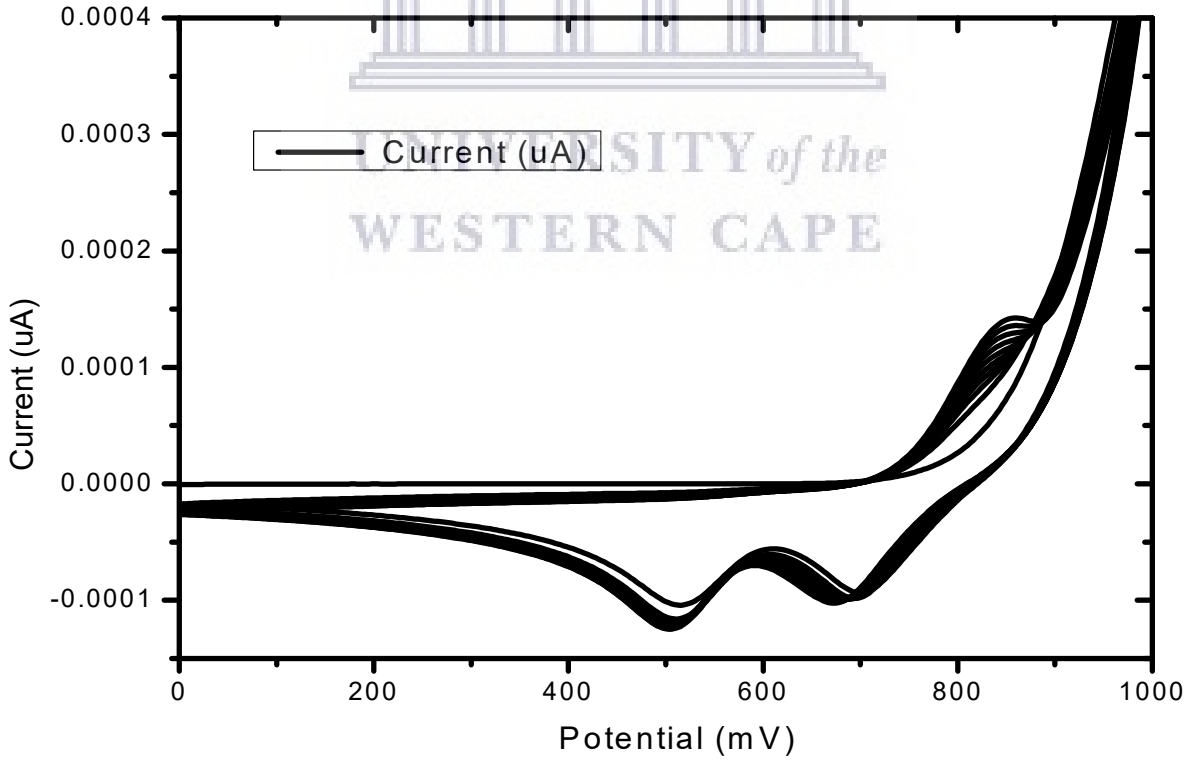

Figure 9: Cyclic voltammetry of PSF-PVA hydrogel in 5 ml of 1 M HCl at the scan rate of 50 mV/s

The cyclic voltammogram of the deposited hydrogel (PSF-PVA) within the potential window ranging from -1200 mV to 1400 mV (figure 9) shows the layers of the thin film on the gold electrode. The cyclic voltammogram showed an anodic peak at 850 mV and a cathodic peak at 750 mV, vs Ag/AgCl. These peaks are ascribed to electron delocalization and the growth of a semi conducting PSF-PVA film on the Au electrode. Strong resonance delocalization of the lone pairs on ester oxygen that happens throughout the structure led to the redox peaks observed. The other reduction peak at 500 mV is ascribed to gold, which is the interface material [118].

4.2. Electrochemical characterization

4.2.1. Cyclic voltammetry of PSF-PVA hydrogel

Electrochemical characterization techniques focused on understanding PSF hydrogel redox behavior in the absence of heavy metals. Electrochemical characterization was performed by cycling the potential scan between - 1200 and + 1400 mV in 5 mL of 0.5 M phosphate buffer solution (PBS) at different scan rates ranging from 10 to 300 mV/s. The platinum (Pt) counter electrode was frequently cleaned before and after analysis. The working electrode was prepared by electrodepositing the hydrogel onto the Au interface by cycling the potential ten times from 0 to 1 V in 0.5 M PBS at the scan rate of 50 mV/s.

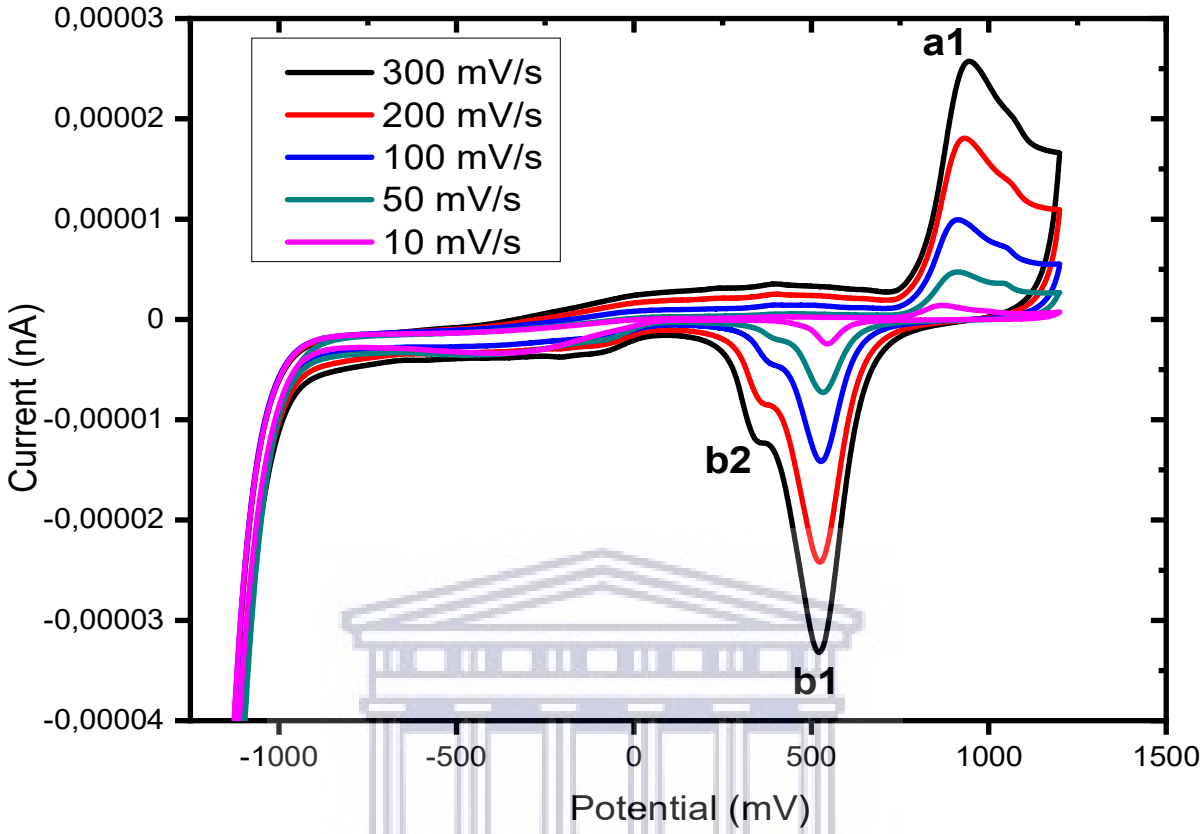

Figure 10: Cyclic voltammetry of PSF-PVA hydrogel in 0.5 M PBS at different scan rate

The synthesized hydrogels exhibited one anodic peak and two cathodic peaks at all used scan rates, as shown in figure 10. The peaks observed in the cyclic voltammogram were attributed to the redox properties of the synthesized hydrogel. Cyclic voltammogram (figure 10) exhibited redox peaks due to electron delocalization and the thickening of a semiconducting polysulfone hydrogel film on the Au interface as the scan rate increases. So far, only a little about polysulfone electrochemistry has been reported. Nevertheless, given organic chemistry aspects, the redox peaks noticed are attributed to delocalization of double bonds. The redox peaks noticed as the scan rate increased could be attributed to resonance delocalization of electron lone pairs on ester oxygen that takes place in the whole structure [119].

Table 2: The oxidation and reduction peak current and potential values for PSF-PVA hydrogel at scan rates of 10, 50, 100, 200 and 300 mV/s

Scan rate (mV/s)	Anodic peak Current Ipa (µA) a1	Cathodic peak current Ipc (µA) b1	Anodic peak potential Epa (mV) a1	Cathodic peak Potential Epc (mV) b1	Formal Potential $E^{o'}$ (mV)	Ipa/Ipc
10	1.016	-1.716	868.52	545.48	323.04	0.592
50	2.806	-5.263	905.62	532.55	373.07	0.533
100	6.486	-9.363	912.83	526.24	386.59	0.693
200	11.426	-15.77	931.17	523.74	407.43	0.725
300	15.836	-21.323	946.70	520.87	425.83	0.743

In table 2, cathodic peaks exhibit higher current response and also shifted to lower potential values but anodic peaks show lower values and shifted to higher potential values. That is, the potential values of the anodic peaks of the hydrogels increased with increasing scan rate whereas the potential at the cathodic peaks decreased with increasing scan rate. Also, the current values for both anodic and cathodic peaks increased with increasing scan rate for the hydrogel. As the scan rate increases the current ratio approaches 1, which means that the hydrogel system approaches reversible electrochemistry, which in turn indicates that the hydrogel system has fast electron transfer kinetics which is best matched by a fast scan rate [108].

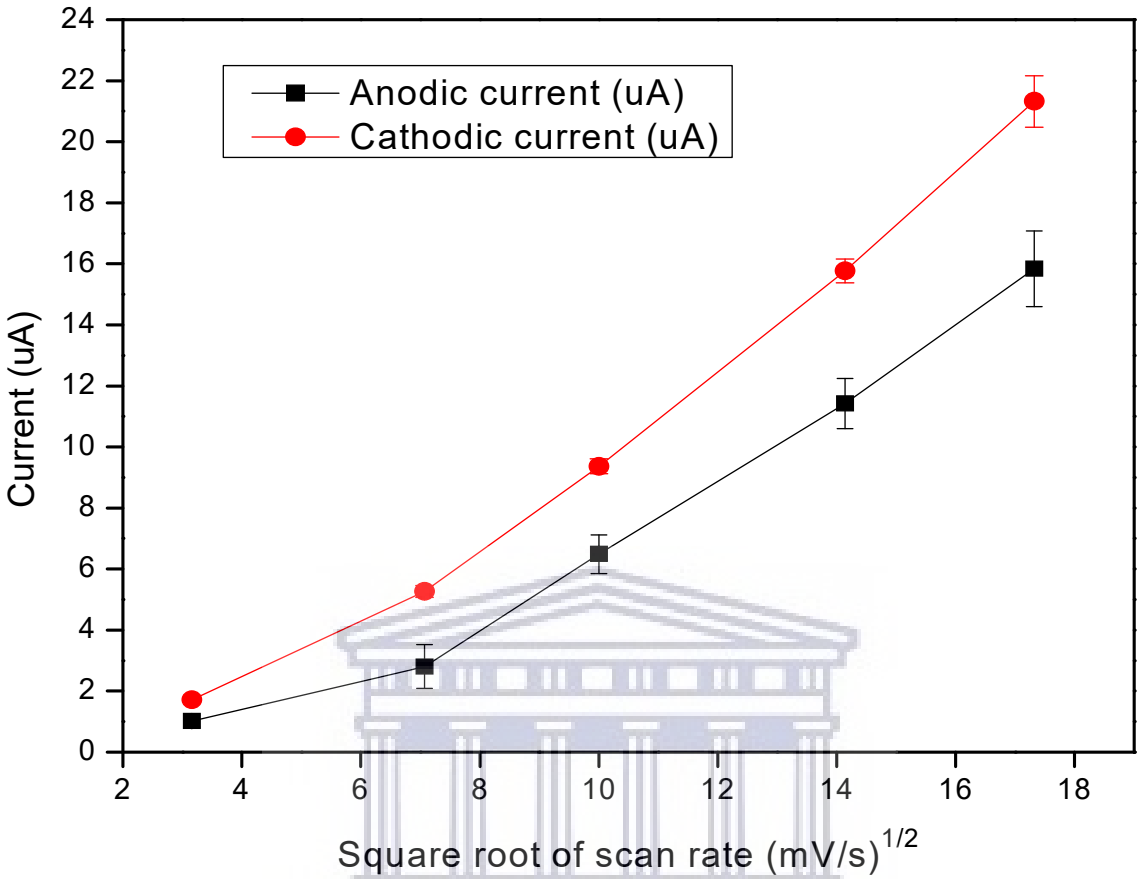

Figure 11: Graph of anodic and cathodic peak current (Ip) vs. square root of scan rate

The diffusion behavior of the hydrogel systems shows elements of quasi to full reversibility, depending on the scan rate applied. For simplicity we have approximated the diffusion coefficient (based on the available data) on the model for full reversibility. The approximated diffusion coefficients of the hydrogels were calculated by plotting the anodic peak current values and cathodic peak current values at different scan rates against the square root of the scan rates (10 to 300 mV/s) as shown in figure 11. A compressed Randle-Sevcik equation for a temperature state of 25 ˚C was used to evaluate the diffusion coefficient of the hydrogels using the equation below.

$$i_p = (2.69 \times 10^{5}) n^{3/2} A D^{1/2} v^{1/2} C \quad (7)$$

and rewritten as,

$$D = \sqrt{\frac{slope}{2.69 \times 10^{5} n^{3/2} AC}} \quad (8)$$

where slope = *I*p *divided by square root of scan rate*, *A* is the surface area of the electrode (in this case gold electrode with the surface area of 0.07 cm^2), *n* is the number of electrons involved in the redox reaction and *C* is the concentration of the analyzed hydrogels. The following equation was used to compute the number of electrons (n):

$$\left|E_p - E_{p/2}\right| = \frac{2303\ RT}{nF} \qquad \text{at} \quad 25\ ^\circ\text{C} \quad (9)$$

Where *E*p is the formal potential, $E_{p/2}$ is half-peak potential, *n* is the number of electrons, *T* is temperature in Kelvin and *F* is faraday constant, *R* is gas constant. By making *n* the subject of the formula and 2.303 *RT* divided by *F* having a value of 59.19 mV at 25 ˚C, where 2.303 *RT* has a value of 0.593 kcal/mol at 25 ˚C and *F* is 23.06 kcal/mol V, the equation is rearranged to;

$$n = \frac{5919\ mV}{E_p - E_{p/2}} \qquad (10)$$

The value of *n* obtained from the equation above for the synthesized hydrogels is 1. The concentration of the synthesized hydrogels was 0.05 M. The approximated diffusion coefficient of the synthesized hydrogels expresses the rate at which the electrons move in the direction of the electrode. The rate of diffusion of the hydrogels shows how fast the hydrogel releases electrons in the direction of the electrode. The values of the approximated diffusion coefficients are 0.33843 cm^2/s for anodic peak and 0.38609 cm^2/s for cathodic peak. The greater cathodic diffusion coefficient agrees with high cathodic current which implies that the hydrogels diffused faster in the cathodic potential scan than in the anodic potential scan. The electron transfer rate constant was calculated to be 0.14 s^{-1} using equation 11.

$$k_s = \frac{\propto nFv_c}{RT} \qquad (11)$$

Where α is the electron transfer coefficient, *n* is the number of electrons, and *F* is faraday constant, v_c is the x-intercept of the anodic line. *R* is gas constant, and *T* is temperature in Kelvin.

4.3. Spectroscopic characterization

4.3.1. Fourier Transform Infrared Spectroscopy (FTIR)

FTIR analysis was carried out using a Perkin Elmer Spectrum Two spectrophotometer in the range from 400 to 4000 cm^{-1} with a resolution of 4 cm^{-1}. A little amount of the hydrogel was sandwiched between two filter papers and a physical force was exerted for dryness. The hydrogel was then allowed to dry for 24 hours at room temperature and thereafter the KBr pellet procedure was followed, where the hydrogel was compressed as a KBr disk, which was prepared by mashing almost 1% mixture of a solid hydrogel in KBr using a hydraulic press. PVA was also studied individually (Figure 10) following the above KBr pellet procedure. Given the bonds between different elements in a sample absorb light at different frequencies, PVA's and PSF hydrogel's absorbance of IR energy was quantified to confirm the materials' molecular content and configuration. Unknown substances are identified by checking the spectrum against a repository of reference spectra. A device called an interferometer was used to identity samples by generating an optical signal with every IR frequency encoded into it. The signal was then deciphered through the application of a Fourier transformation technique. A mapping of the spectral information was then produced by this computer-generated process and that resultant spectrum was then compared with reference libraries for identification. The spectrum of the PSF-PVA hydrogel confirmed the cross-linking of the two polymers by the presence of both functional groups found in PSF and PVA with a band C-H at 3125 cm^{-1}, C=C at 1800 cm^{-1}, SO_2 at 1300 cm^{-1} and C-C at 1100 cm^{-1}. The absence of OH groups from PVA was interpreted as evidence of its involvement in crosslinking (Figure 12) [120], [121], [122], [123].

Table 3: Fourier transform Infrared peak assignment

Functional groups	Wave numbers
C=C	1600-1500
C-C	1200-1600
C-H	3000-2800
C-H	1500-1400
OH	3600-2400
SO_2	1150-1300

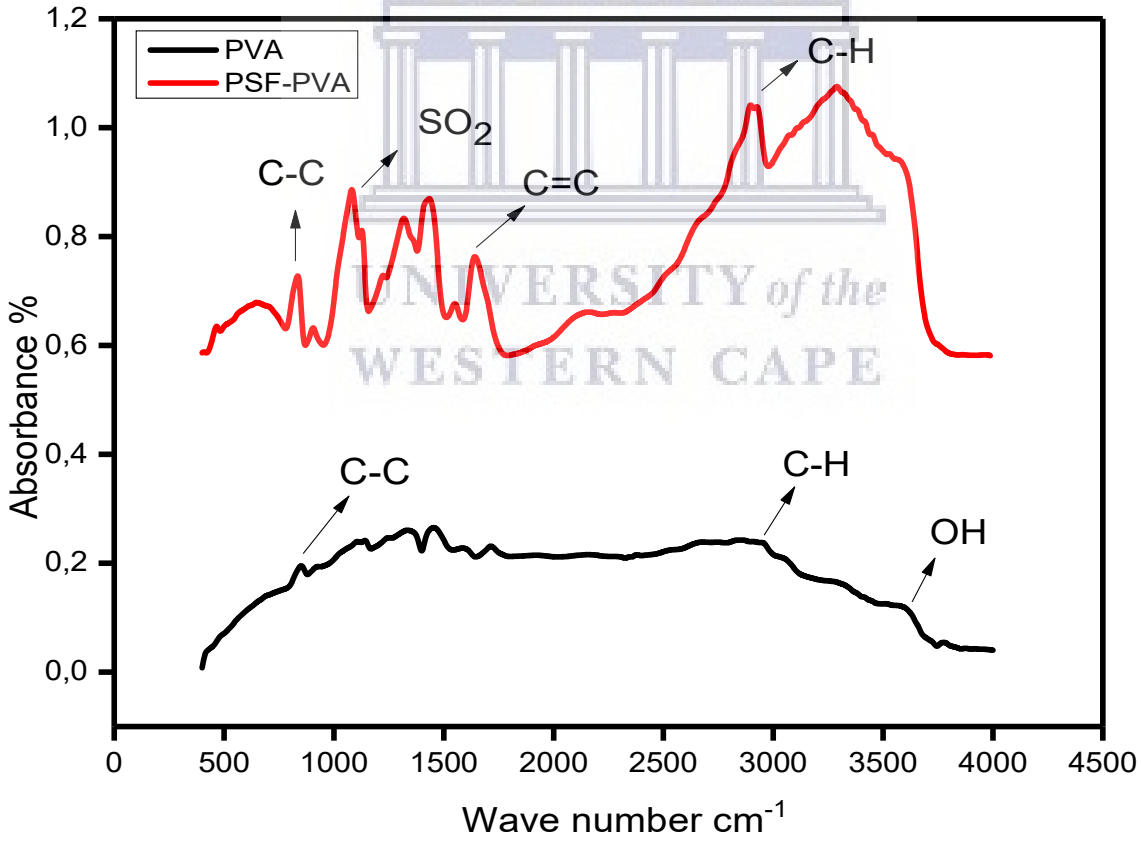

Figure 12: Spectrum of PVA and PSF-PVA hydrogel

From the suggested mechanism the two possibilities were identified for the position at which carbocation bonding could take place either at the ester oxygen, or sulphur oxygen. Fourier transform infrared analysis provides some evidence of point of linkage. The spectra of the PSF-PVA hydrogels confirmed cross-linking of the two polymers by the absence C-O-C which is involved in cross linking (Figure 12) [123]. This indicates that the ester oxygen was the site for cross linking to form the hydrogel. The sulfone oxygen vibrations were still visible in the spectrum of the synthesized hydrogel.

4.4. Microscopic characterization

4.4.1. Scanning electron microscopy

4.4.1.1. Polysulfone film preparation

Preparation of thin films was done by drop coating 10 µL aliquot of polysulfone (PSF) solution and PSF hydrogels onto separate screen-printed carbon electrodes (SPCE) with a micropipette and allowed to dry overnight prior to imaging. Both samples were covered with a thin Au layer for viewing. The SEM study was carried out using the LEO 1450 scanning electron microscope coupled with an Energy Dispersive X-ray spectrometer. A 2 µm secondary electron (SE) image resolution was achieved at 20 kV accelerating voltage and 10 000 X magnification.

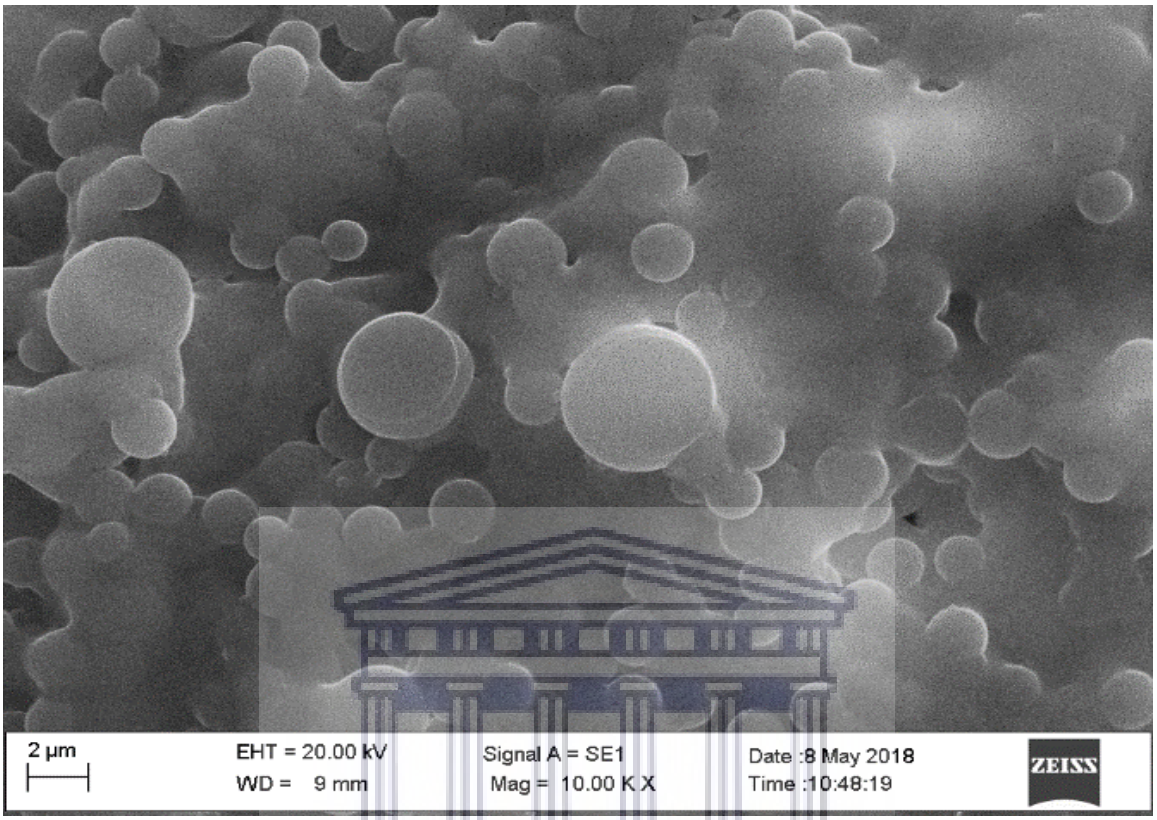

Figure 13: SEM images of polysulfone

Scanning electron microscopic image (Figure 13) reveals that polysulfone is of a spherical shape with moderately even size distribution of spheres. The steadiness in color of the image showed the absence of charging owing to interaction with the incident electron beam.

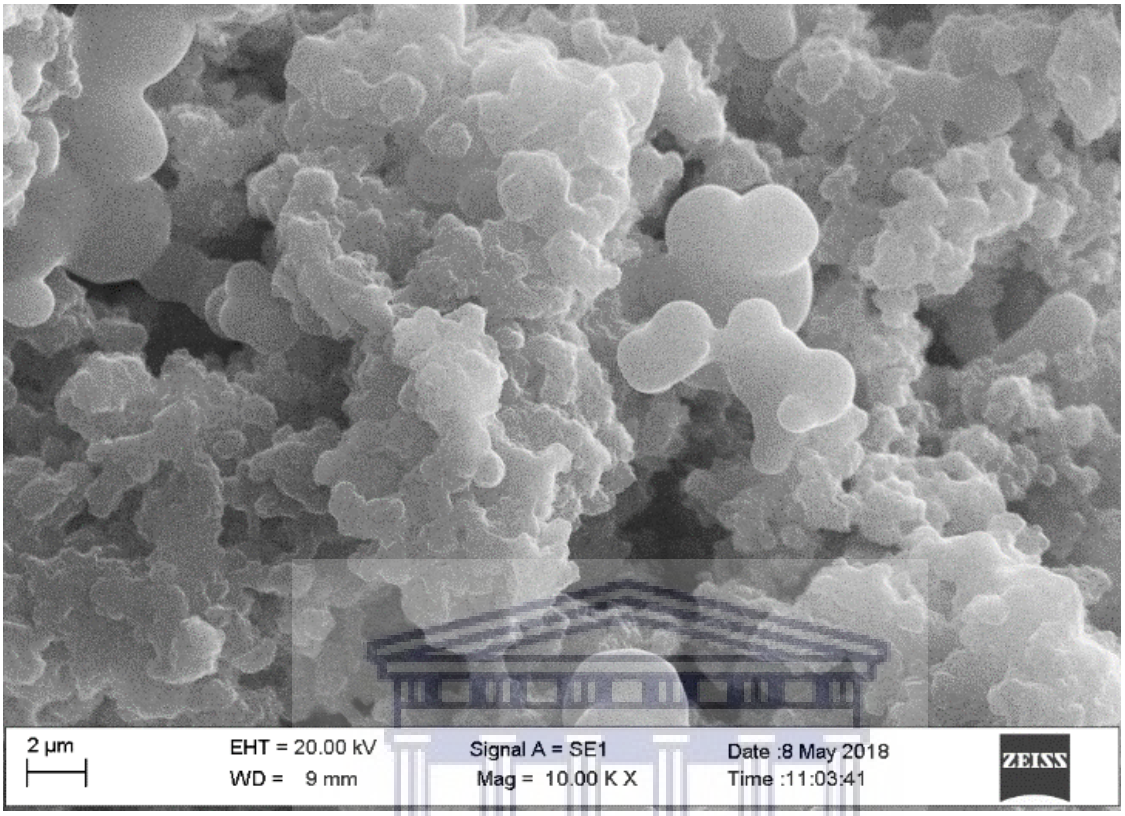

Figure 14: SEM images of PSF-PVA hydrogel

Figure 14 displays PSF-PVA hydrogel material which when compared to polysulfone alone, attested a transformation in morphology owing to the combination of PVA and PSF. The incorporation of polyvinyl alcohol resulted in a dwindled size of the surface morphology characteristics. Quite small PSF spheres were observable, but it was clear that PSF spheres controlled the expansion of PVA polymer, which is compatible with prospect for effectual crosslinking. The role played by morphology in membrane technology, mechanical characteristics and electrical conductivity of the materials is critical [124]. It could be concluded by reason of the color and size distribution exhibited by PVA-PSF hydrogel that effectual crosslinking was accomplished with confirmation of PSF spheres controlling the morphology of crosslinking. The size of our hydrogel is 2µm but the ideal size distribution is about 100 nm as Salmaan H. et al prepared hydrogel ultrathin films of ∼100 nm size for sensors for biological applications [125], and Rui Wu et al. synthesized an amine-functionalized polyacrylamide hydrogel and experimental results indicate that the particle size range from 80–120 nm hydrogel is more efficient [126].

4.4.2. Atomic force microscopy

Atomic force microscopy has been utilized to study the roughness of the surface which is considered a significant surface property. The role played by this characteristic in membrane permeability and fouling behavior is critical. Roughness parameters such as root mean square roughness (*Rrms*) and average roughness (*Ra*) are used to determine surface roughness, which could in turn be related to the thin film's hydrophobicity [127]. The sample, the hydrogel, was electrodeposited on the Au interface by cycling the potential ten times from 0 to 1 V in 1 M HCl. AFM was carried out using the Veeco Atomic Force Microscope. The sample was scanned with contact mode. In contact mode, as the tip is scanned across the sample surface, it is diverted up or down as it makes contact with the morphological details of the sample surface. In constant force mode, the tip is continuously adjusted to keep a constant deflection that holds the tip of the probe at a constant height above the surface. This height adjustment is shown as data.

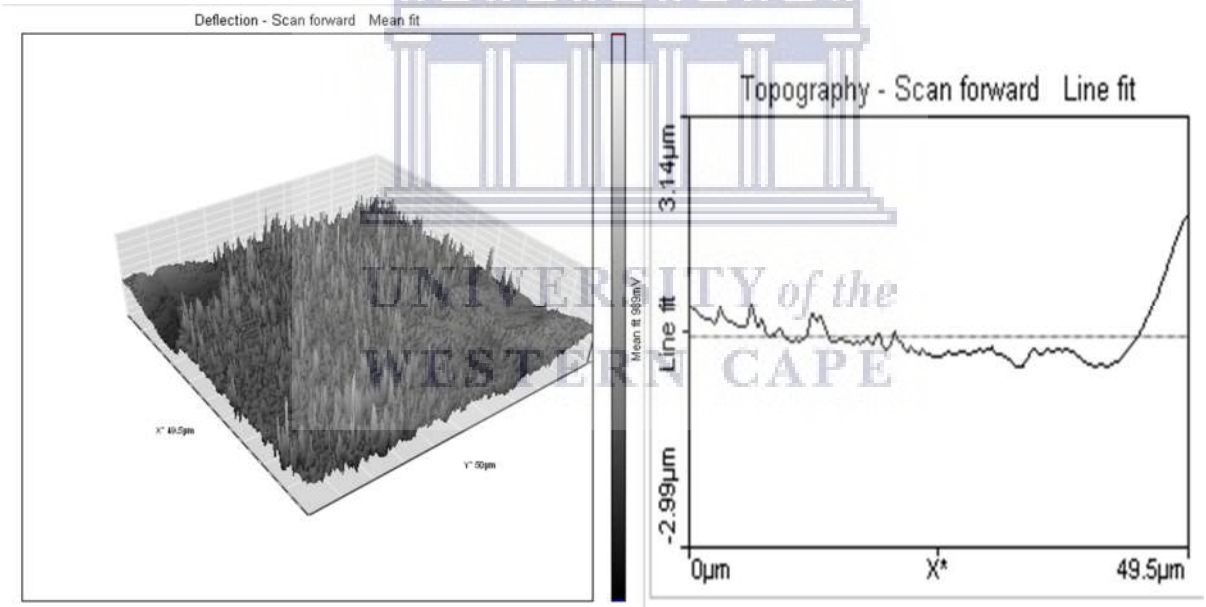

Figure 15: AFM images of the bare gold electrode

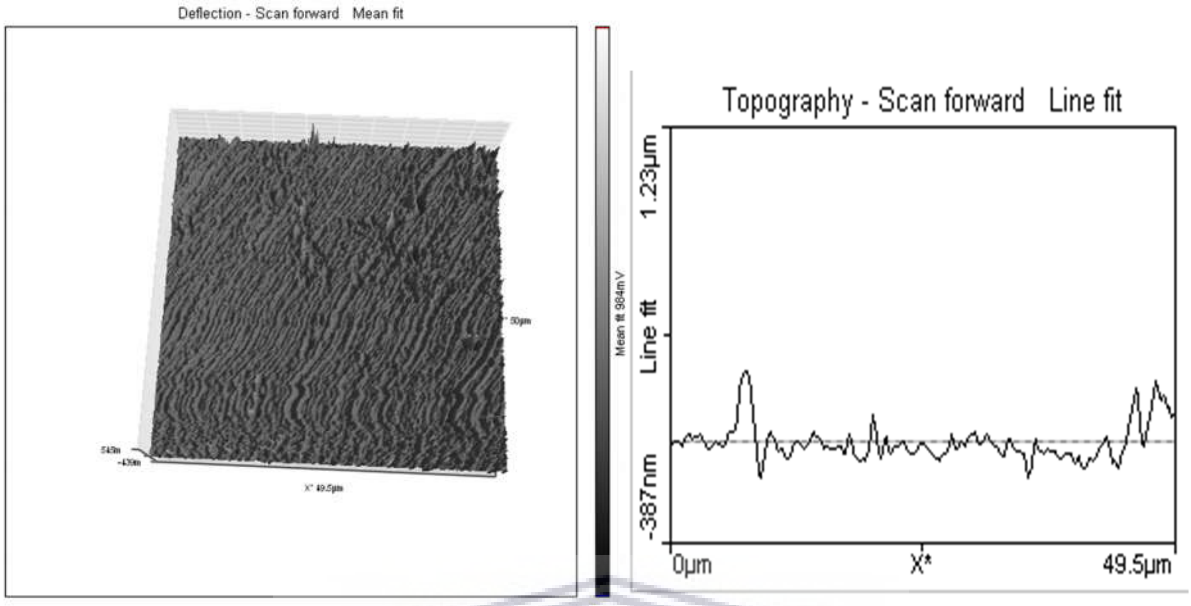

Figure 16: AFM images of PSF-PVA hydrogel

The surface roughness of the bare gold electrode (Figure 15) was measured and found to be higher (53.349 mV) compared to that of PSF-PVA hydrogels (Figure 16), which is 23.666 mV. This lower surface roughness of the hydrogel corroborates the observed surface properties from SEM, and an evident decrease in height can be ascribed to modification with PVA. The hydrophobicity of a material could be linked to surface roughness, the rougher the surface the more it becomes hydrophilic [127]. The observed topographic features agree with SEM images where a dwindled size of the surface morphology was observed after the crosslinking of PSF and PVA, which in turn confirms that the hydrophobic nature of polysulfone was reduced.

Chapter 5

Results and discussion

This chapter presents results generated from SWV carried out on three different heavy metals. Measurements of three replicates were performed for the detection of Cu (II), Cd (II) and Pb (II) respectively with the bare gold electrode (AuE), hydrogel-modified gold electrode (AuE/HGL) and the humic acid-modified gold electrode (AuE/HGL/HA).

5. Part II: Electrochemical studies of heavy metals

5.1. Procedure for complexation of copper with PSF hydrogel and PSF hydrogel-HA

The application of the PSF hydrogel for copper complexation is not captured in literature. This is an expansion to the applications of the recently developed hydrogel. The complexation of metal ions (Cu, Cd and Pb) by PSF hydrogel and PSF hydrogel-humic acid in an aqueous solution was studied by square wave voltammetry (SWV) in a three-electrode electrochemical system. About 1ml of PSF hydrogel was transferred into the cell containing 5ml of 1 M HCl. The PSF hydrogel was electrodeposited on the gold electrode (AuE) interface by cycling the potential from 0 to 1 V ten times. The deposited hydrogel on the AuE interface was allowed to dry for an hour. The electrolyte, 5 ml of 0.5 M phosphate buffer (PBS), was purged with argon. Metals solutions were sequentially added in 2 µl aliquots to the cell. Quantification of metal ions with the hydrogel was studied by SWV using the following parameters: potential window: -0.8 V to 0.6 V, amplitude: 0.2 V, scan rate: 100 mV/s, frequency: 10 Hz, and E-step: 0.01 V. We have selected 100 mV/s as the analytical scan rate because it represents the best match in analytical redox of the metal ions with the electron transfer capabilities of the hydrogel systems. The potential scan was started in the oxidation (anodic) direction after 2 second rest period and it was repeated. For quantification of metal ions with PSF hydrogel-HA, the dry PSF hydrogel thin film on the AuE interface was impregnated with HA by submerging in 2 ml HA solution for 30 minutes. Quantification of metals with PSF hydrogel-HA was then carried out with SWV following the same procedure as described

above. The obtained results showed an increase in peak current as a function of an increase in concentration of the analyte. The detected concentrations varied from 1.78 µM to 54 µM in 0.5 M PBS, pH 7.0. For evaluation of the linearity of the sensor, the calibration curves were plotted to compute correlation coefficient, intercept and slope values. The limits of detection for Cu (II), Cd (II) and Pb (II) were estimated based on equation 12.

$$\text{LOD} = 33 \times \left(S_{Y/a}\right) \quad (12) \ [128]$$

Where S_Y denotes the standard deviation (SD) of responses and "a" for the slope of a linear calibration line. The lowest concentration that can be measured in a sample at an acceptable level of accuracy and precision, that is limit of quantitation, was computed using standard deviation of the response and the slope method expressed as displayed in equation 13 [129].

$$LOQ = 10 \times \left(S_{Y/a}\right) \quad (13)$$

Measurements of three replicates were performed and expressed as RSD % among responses using equation 14.

$$RSD = \left(\frac{SD}{Mean}\right) \times 100\,\% \quad (14) \ [129]$$

The current readings were captured for quantitative analysis.

The surface concentration of PSF hydrogel on the surface of the AuE can be determined by using the Brown Anson approximation, equation 15.

$$Ip, a = \frac{n^2 F^2 A\Gamma}{4RT} V \quad (15)$$

Where:

$I_{p,a}$ is the peak current (A)

n is the number of electrons (1)

F is Faradays constant (96485 C.mol^{-1})

A is the geometric area of the electrode surface (0.07 cm^2)

R is the gas constant in J mol^{-1} K^{-1} (8.314 J.mol^{-1}K^{-1})

T is presented by the absolute temperature (298.15 K)

v is the scan rate in ($V.s^{-1}$)

Γ represents the surface concentration coverage/density ($mol.cm^{-2}$).

Therefore, Γ for PSF hydrogel is calculated to be 8.64×10^{-10} $mol.cm^{-2}$.

Preparation of Au electrode interface

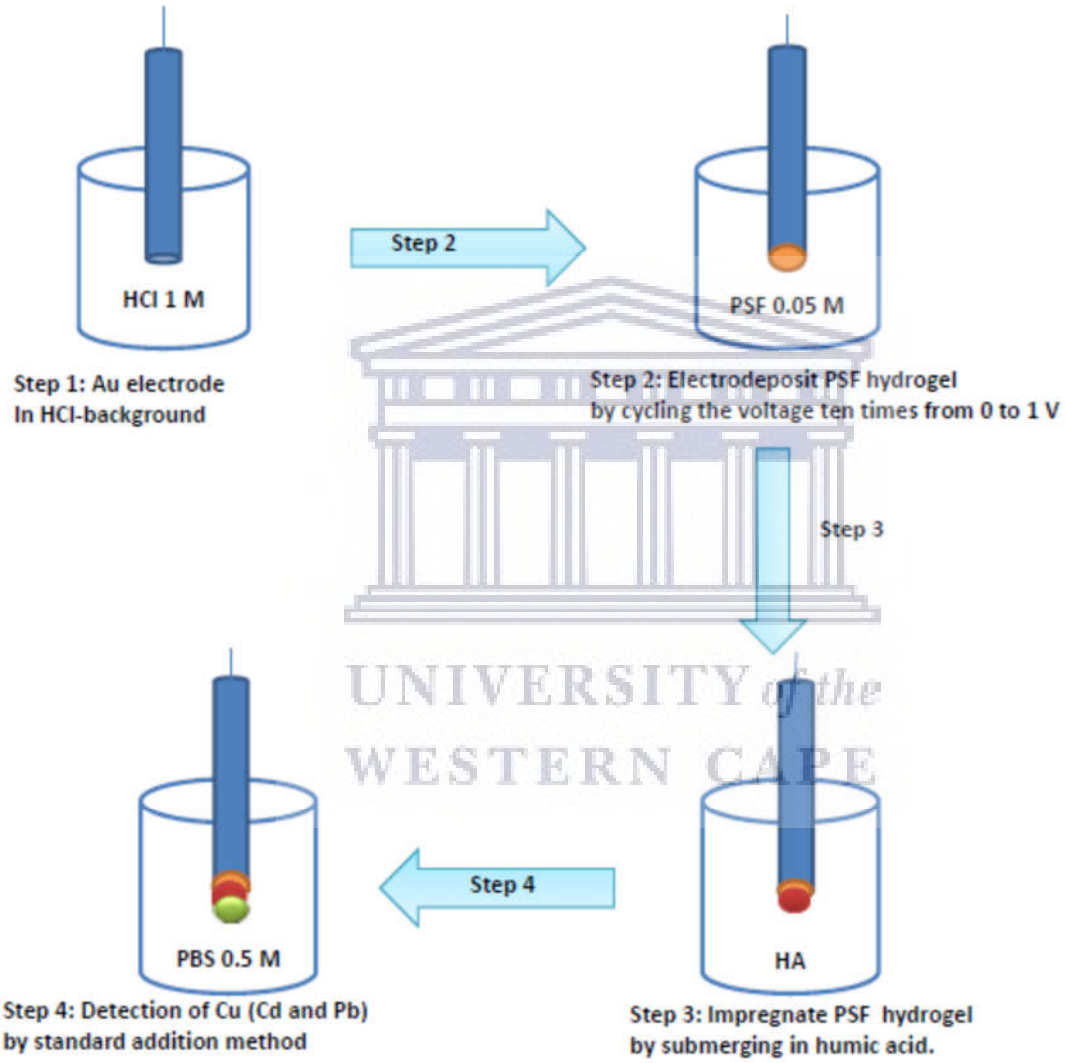

Scheme 3: Steps of electrode preparation

Commercial Au electrodes were modified with PSF hydrogel and HA as indicated (Scheme 3). The metal ions in solution were quantified by standard addition method using cyclic voltammetry and square wave voltammetry.

5.2. Electrochemical study of transducer modification

Square wave voltammetry analysis used to evaluate the redox chemistry of metal ions at the hydrogel and hydrogel/HA electrode interfaces, respectively. The electrochemical window was fixed from -0.8 to 0.6 V and the scan rates were incremented in the range 10-300 mV/s.

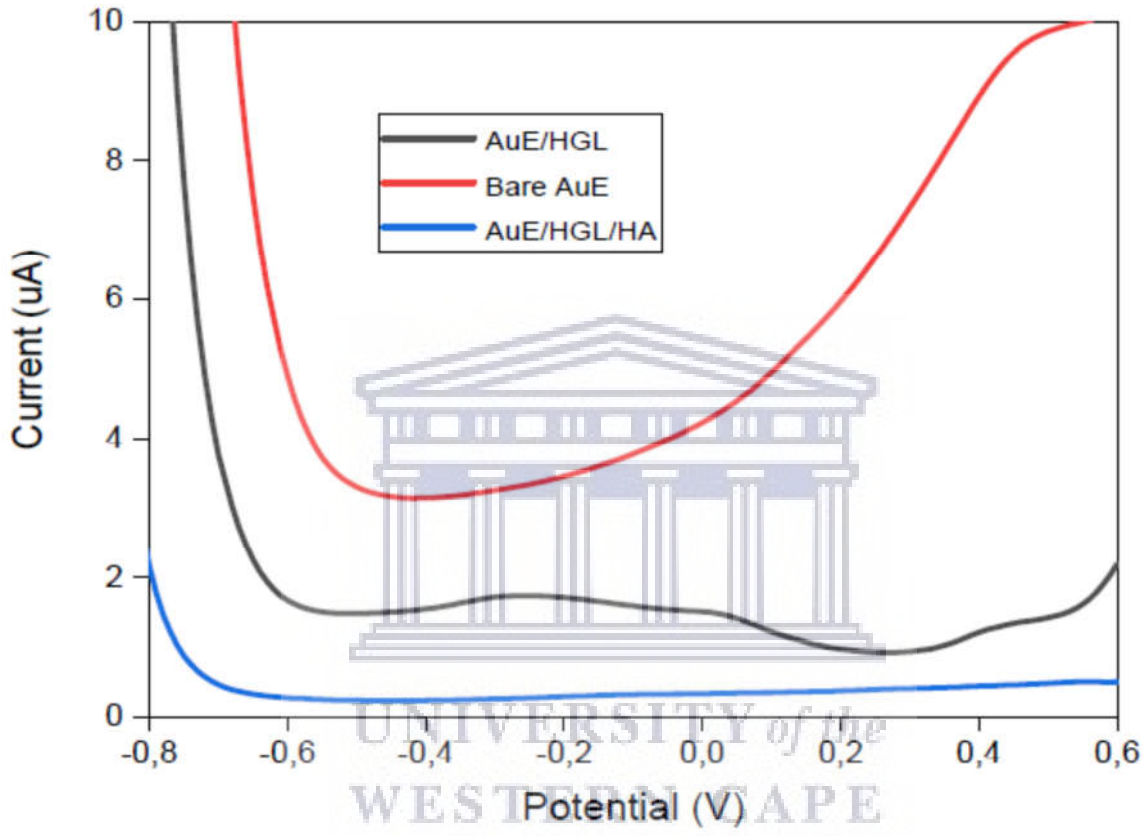

Figure 17: Square wave voltammetry of the bare AuE, PSF hydrogel and HA in phosphate buffer solution at the gold electrode in the potential range from -0.8 V to 0.6 V. Scan rate 100 mV/s

The Au electrode interface was modified with PSF hydrogel as evidenced by the development of peaks at – 0.3 and 0 V and a noticeable decrease in current response (figure 17). Upon further modification with HA, no peak was observed and a further decrease in current was observed. The quantitative analysis of Cu, Cd and Pb ions were evaluated at the hydrogel and hydrogel encapsulated humic acid electrode interfaces. Humic acid is a complexing agent of choice since it, firstly, contains several functional groups that are involved in complexation of metals and, secondly, the waste material of the sensor is environmentally friendly since humic acid is a naturally occurring complexing agent unlike several other ligands.

5.3. Electrochemical studies of copper

5.3.1. Electrochemical study of copper at the bare glassy carbon electrode (GCE)

Quantification of copper at the bare GCE was carried out by standard addition method, where copper amounts were added in 10 µl increments to the cell with 5 ml of 1 M HCl. HCl is a standard electrolyte and most metals are soluble in it. It is a strong electrolyte that reduces and oxidizes metals at the bare electrode. There might have been lack of sensitivity for lower concentrations but the focus here was not the study of the analytical profile of metals but the behaviour, to identify electrochemical peaks at the bare GCE. The potential was applied and resulted in a steady increase in current response.

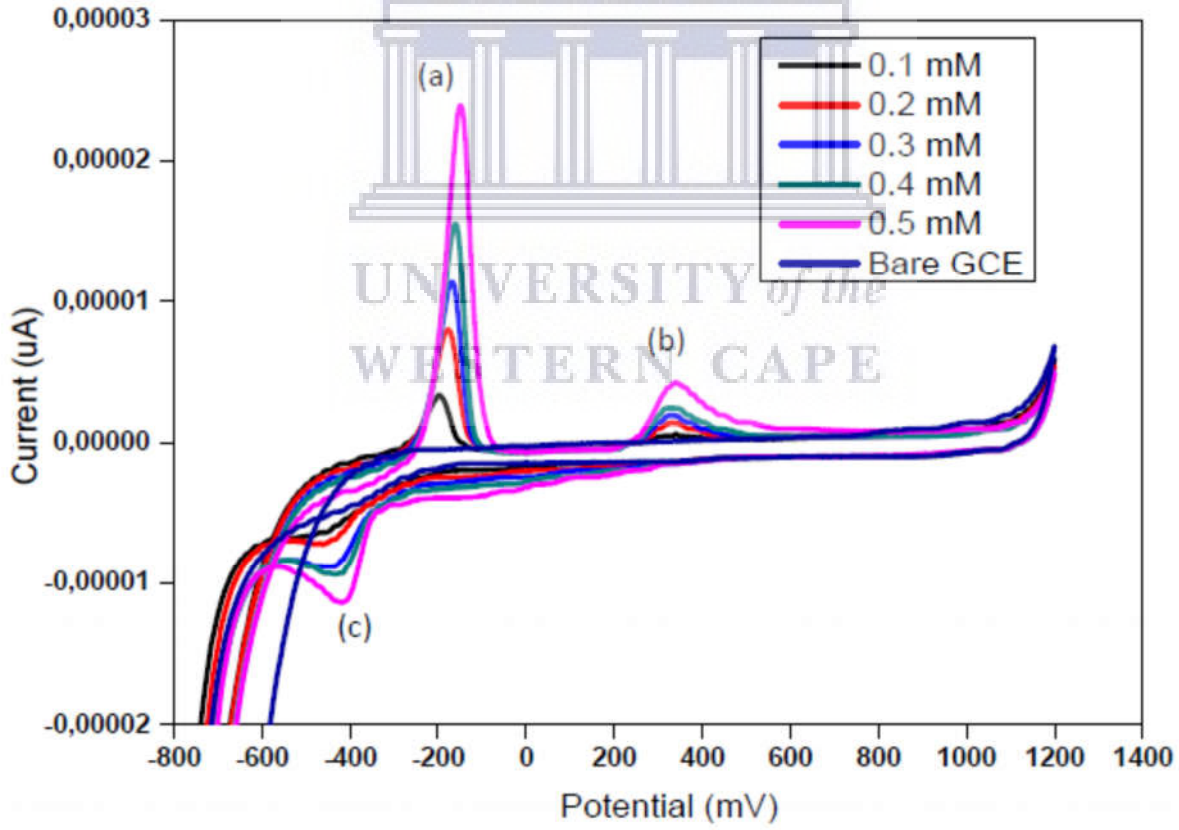

Figure 18: Cyclic voltammetry of copper in HCl solution at the bare GC electrode in the potential range from -800 V to 1200 V. Scan rate 50 mV/s

Cyclic voltammetry of copper at bare GCE offered a clear-cut voltammogram as shown in figure 18 and it displays two oxidation peaks. There was no peak observed prior to the addition of copper solution, but upon the addition of copper peaks were observed. As copper was incremented an increase in peak current response was observed and hence all the peaks are attributed to free copper ions in the solution. The calibration curve for quantification of copper at bare GCE (figure 19) was used to determine corresponding coefficients of peak (a), where limit of detection (LOD) was found to be 2.1375×10^{-4} M, limit of quantification was 6.4786×10^{-4} M, sensitivity of 53.9607 µA/mM was achieved and R-squared value was 0.98846. This data reveals that GCE has good sensitivity towards copper. GCE could not be modified with PSF hydrogel due to its low affinity for the hydrogel, meaning it would easily fall off the GCE interface. Cyclic voltammetry of copper could only be successfully performed at the bare GCE but showed inadequate sensitivity at Au interface.

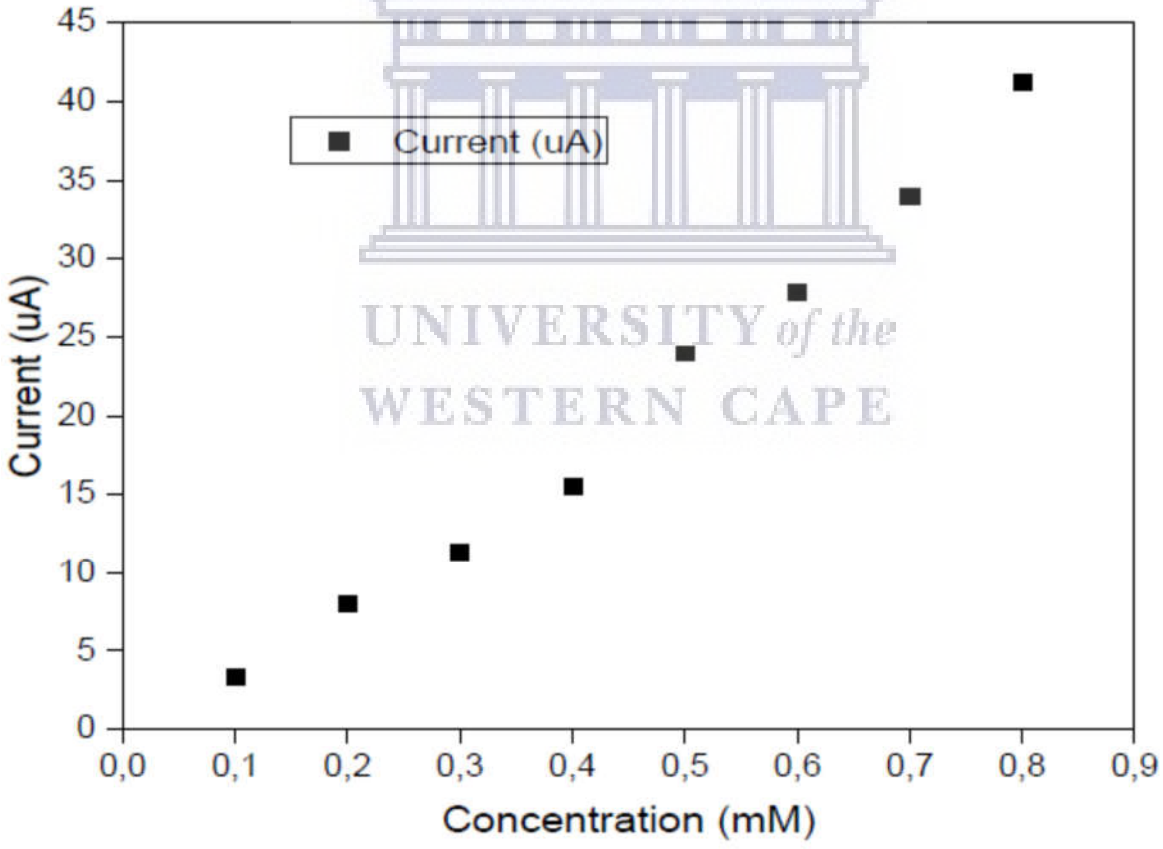

Figure 19: Calibration plot for detection of copper at the bare glassy carbon electrode

5.3.2. Electrochemical study of copper at the bare gold electrode (AuE)

Square wave voltammetry of copper at the bare gold electrode (AuE) gave a well-defined voltammogram as shown in figure 20 and it exhibits three oxidation peaks, whose development confirms that copper (II) is redox-active at our AuE sensor and hence it was inferred that copper could also be redox-active at the modified interface. All the peaks can be ascribed to copper since no peak was observed for the bare AuE prior to the addition of copper solution into the electrolyte. As the concentration of copper increased the peak current responses also increased steadily. It is assumed that the observed increase in current response is due to the detection of free copper ions in the solution.

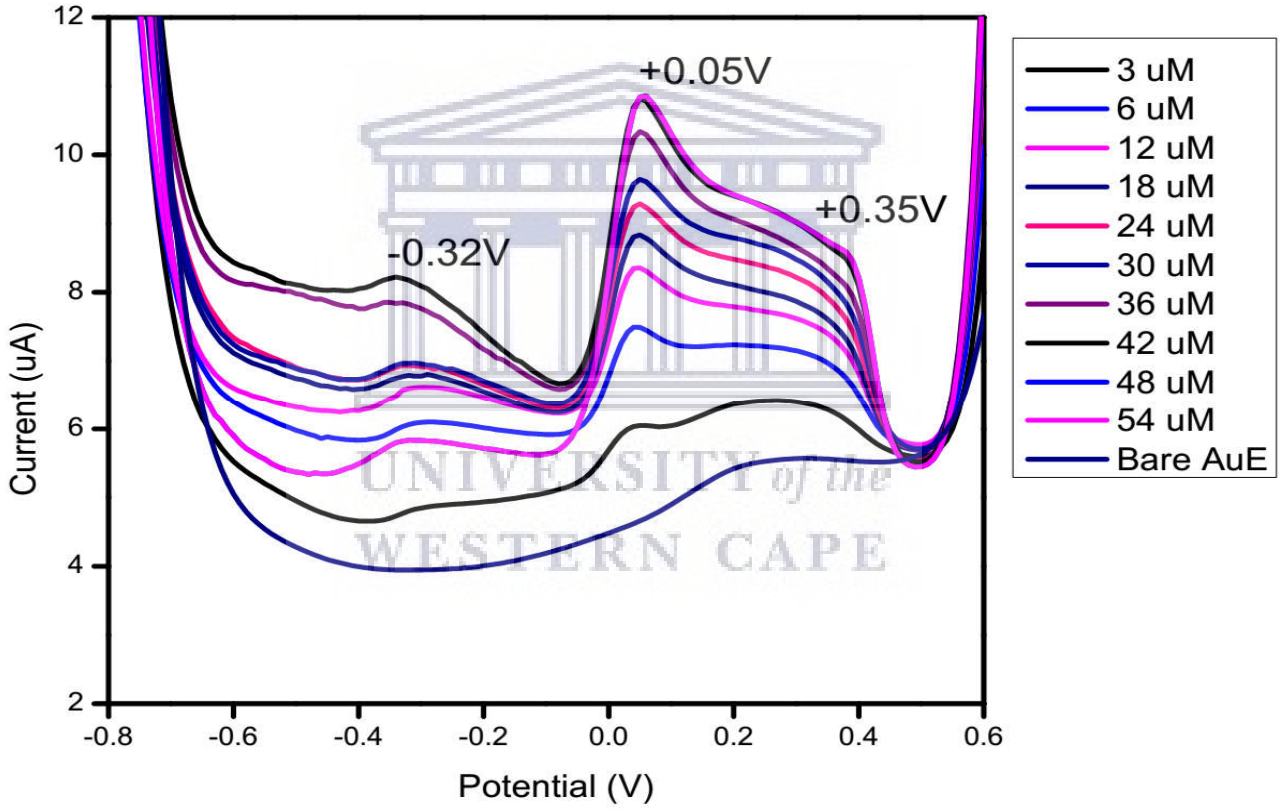

Figure 20: Square wave voltammetry of copper in phosphate buffer solution at the bare gold electrode in the potential range from -0.8 V to 0.2 V. Scan rate 100 mV/s

Figure 21 shows the calibration curves for replicate measurements of Cu(II) at bare Au electrode and since there is always some error associated with the measurement of any signal (due to material differences during preparation as well as human error), this figure shows the differences between measurements. The detections were performed in triplicates and the average current response

measured as a function of concentration for the oxidation of Cu(I) to Cu(II) at bare Au electrode was used for the construction of the calibration curve in figure 22 to determine more parameters. The standard deviations of current response were used to determine error bars. As the concentration increases, error bars increase. The calibration curve for determination of copper at bare gold electrode is displayed in figure 22 and its corresponding coefficients in table 4, where the values of limits of detection and quantitation, sensitivity, RSD, and also the coefficient of determination (R^2) are presented. The attained variation is evidently nonlinear with high error bars, which may be due to slight variation in electrode characteristics such as electron exchange ability, electronic structure and density of states which are significant reaction kinetics. When comparing the three measurements at the bare electrode (table 4) their slopes (sensitivities) were different given high RSD.

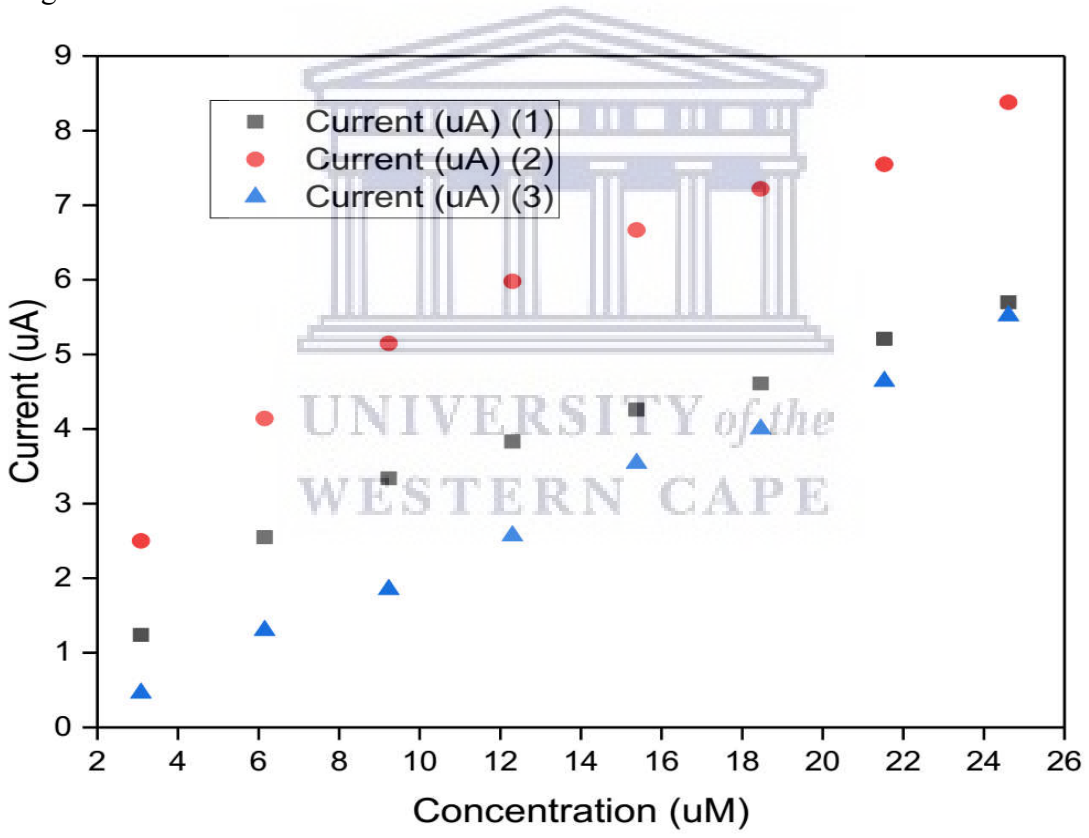

Figure 21: Calibration plot for the triplicate detections of copper at the bare gold electrode

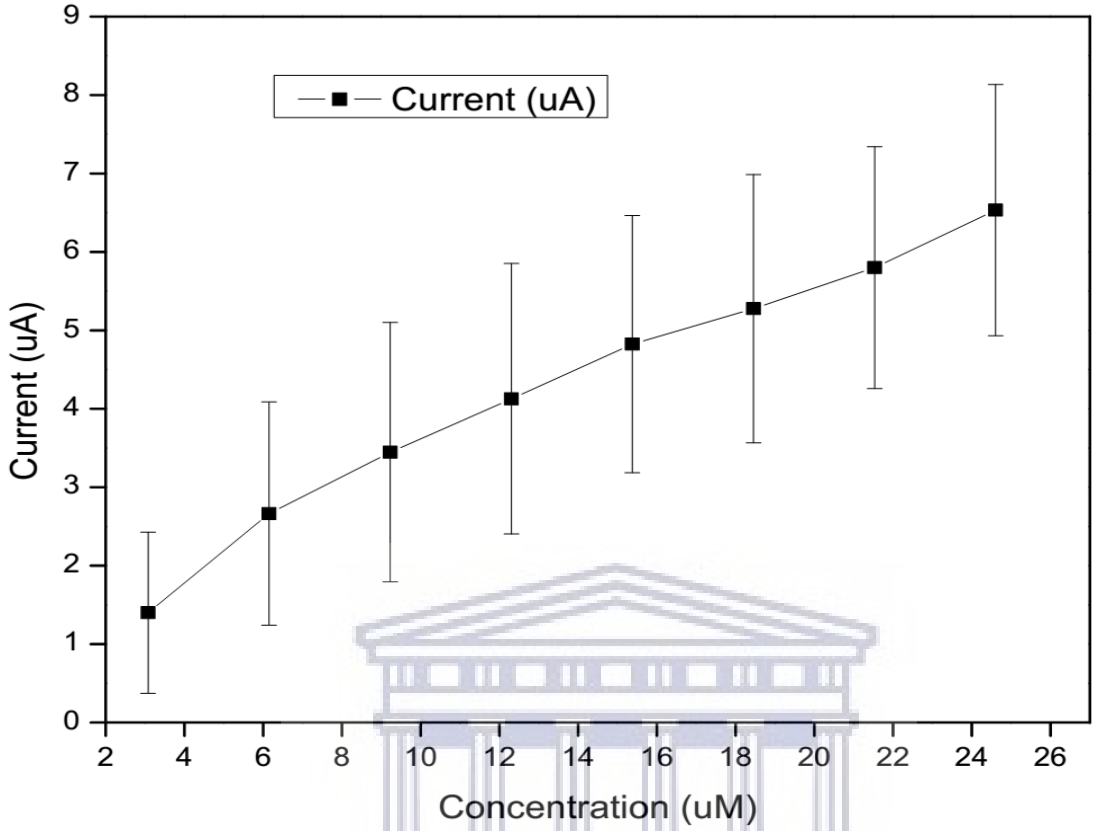

Figure 22: Calibration plot for the detection of copper at the bare gold electrode. The error bars represent the standard deviation of measurements from 3 times repetitions

Table 4: Data for copper detection with the bare gold electrode

Electrode Number	Sensitivity (µA/µM)	LOD (µM)	LOQ (µM)	R-square	RSD% (Sensitivity)
Bare AuE 1	0.2379	10.6954	32.4103	0.92391	19.51%
Bare AuE 2	0.3310	7.8196	23.6958	0.95820	
Bare AuE 3	0.2415	3.8992	11.8158	0.98935	

5.3.3. Electrochemical study of copper at the PSF hydrogel-modified gold electrode (AuE)

Square wave voltammetry has been used to investigate metal-complexing capability of the synthesized and electrodeposited hydrogels. As shown in figure 23, the peak current increased with metal concentration and three peaks were observed. Square wave voltammetry (SWV) reveals

a distinctive peak at + 0.05 V, associated with oxidization of Cu/Cu^{2+} on a HGL-modified AuE [130]. A minor peak was observed around -0.4 V in figure 21, due to the partial reduction of entrapped Cu^{2+} to Cu^{+} [131], [132]. The hydrogel used to modify the surface of the gold electrode has been found to have a considerable influence on the peaks. The peaks observed at +0.05 V and +0.35 V became broader than at the ones observed at bare electrode, which could be linked with copper complexation by the hydrogel on the surface of the electrode.

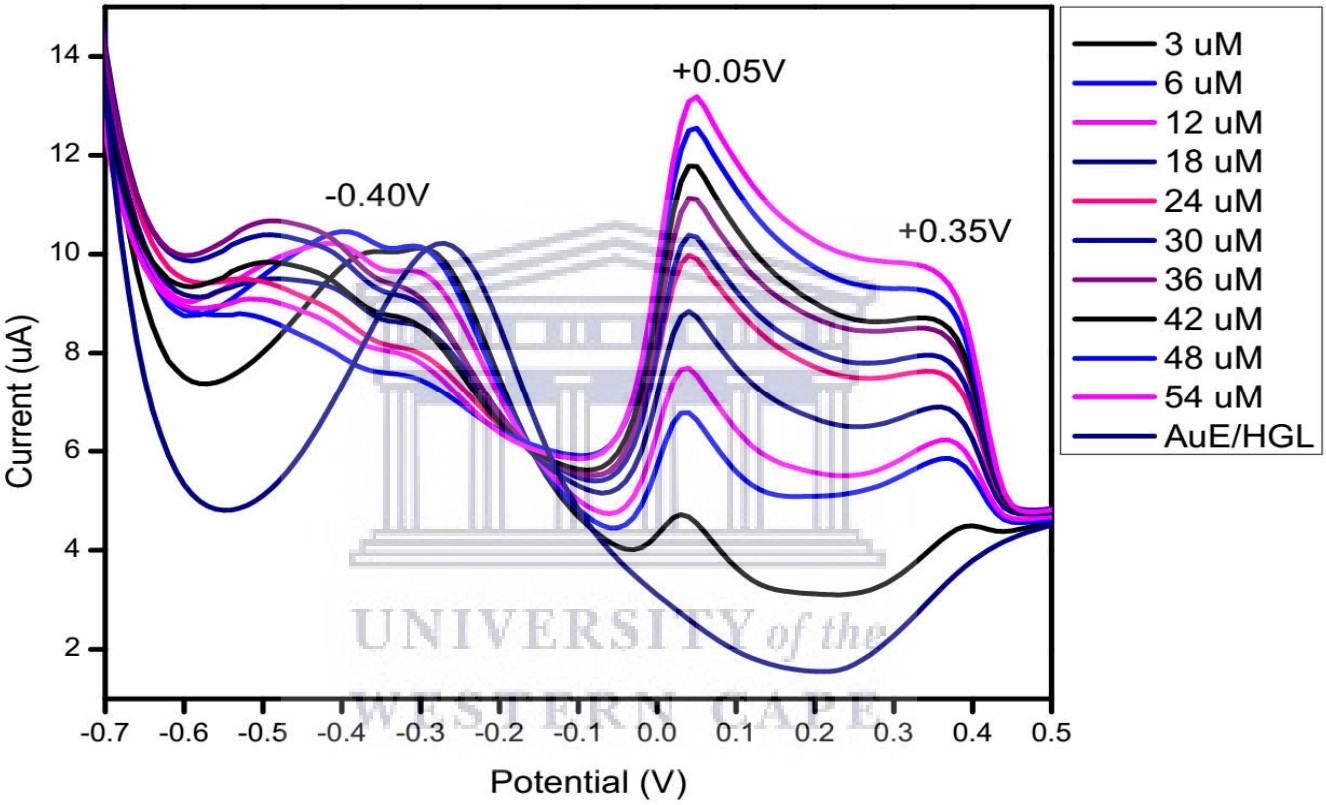

Figure 23: Square wave voltammetry of copper in phosphate buffer solution at the PSF hydrogel modified gold electrode in the potential range from -0.8 V to 0.2 V. Scan rate 100 mV/s

Figure 24 shows the calibration curves for replicate measurements of Cu(II) at the Au/HGL electrode and since there is always some error associated with the measurement of any signal (due to material differences during preparation as well as human error), this figure shows the differences between measurements. The detections were performed in triplicates and the average current response measured as a function of concentration for the oxidation of Cu(I) to Cu(II) at the Au/HGL electrode was used for the construction of the calibration curve in figure 25 for

determination of more parameters. The standard deviations of current response were used to determine error bars. As the concentration increases, error bars increase. The observed slope change in figure 25 was attributed to near-saturation of the polysulfone hydrogel with Cu. Supposing that there is a direct correlation between the linear section and the binding capacity of the hydrogel for Cu, this binding ability is of the order of ~ 16 µM Cu for 8.64 $\times 10^{-10}$ mol.cm^{-2} PSF hydrogel. The related coefficients are shown in table 5, where the values of sensitivity, the coefficient of measurement and limits of detection and quantitation are shown. The limit of detection was calculated as the values in table 5 according to equation 12 for AuE/HGL sensor.

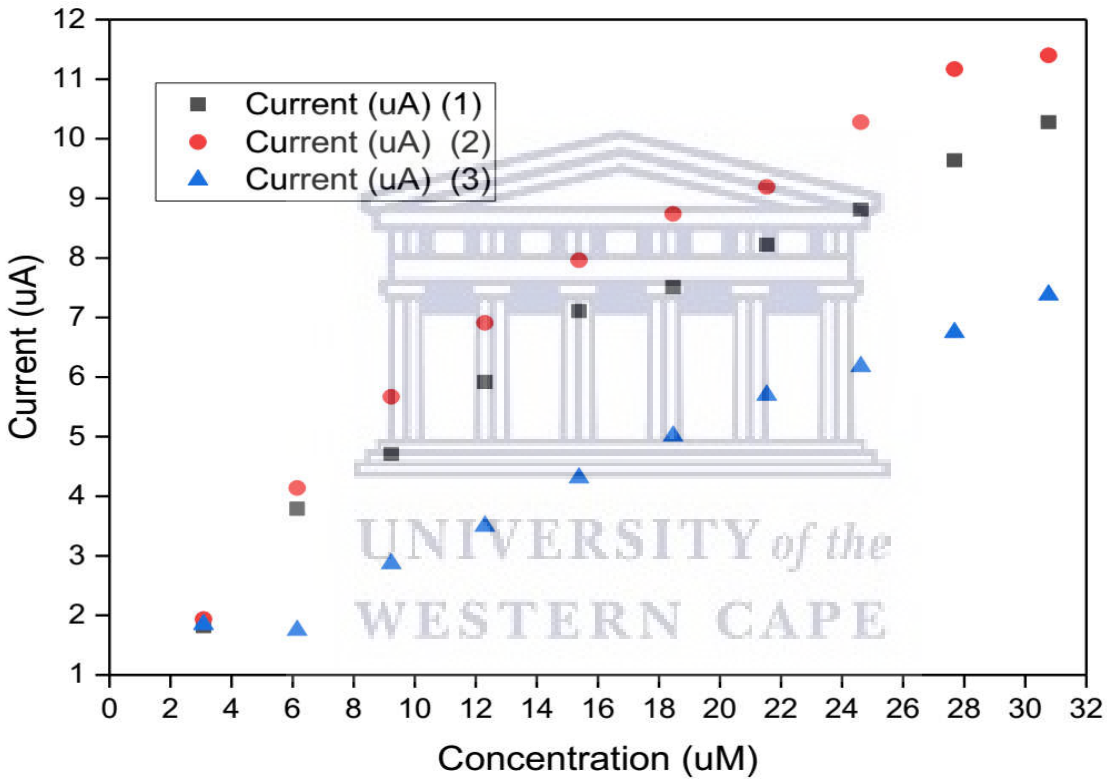

Figure 24: Calibration plot for the triplicate detections of copper at the PSF hydrogel-modified gold electrode

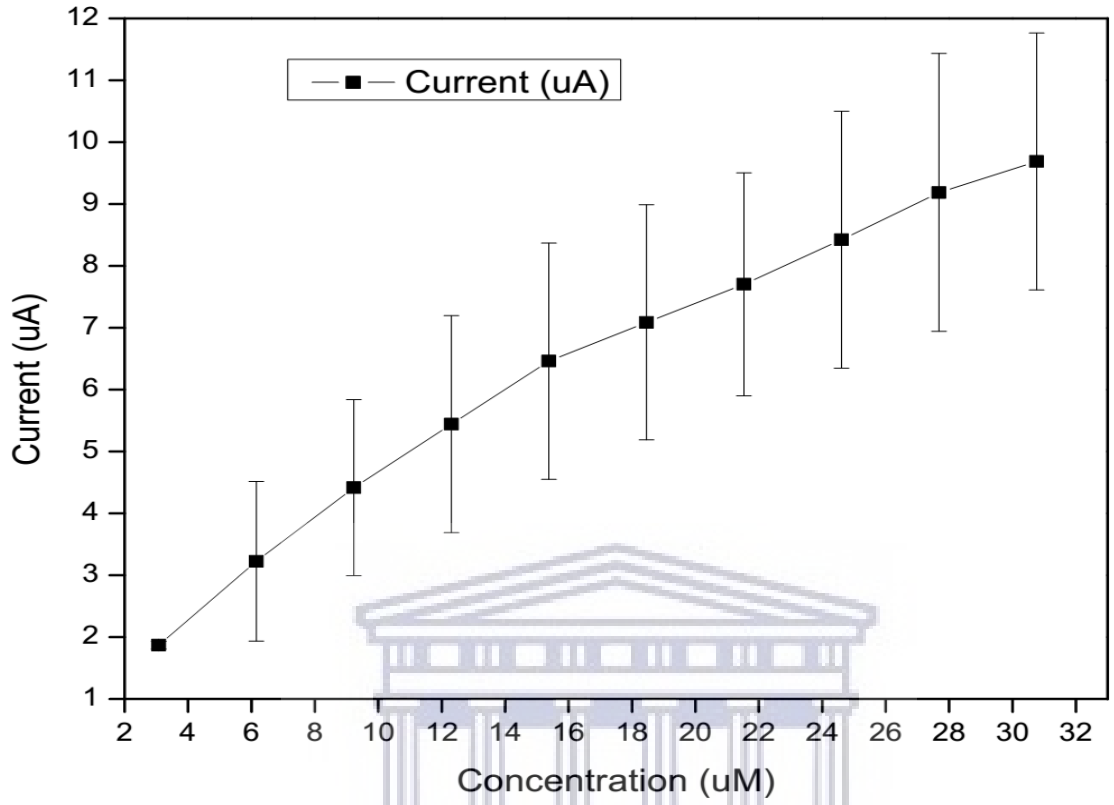

Figure 25: Calibration plot for the detection of copper at the PSF hydrogel modified gold electrode. The error bars represent the standard deviation of measurements from 3 times repetitions

Table 5: Data for copper detection with PSF hydrogel-modified gold electrode

Electrode Number	Sensitivity (µA/µM)	LOD (µM)	LOQ (µM)	R-square	RSD% (Sensitivity)
AuE/HGL 1	0.4130	5.5185	16.7228	0.97887	36.19%
AuE/HGL 2	0.4815	6.5839	19.9512	0.97009	
AuE/HGL 3	0.2217	7.8982	23.9338	0.97959	

5.3.4. Electrochemical study of copper at the PSF hydrogel/humic acid-modified gold electrode (AuE)

The electrodeposited hydrogel was functionalized with humic acid and square wave voltammetry was used to study the metal complexation ability of the hydrogel-humic acid sensor. The forward

potential scan produced three oxidation peaks, as shown in figure 26, which could all be associated with copper since the hydrogel-humic acid background exhibited no peak. The effect of humic acid was attested by the uniform spacing between peaks given the overlapping peaks observed at the bare electrode and at the hydrogel-modified electrode, especially the peaks at – 0.25 V and + 0.35 V. Other studies [133] have already shown that the adsorption of copper ions rises with the amount of suspended humic substances and declines with low pH levels or a rise in dissolved organic substances. Since the electrolyte pH of ~7 was kept constant prior to and after the entrapment of humic acid in the hydrogel, it is therefore evident that the observed decrease in current response is due to the fact that the adsorption of Cu (II) ions increased when humic acid was incorporated in the hydrogel matrix which reduced the number of free Cu (II) ions in the solution and hence low current response. Humic materials constitute a diverse range of functional groups, including hydroxyl (OH), carboxyl (COOH), and carbonyl (C=O) and these are some of the active sites through which metal ions are bonded to form complexes after loss of protons from this ligand [134]. The swelling of the hydrogels increases with pH [135], but the rationale for constant neutral pH is that copper adsorption tends to decline at high pH levels owing to the development of hydroxides of metals or dissolvable organic metal complexes [136].

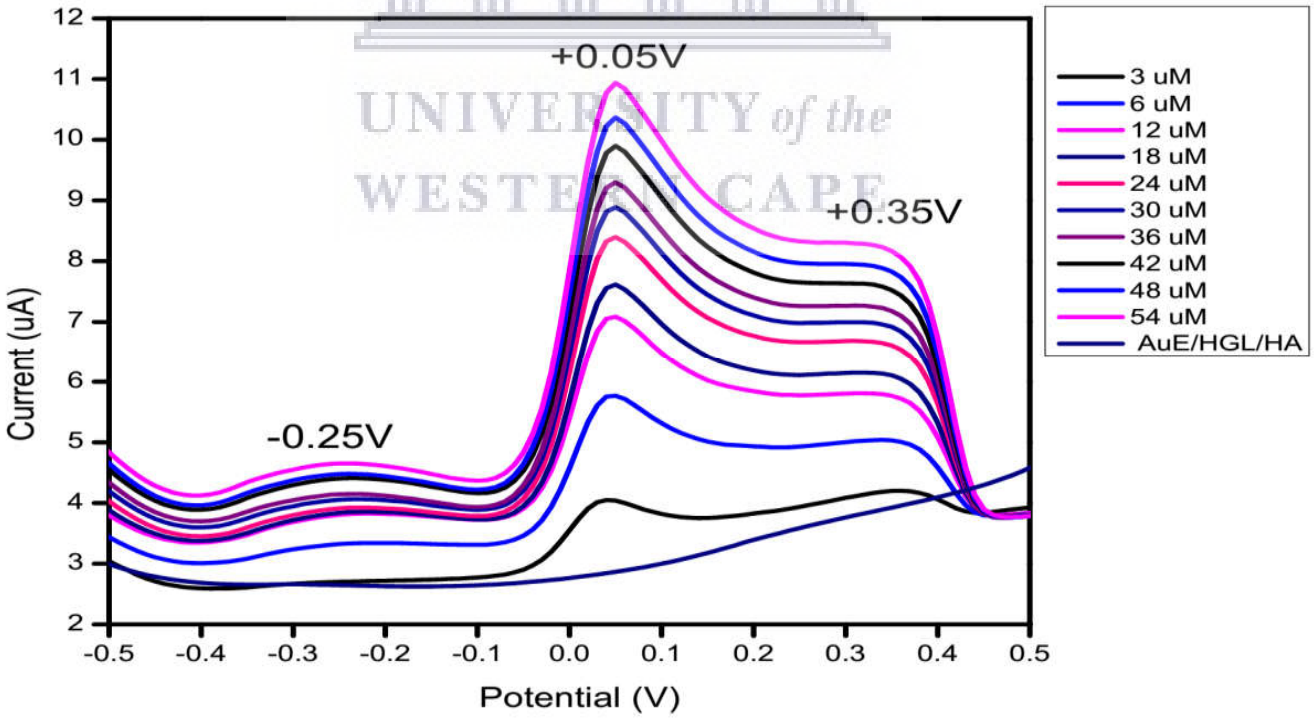

Figure 26: Square wave voltammetry of copper in phosphate buffer solution at the PSF hydrogel/ humic acid-modified gold electrode in the potential range from -0.8 V to 0.2 V. Scan rate 100 mV/s

Figure 27 shows the calibration curves for replicate measurements of Cu(II) at the Au/HGL/HA electrode and since there is always some error associated with the measurement of any signal (due to material differences during preparation as well as human error), this figure shows the differences between measurements. The detections were performed in triplicates and the average current response measured as a function of concentration for the oxidation of Cu(I) to Cu(II) at the Au/HGL/HA electrode was used for the construction of the calibration curve in figure 28 for determination of more parameters. The standard deviations of current response were used to determine error bars. As the concentration increases, error bars increase. The observed change in slope in figure 28 was accredited to near-saturation of the HA with Cu. Presuming that the linear section is directly proportional to the binding ability of the HA for Cu, this binding ability is of the order of ~ 18 µM Cu for 0.25 ml of HA. Table 6 presents the corresponding coefficients, including the coefficient of determination (R^2), sensitivity, limit of detection and limit of quantitation. HA has a great metal complexing ability as it has carboxylic groups and phenolic-OH as predominant sites for metal complexation. The ability of HA to form stable chelate complexes varies with metals [137]. The results of IR spectrophotometer of humic acid exhibit that a broad peak was observed at 1640–1588 cm^{-1}, linked to the carbonyl of the carboxylic acid group, and a great peak at 3416.6 cm^{-1}, linked with phenols, alcohols and carboxylates [138]. It is generally approved that metals can also be held firmly through binding specifically with N and S groups on humic acid which favourably bind metals like copper among others [139].

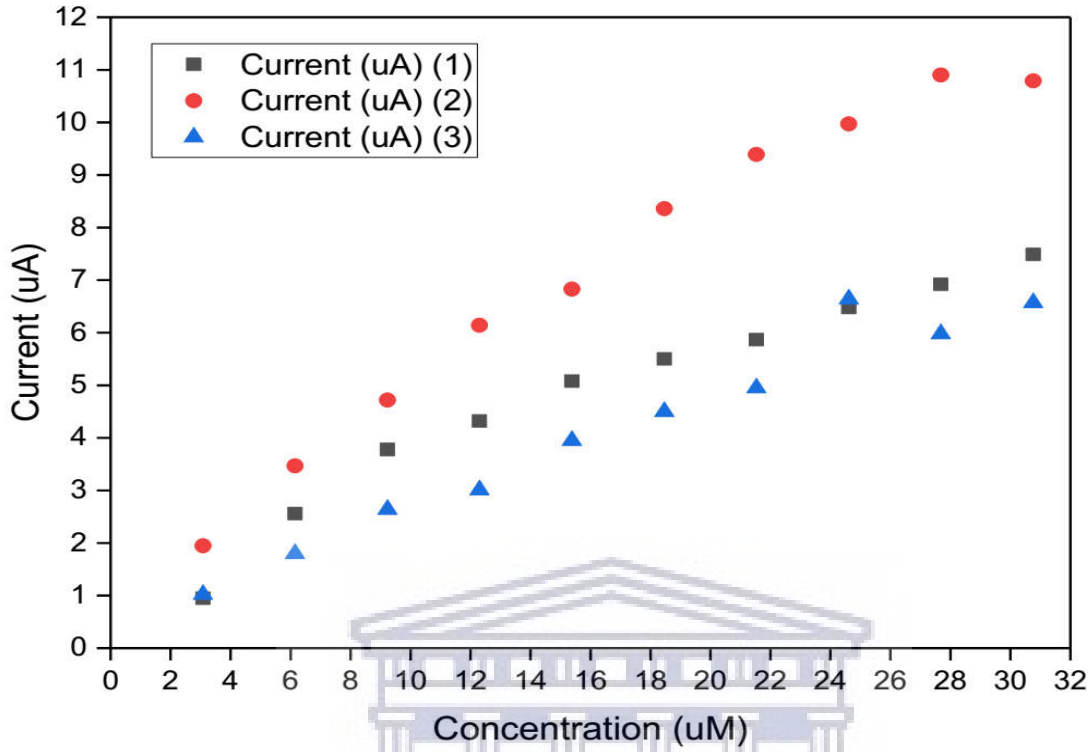

Figure 27: Calibration plot for the triplicate detections of copper at the PSF hydrogel/humic acid -modified gold electrode

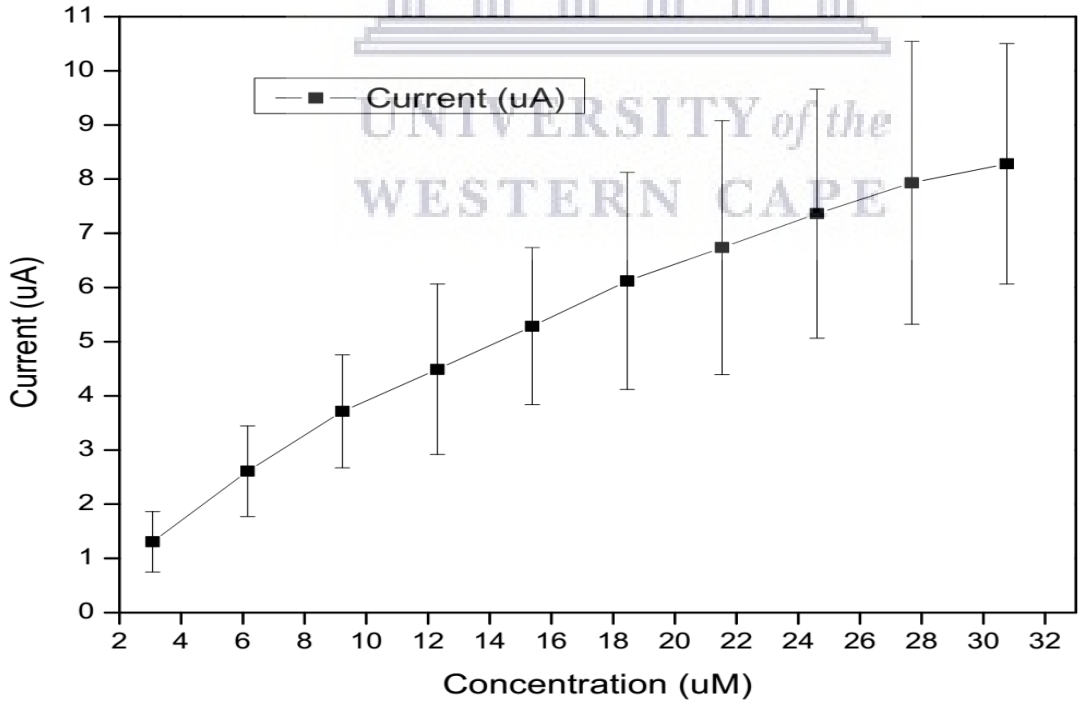

Figure 28: Calibration plot for the detection of copper at the PSF hydrogel/ humic acid-modified gold electrode. The error bars represent the standard deviation of measurements from 3 times repetitions

Table 6: Data for copper detection with PSF hydrogel/humic acid-modified gold electrode

Electrode Number	Sensitivity (µA/µM)	LOD (µM)	LOQ (µM)	R-square	RSD% (Sensitivity)
AuE/HGL/HA 1	0.3250	9.3452	28.3189	0.94134	28.24%
AuE/HGL/HA 2	0.4041	5.0111	15.1854	0.98251	
AuE/HGL/HA 3	0.2249	4.3651	13.2276	0.98993	

5.3.5. Conclusions on the electrochemical study of copper

Simple square wave voltammetric sensors based on gold electrode/polysulfone hydrogel (AuE/HGL) and gold electrode/polysulfone hydrogel/humic acid (AuE/HGL/HA) have been developed for complexation of copper (II) ions. Comparison of sensitivity values for the modified and unmodified electrodes shows that modification of AuE with HGL improved the sensitivity of the electrode and further modification with humic acid further enhanced the sensitivity according to the limits of detection. The redox chemistry of copper exhibited the same number analytical peaks at both modified and unmodified interfaces. Humic acid is understood to have the effect of a surface-active agent which could be greater than the propensity for the adsorption of Cu-HA; this is the most likely reason behind the absence of an observable rise in linear range in spite of greater concentrations whereas the sensitivity rose [140]. The measurements were performed in triplicates and the slope and standard deviation of the calibration curves have been used for the determination of limit of detection (LOD) of the sensors. The AuE/HGL sensor in our study achieved the average limit of detection of 6.6669 µM, which makes it less sensitive than the electrochemical Cu (II) sensor constructed by Oztekin et al [141]; where the limit of detection (LOD) was calculated as 5.0 x 10^{-12} M for a gold electrode modified with 4-formylphenylboronic acid, and Lu et al [142] used nafion modified electrode to determine Cu (II), which achieved an LOD of 0.021 µM. The lower sensitivity of our AuE/HGL sensor could be ascribed to lesser adsorption groups on our hydrogel. In our work, the average LOD values were found to be 7.4714 µM for the bare AuE sensor, 6.6669 µM for the AuE/HGL sensor and 6.2405 µM for the AuE/HGL/HA sensor. The humic acid sensor shows the lowest LOD, which implies that it can detect copper ions at lower concentrations than the other two sensors. The rationale for a very small difference between the LOD values of the hydrogel sensor and the humic acid sensor

is the small amount of the entrapped humic acid in the hydrogel matrix, meaning adsorption increases with dissolved humic substances. The humic acid sensor (AuE/HGL/HA) in our study was found to be less sensitive than the sensor developed by Marta Radaelli et al. [143]; which yielded the (LOD) of 0.52 nM for Cu ions by DPASV. The sensor constructed by Eub-Duck Jeon et al. [144] also exhibited higher sensitivity and the determined LOD was 8.0 X 10^{-8} M. The explanation for the lower sensitivity of our humic acid sensor could be that the amount of the ligand that interacted with copper ions was limited owing to the small surface concentration of the hydrogel which could not entrap a large amount of humic acid. Another reason might be that some of the active sites on the entrapped humic acid could not be reached by metal ions due to the conformation of the ligand. Our hydrogel-humic acid sensor achieved an LOD lower than the WHO's guideline value of 2 mg/L and this is advantageous since it would allow for detection of even lower concentrations. Given the LOD value and linear range fall within the range of copper concentrations in water, which is from 0.0005 to 1 mg/L, the sensor is more suitable for water quality monitoring. Our sensor has been constructed in such a way that it would be environmentally friendly since the modification layer, the hydrogel, was synthesized by incorporating PVA, which is biodegradable under both aerobic and anaerobic conditions, and PSF which is a green material due to its biodegradability. Humic acid is an environmentally friendly adsorbent and enhances soil fertility and removes polluting agents. Therefore, the modification layer does not increase but decreases toxicity in the environment due to its dominant organic content. The reduction potential for free Cu(II) ions is 0.34 V [145], whereas in complexed form, Cu(II)-HGL, it reduced to 0.057 V. After modification of the hydrogel thin film with humic acid, the reduction potential of the complexed state, Cu-HGL-HA, decreased more to -0.123 V. The observed decreasing pattern of the reduction potential after complexation is ascribed to higher complexing agent (HGL and HA) stabilization of Cu(II) than Cu and consequently it decreases the reduction potential of Cu(II)-Cu redox couple. Tabbì et al [146] obtained a shifted formal potential of -0.118 V for Cu(II) complex with ligands having oxygen and nitrogen as donor atoms, which coordinate Cu(II) in a square planar arrangement.

5.4. Electrochemical study of cadmium

Square wave voltammetry of cadmium was performed successfully at Au interface but cyclic voltammetry showed inadequate sensitivity at Au interface.

5.4.1. Electrochemical study of cadmium at the bare gold electrode (AuE)

The electrochemical study of cadmium at the bare gold electrode resulted in the development of one oxidation peak as exhibited in figure 29. No peak was observed in the absence of metal ions but the effect of the increasing concentration of cadmium ions led to the observed increase of peak height and hence it is assumed that it was the detection of free cadmium ions that lead the observed increased in current response.

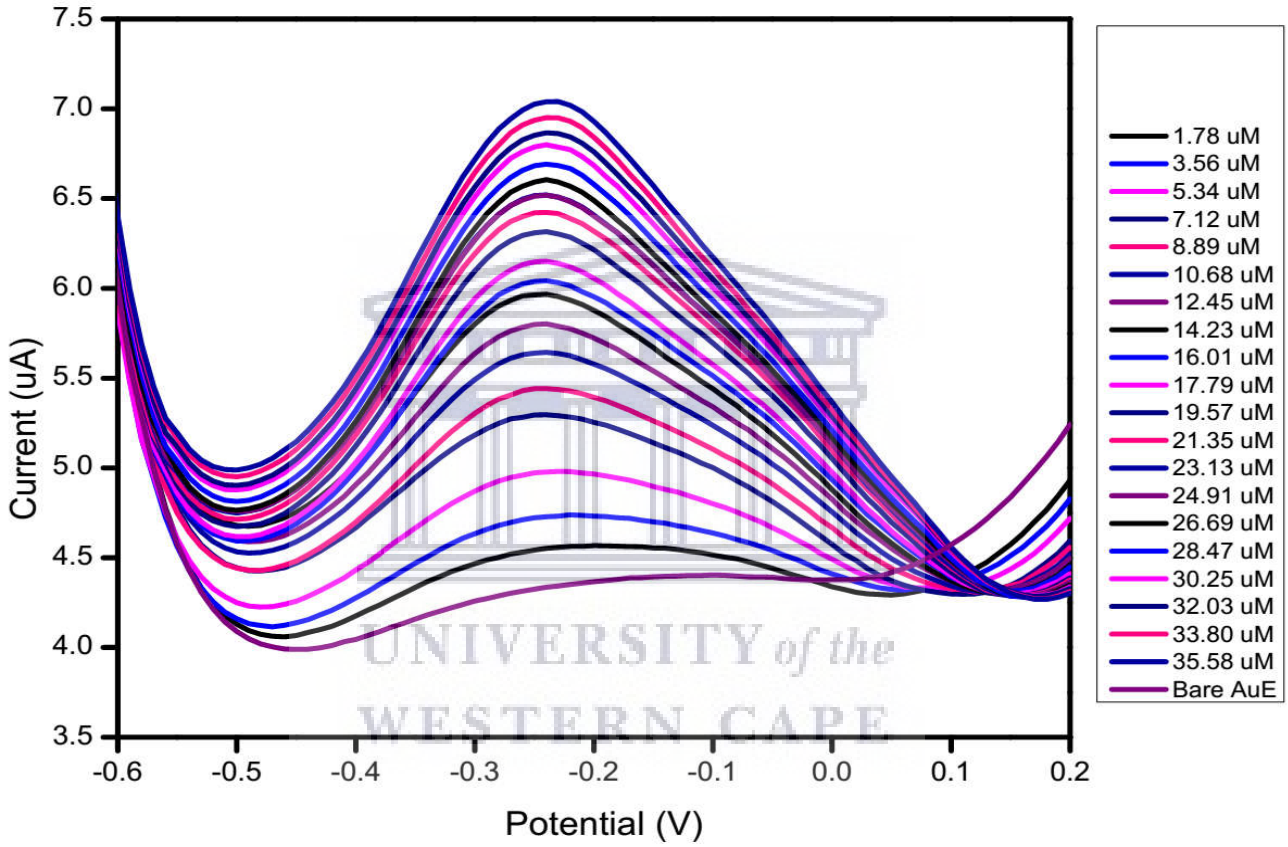

Figure 29: Square wave voltammetry of cadmium in phosphate buffer solution at the bare gold electrode in the potential range from -0.8 V to 0.2 V. Scan rate 100 mV/s

Figure 30 shows the calibration curves for replicate measurements of Cd(II) at bare Au electrode and since there is always some error associated with the measurement of any signal (due to material differences during preparation as well as human error), this figure shows the differences between measurements. The detections were performed in triplicates and the average current response measured as a function of concentration for the oxidation of Cd to Cd(II) at bare Au electrode was used for the construction of the calibration curve in figure 31 for determination of more parameters.

The standard deviations of current response were used to determine error bars. As the concentration increases, error bars increase. The values of sensitivity, limits of detection (LOD) and quantitation (LOQ), RSD and the coefficient of determination (R^2) are presented in table 7. When comparing the three detections at the bare electrode (table 7), the achieved sensitivities are almost the same as attested by their RSD, which is also the case with the achieved values of LOD. The values of R^2 obtained display the very good reliability of the method.

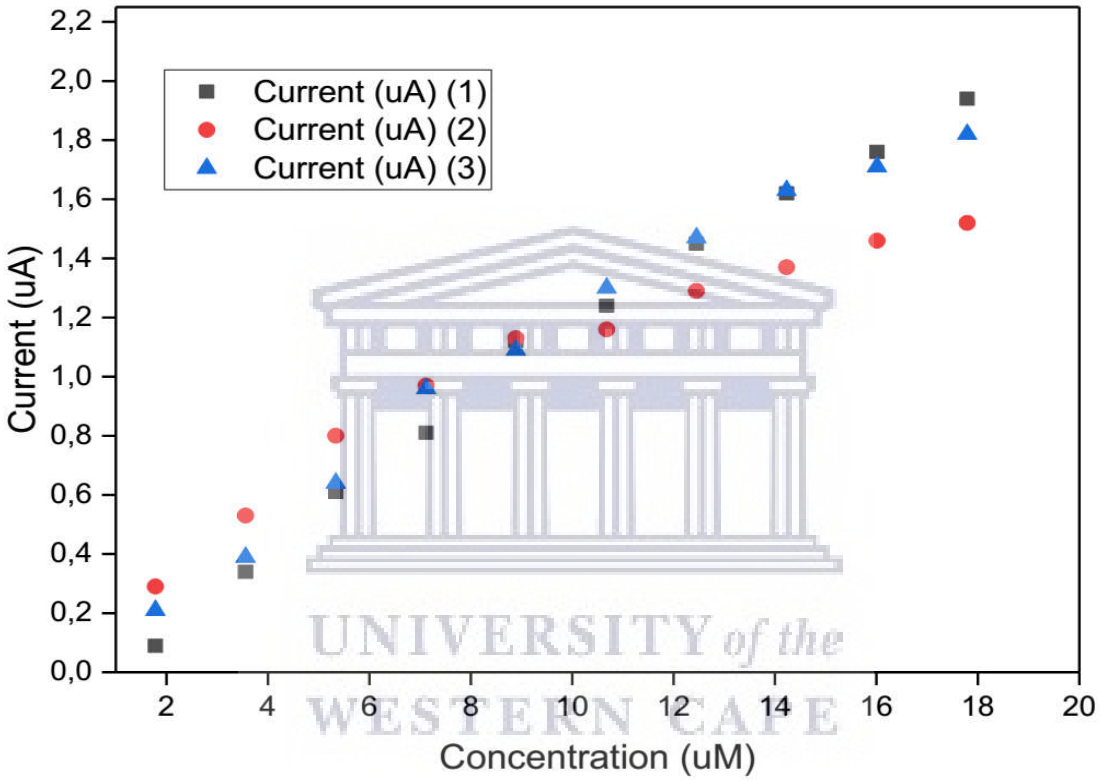

Figure 30: Calibration plot for the triplicate detections of cadmium at the bare gold electrode

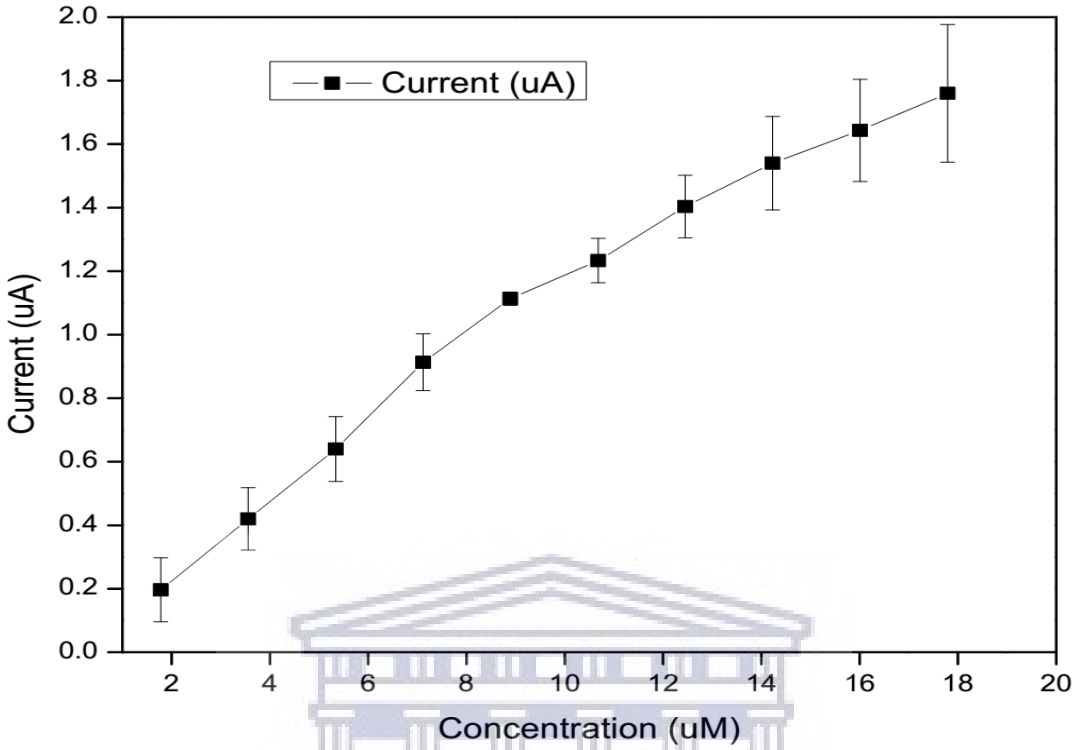

Figure 31: Calibration plot for the detection of cadmium at the bare gold electrode. The error bars represent the standard deviation of measurements from 3 times repetitions

Table 7: Data for cadmium detection with the bare gold electrode

Electrode number	Sensitivity (µA/µM)	LOD (µM)	LOQ (µM)	R-square	RSD% (Sensitivity)
Bare AuE 1	0.1283	2.7831	8.4336	0.99045	3.83%
Bare AuE 2	0.1193	2.8031	8.4942	0.98632	
Bare AuE 3	0.1264	2.8722	8.7037	0.98699	

5.4.2. Electrochemical study of cadmium at the PSF hydrogel-modified gold electrode (AuE)

The gold electrode was modified with the hydrogel to produce a sensor for detection of cadmium ions. The forward (oxidation) potential scan produced two peaks as shown in figure 32. The shifting of the broader peak to a less negative potential value, i.e. -0.3 V, could be attributed to the formation of a complex between the hydrogel and cadmium ions. The development of the second

anodic peak could also be linked to the interaction between the hydrogel and cadmium ions given the absence of the second peak when cadmium was detected with the bare electrode.

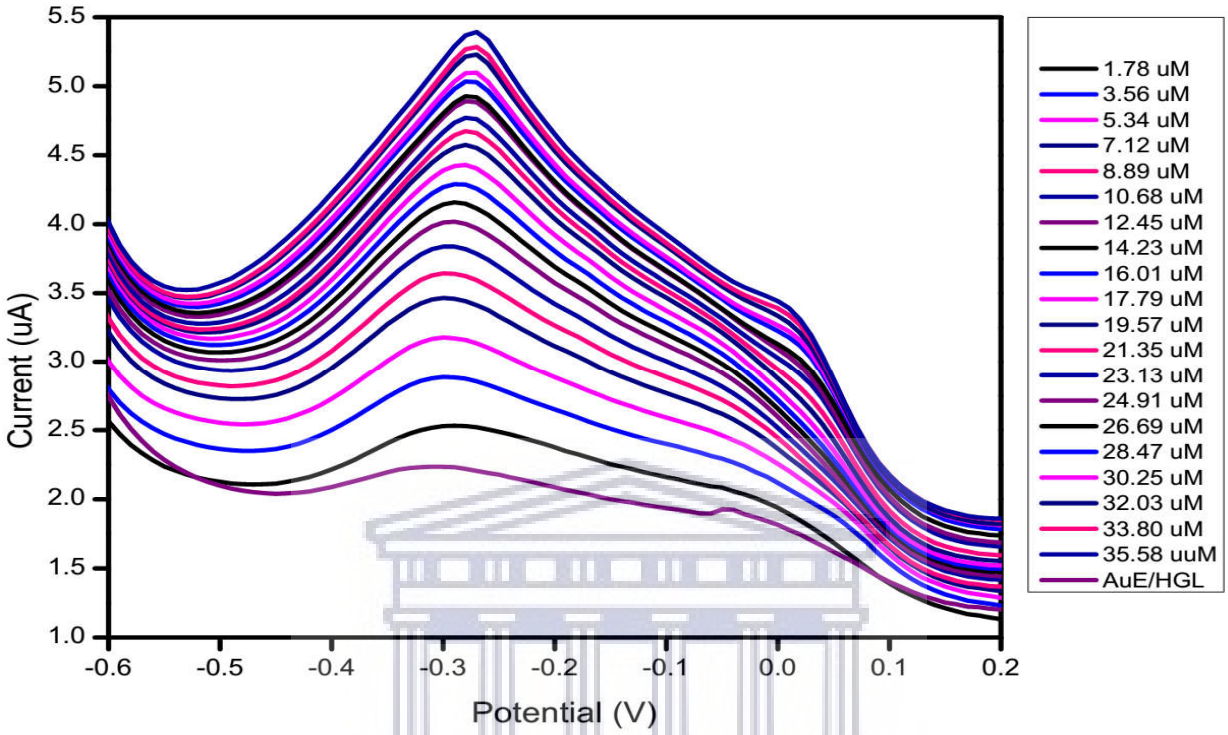

Figure 32: Square wave voltammetry of cadmium in phosphate buffer solution at the PSF hydrogel -modified gold electrode in the potential range from -0.8 V to 0.2 V. Scan rate 100 mV/s

Figure 33 shows the calibration curves for replicate measurements of Cd(II) at the Au/HGL electrode and since there is always some error associated with the measurement of any signal (due to material differences during preparation as well as human error), this figure shows the differences between measurements. The detections were performed in triplicates and the average current response measured as a function of concentration for the oxidation of Cd to Cd(II) at the Au/HGL electrode was used for the construction of the calibration curve in figure 34 for determination of more parameters. The standard deviations of current response were used to determine error bars. As the concentration increases, error bars increase. The big error bars may be as a result of slightly different hydrogel surface concentration which presented different amounts of binding sites on the modified interface. Table 8 presents values of sensitivity, limits of detection (LOD) and quantitation (LOQ), RSD and the coefficient of determination (R^2). The observed slope change was attributed to near-saturation of the PSF hydrogel with Cd. Supposing that there is a direct

correlation between the linear section and the binding capacity of PSF hydrogel for Cd, this binding ability is of the order of ~ 12.5 µM Cd for ~ 8.64 ×10 $^{-10}$ mol.cm^{-2} PSF hydrogel. The obtained values of R^2 show good reliability of the method. When comparing the three measurements at the hydrogel-modified electrode, only two values of achieved sensitivity are comparable and hence their high RSD.

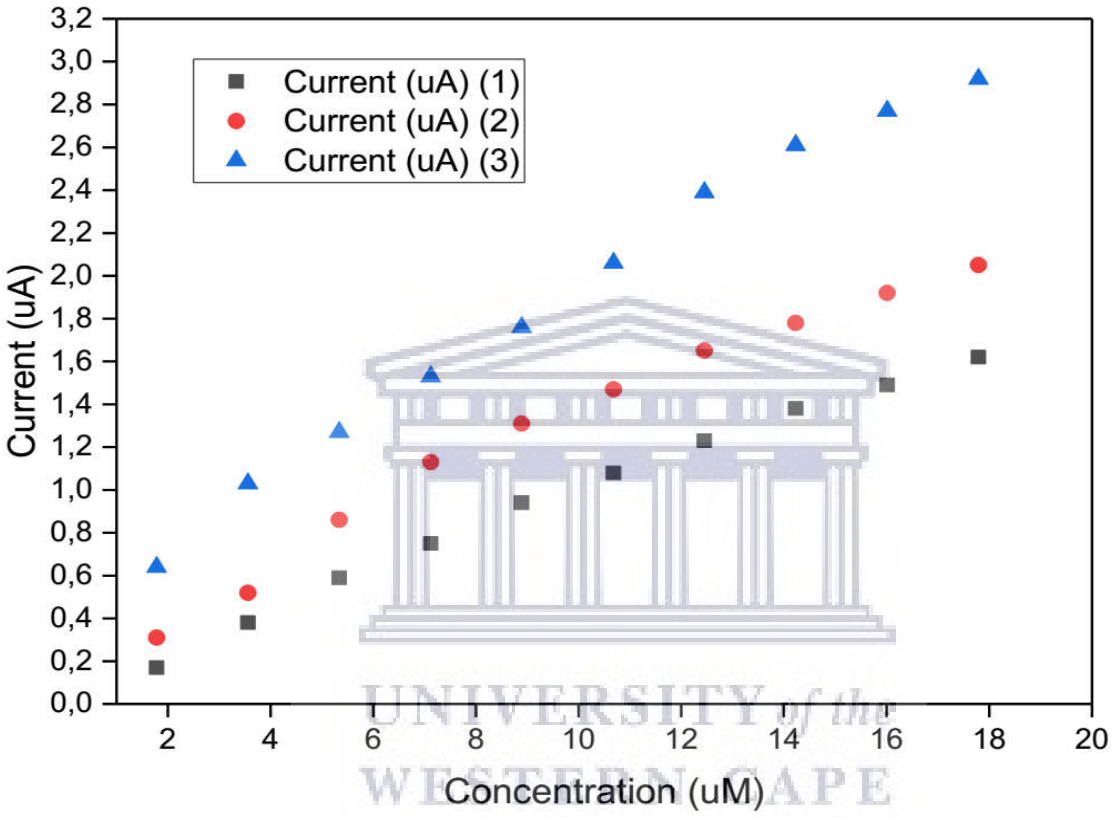

Figure 33: Calibration plot for the triplicate detections of cadmium at the PSF hydrogel-modified gold electrode

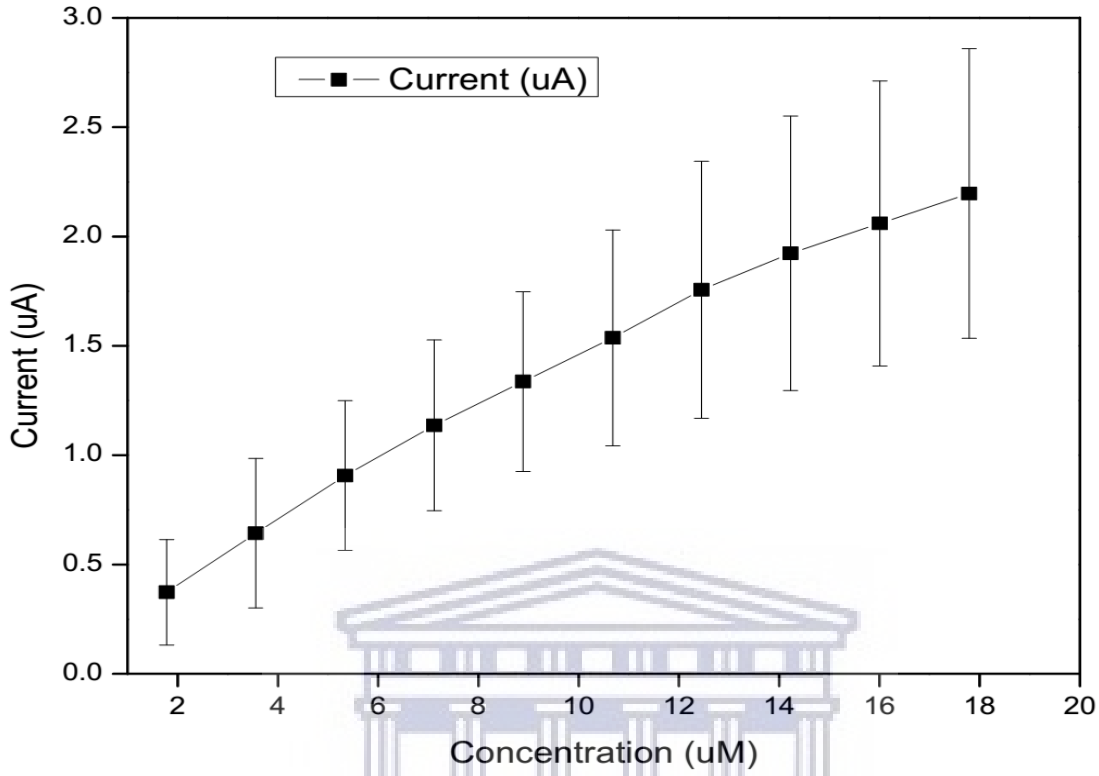

Figure 34: Calibration plot for the detection of cadmium at the PSF hydrogel modified gold electrode. The error bars represent the standard deviation of measurements from 3 times repetitions

Table 8: Data for cadmium detection with PSF hydrogel-modified gold electrode

Electrode number	Sensitivity (µA/µM)	LOD (µM)	LOQ (µM)	R-square	RSD% (Sensitivity)
AuE/HGL 1	0.0990	2.2454	6.8041	0.99376	27.35%
AuE/HGL 2	0.1016	4.6338	14.0142	0.98454	
AuE/HGL 3	0.1566	2.1149	6.4087	0.99447	

5.4.3. Electrochemical study of cadmium at the PSF hydrogel/humic acid-modified gold electrode (AuE)

The hydrogel thin film was functionalized with humic acid to produce a sensor for detection of cadmium. As shown in figure 35, the forward scan led to the development of two oxidation peaks. The wide peak separation at -0.3 V could be the effect of humic acid since peak separation around

that potential was smaller when detection was performed with the bare electrode and with the hydrogel-modified electrode. The second oxidation peak around 0 V decreased considerably and this could be due to complex formation between humic acid and cadmium ions. Once humic acid was incorporated into the hydrogel a decrease in current response was observed and this could be attributed to an increase in binding capacity as a result of modification with humic acid. The explanation for lower current response could be that humic acid, through its functional groups, complexed most of the free copper (II) ions in the solution. Cadmium preferably interacts with the ionizable carboxyl groups that are available for complexation [147]. It is understood that complexation capacity increases with pH and the amount of both metals and dissolved organic substances, the explanation being that as pH increases more functional groups are ionized and become available for complexation and an increase in the amount of organic substances increases the number of functional groups which could be ionized to interact with metal ions. Therefore, this increase in adsorption capacity can only be ascribed to the presence of humic acid since the pH of ~7 was kept constant throughout the measurements.

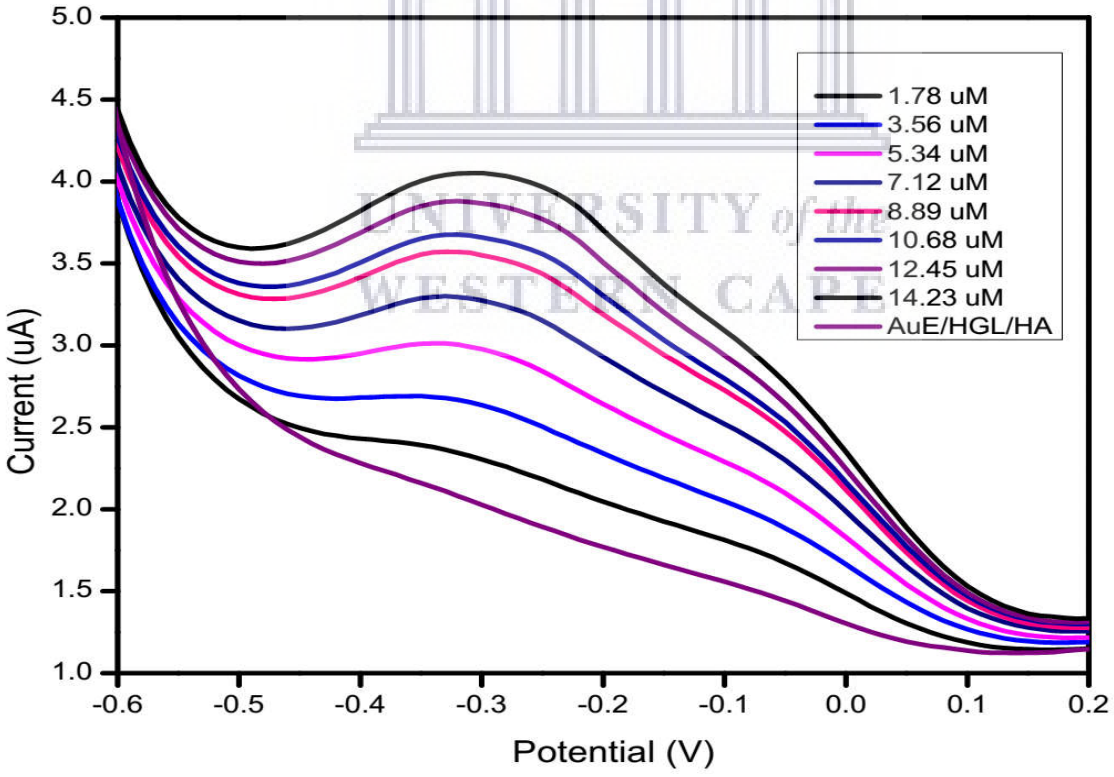

Figure 35: Square wave voltammetry of cadmium in phosphate buffer solution at the PSF hydrogel/ humic acid modified gold electrode in the potential range from -0.8 V to 0.2 V. Scan rate 100 mV/s

Figure 36 shows the calibration curves for replicate measurements of Cd(II) at the Au/HGL/HA electrode and since there is always some error associated with the measurement of any signal (due to material differences during preparation as well as human error), this figure shows the differences between measurements. The detections were performed in triplicates and the average current response measured as a function of concentration for the oxidation of Cd to Cd(II) at the Au/HGL/HA electrode was used for the construction of the calibration curve in figure 37 for determination of more parameters. The standard deviations of current response were used to determine error bars. As the concentration increases, error bars increase. The error bars are high, which is indicative of nonlinear variation and could be attributed to leaching of the hydrogel into the electrolyte, leading to various amounts of the adsorbent on the interface of the three modified electrodes. The observed change in slope in figure 37 was accredited to near-saturation of the HA with Cd. Presuming that the linear section is directly proportional to the binding ability of the HA for Cd, this binding ability is of the order of ~ 12.5 μM Cd for 0.25 ml of HA. The corresponding coefficients are presented in table 9, in which the values of limits of detection (LOD) and quantitation (LOQ), the coefficient of determination (R^2), sensitivity, RSD and are displayed. Comparing the three detections in table 9, the three sensitivity values are different and high and that could be associated with formation of complexes between humic acid and cadmium ions. The R^2 values obtained show good reliability of this method.

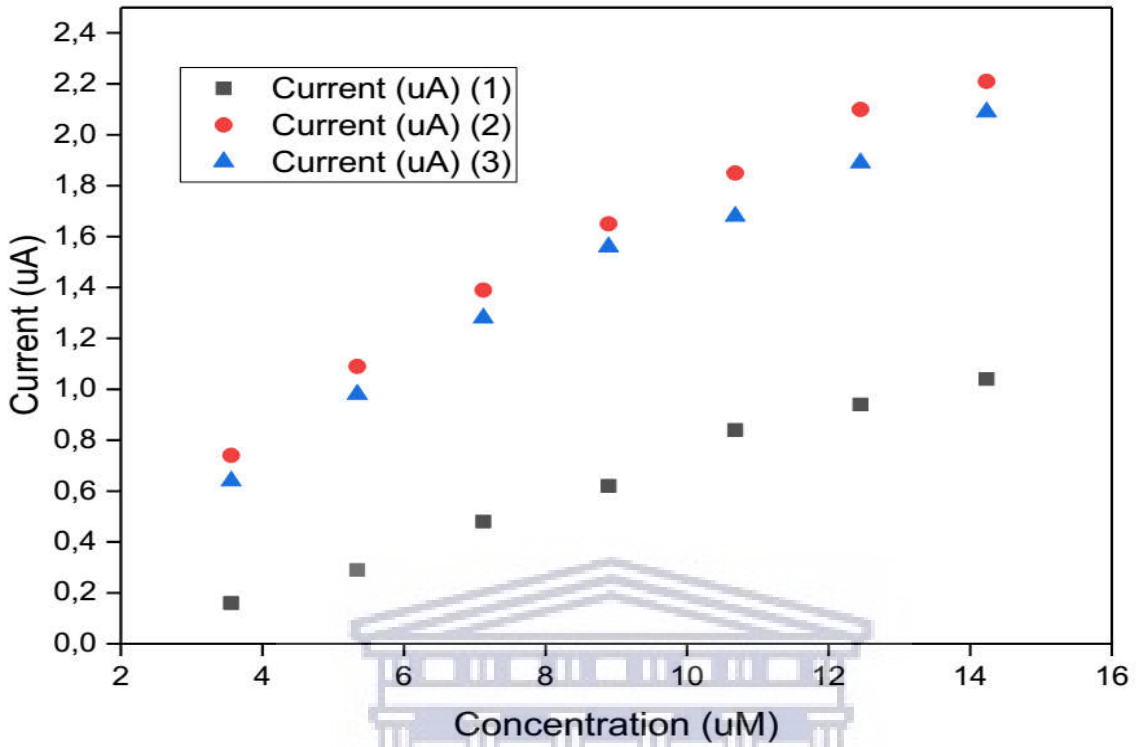

Figure 36: Calibration plot for the triplicate detections of cadmium at the PSF hydrogel/humic acid-modified gold electrode

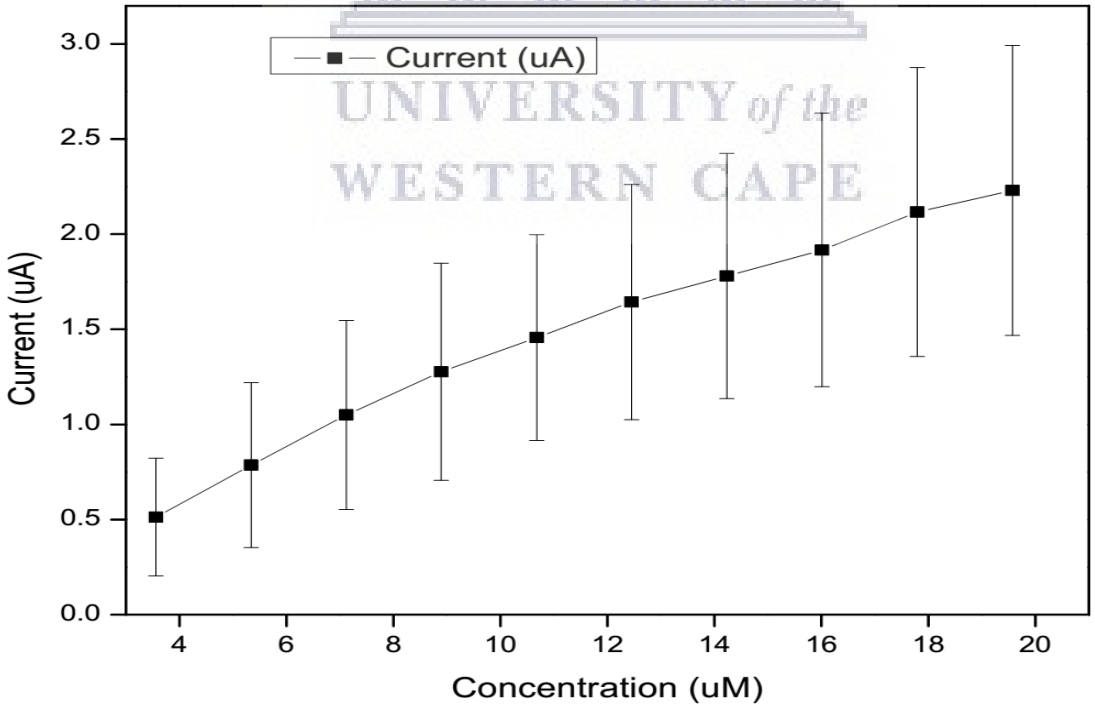

Figure 37: Calibration plot for the detection of cadmium at the PSF hydrogel/humic acid-modified gold electrode. The error bars represent the standard deviation of measurements from 3 times repetition

Table 9: Data for cadmium detection with hydrogel/humic acid-modified gold electrode

Electrode number	Sensitivity (µA/µM)	LOD (µM)	LOQ (µM)	R-square	RSD% (Sensitivity)
AuE/HGL/HA 1	0.1783	4.1468	12.5661	0.99499	31.74%
AuE/HGL/HA 2	0.0950	2.7043	8.1949	0.99064	
AuE/HGL/HA 3	0.1766	0.9752	2.9551	0.9880	

5.4.4. Conclusions on the electrochemical study of cadmium

The development of a voltammetric sensor based on gold electrode/polysulfone hydrogel/humic acid for detection of cadmium (II) ions has been achieved. When comparing sensitivity values for the bare sensor and modified sensor, the AuE/HGL/HA sensor is way high and this could be attributed to functionalization of the hydrogel thin film on the gold interface. The number of analytical peaks observed for cadmium increased from one to two upon electrode modification, which could be due to the formation of complexes between the hydrogel and cadmium ions. The measurements were performed in triplicates and the slope and standard deviations were used to determine the average LOD values. The average LOD for Cd(II) detection with AuE/HGL sensor was found to be 2.9980 µM which makes it more sensitive than the sensor constructed with Bi/Nafion/thiolatedpolyaniline/GCE treated with SWASV by Chen et al, whose LOD was found to be 3.56 $\times 10^{-4}$ M [148]. The LOD value of the AuE/HGL sensor was also compared with some LOD values achieved by other researchers and found to be less sensitive. The other more sensitive sensors include the one constructed with polycyclodextrin-modified carbon paste electrode treated with anodic stripping voltammetry by Roa et al [149]; where the LOD was reported as 2.51 µM, graphene/polyaniline/polystyrene (G/PANI/PS) nanoporous fiber modified SPCE by Promphet et al, whose LOD was found to be 1.59×10^{-8} M [150], and a nafion modified electrode treated with DPASV by Lu et al. [142] whose LOD was found to be 0.035 µM. This lower sensitivity of our sensor compared with the abovementioned sensors could be attributed to less binding sites on the hydrogel and lower surface concentration. The humic acid sensor, AuE/HGL/HA, constructed in the current work achieved the average LOD of 2.6088 µM, which makes it more sensitive than the hydrogel sensor, AuE/HGL, prior to its functionalization with humic acid. This attests to the binding capacity of humic acid for cadmium ions through its many functional groups. The

sensitivity of the constructed humic acid sensor in the current work was compared with other works and found to be less sensitive. The other works include the study by Grabarczyk and Koper [151]; where an LOD of 3 x 10^{-10} M was achieved. The other investigation was conducted by Radaelli et al. [143] and achieved an LOD of 0.097 nM. The explanation for the lower sensitivity of the humic acid sensor in the current work could be that the humic acids of different molecular weights were used. Molecular weight (Mw) is an important property of humic acid and its increase leads to a decrease in the concentration of acidic functional groups, so the larger Mw of the humic acid in the current study could be one of the reasons for the lower binding capacity of the sensor. Our hydrogel-humic acid sensor offered an LOD way higher than the WHO's guideline value of 0.003 mg/L. Both the LOD and linear range do not allow for the detection of Cd at or below the guideline value since they are above. Our sensor is more suitable for food quality monitoring since the LOD and linear range fall within the range of Cd concentration in food, which is from 10 to 1000 µg/kg. Our sensor was developed so that it would be environmentally friendly. The modification layer was made up of the hydrogel, which was produced by blending two polymers, PVA and PSF, which are mostly organic and therefore green materials because of their biodegradability. The hydrogel was further modified with HA which is a naturally occurring organic substance, meaning it does no harm to the environment. Therefore, the modification layer, which would be waste material after detections, would not increase toxicity in the environment. The reduction potential of free Cd(II) ions is -0.40 V [145], while in complexed form, Cd(II)-HA, it reduced to -0.300 V. The observed decline in reduction potential after complexation implies that the oxidized form, Cd(II), becomes more stable after complexation and this is attributed to higher complexing agent, HA, stabilization of Cd(II) than Cd and as a result, it reduces the reduction potential of Cd(II)-Cd redox couple. Cadmium-methionine complex was studied by Rangarajan et al. [152]; where a shifted formal potential of -0.569 V was obtained.

5.5. Electrochemical study of lead

Square wave voltammetry of lead was performed successfully at Au interface but cyclic voltammetry showed inadequate sensitivity at Au interface.

5.5.1. Electrochemical study of lead at the bare gold electrode (AuE)

The electrochemical study of lead at the bare gold electrode resulted in no peak in the absence of cadmium as shown in figure 38. The anodic potential scan resulted in the development of two oxidation peaks as soon as lead was introduced and the broader peak being around -0.3 V and the other one around -0.1 V. As the concentration of lead ions increased, the current responses increased accordingly and hence it is assumed that it was the detection of free lead ions that lead to an increase in current response.

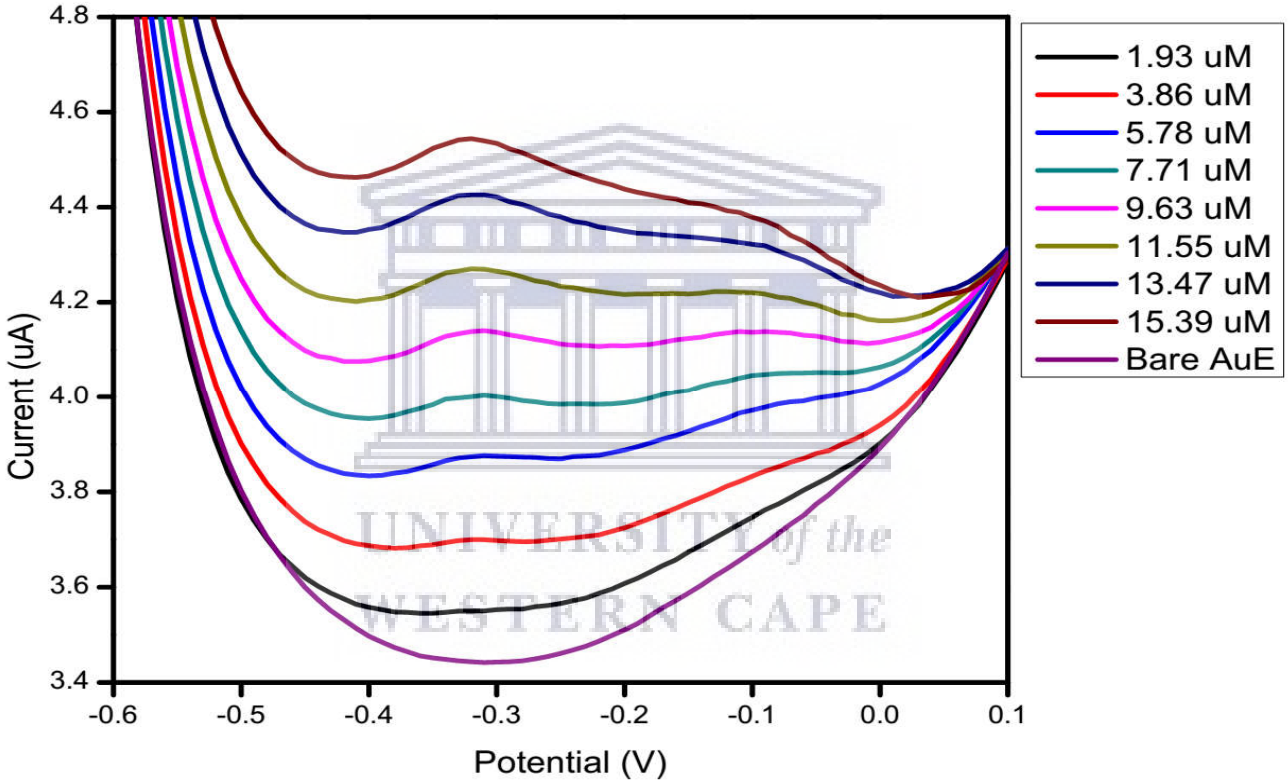

Figure 38: Square wave voltammetry of lead in phosphate buffer solution at the bare gold electrode in the potential range from -0.8 V to 0.2 V. Scan rate 100 mV/s

Figure 39 shows the calibration curves for replicate measurements of Pb(II) at bare Au electrode and since there is always some error associated with the measurement of any signal (due to material differences during preparation as well as human error), this figure shows the differences between measurements. The detections were performed in triplicates and the average current response measured as a function of concentration for the oxidation of Pb to Pb(II) at bare Au electrode was

used for the construction of the calibration curve in figure 40 for determination of more parameters. The standard deviations of current response were used to determine error bars. As the concentration increases, error bars increase. The corresponding values of sensitivity, LOD, LOQ and R^2 are shown in table 10. The achieved sensitivities of the three measurements are almost the same as attested by low RSD. Only two values of the LOD are comparable.

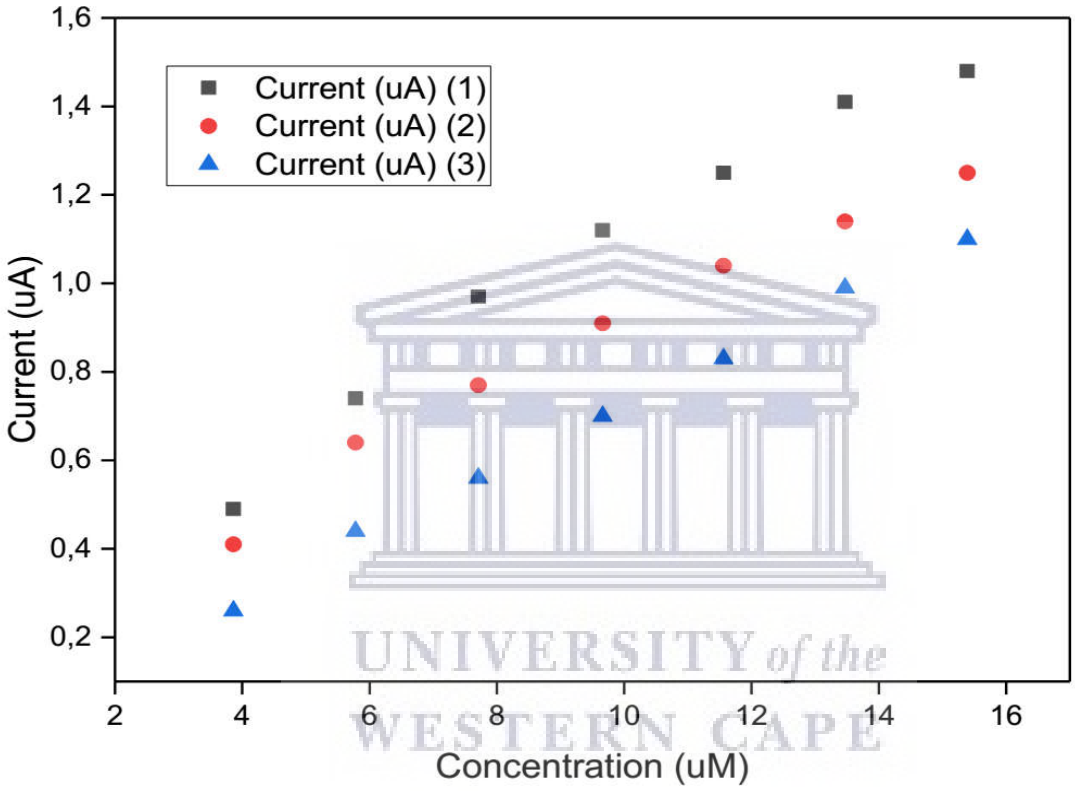

Figure 39: Calibration plot for the triplicate detections of lead at the bare gold electrode

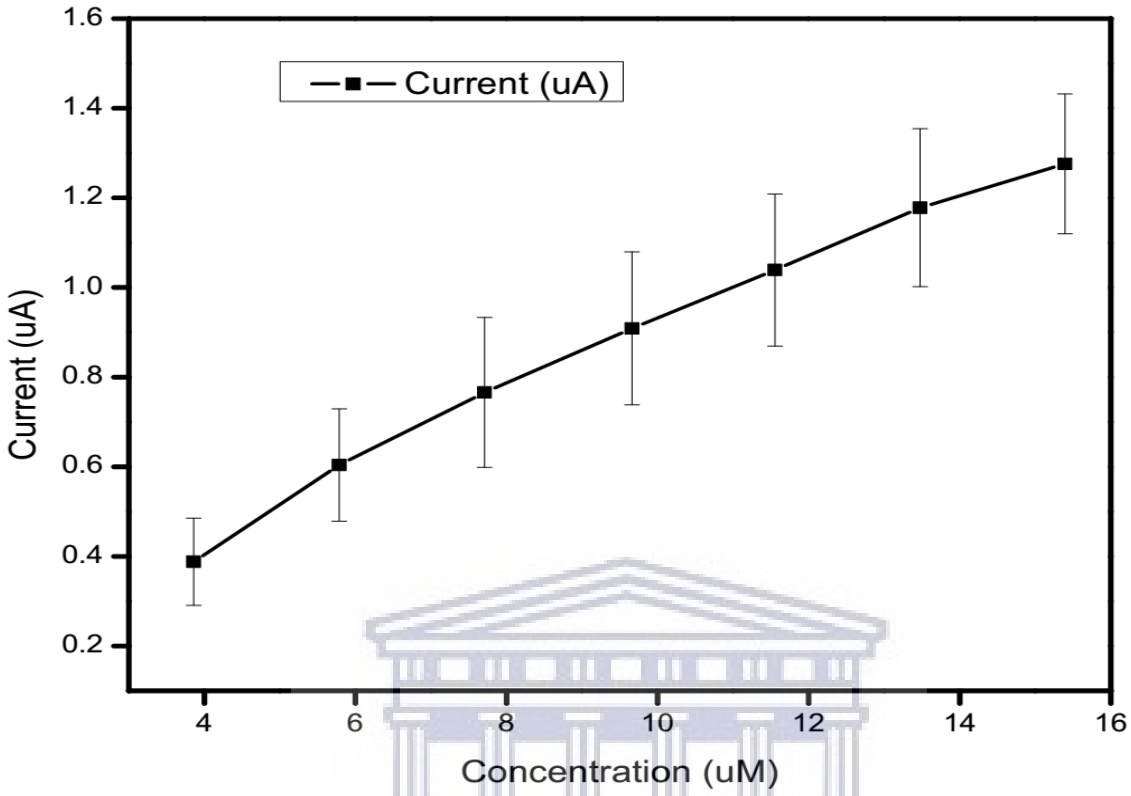

Figure 40: Calibration plot for the detection of lead at the bare gold electrode. The error bars represent the standard deviation of measurements from 3 times repetitions

Table 10: Data for lead detection with the bare gold electrode

Electrode Number	Sensitivity (µA/µM)	LOD (µM)	LOQ (µM)	R-square	RSD% (Sensitivity)
Bare AuE 1	0.0850	6.6180	20.0548	0.96883	9.40%
Bare AuE 2	0.0704	5.0501	15.3032	0.98163	
Bare AuE 3	0.0697	2.7934	8.4650	0.99526	

5.5.2. Electrochemical study of lead at the PSF hydrogel-modified gold electrode (AuE)

The electrode was electrochemically modified with the hydrogel for detection of lead. As shown in figure 41, the anodic potential scan produced two oxidation peaks, one around -0.3 V and the other around 0 V. The increasing lead concentration resulted in corresponding increase in peak height. The broadened peak around 0 V could be due to complex formation between the hydrogel

and lead ions. In figure 41 there is a little decrease in current response and that could be due to the complexation of free Pb ions from the solution with the hydrogel thin film.

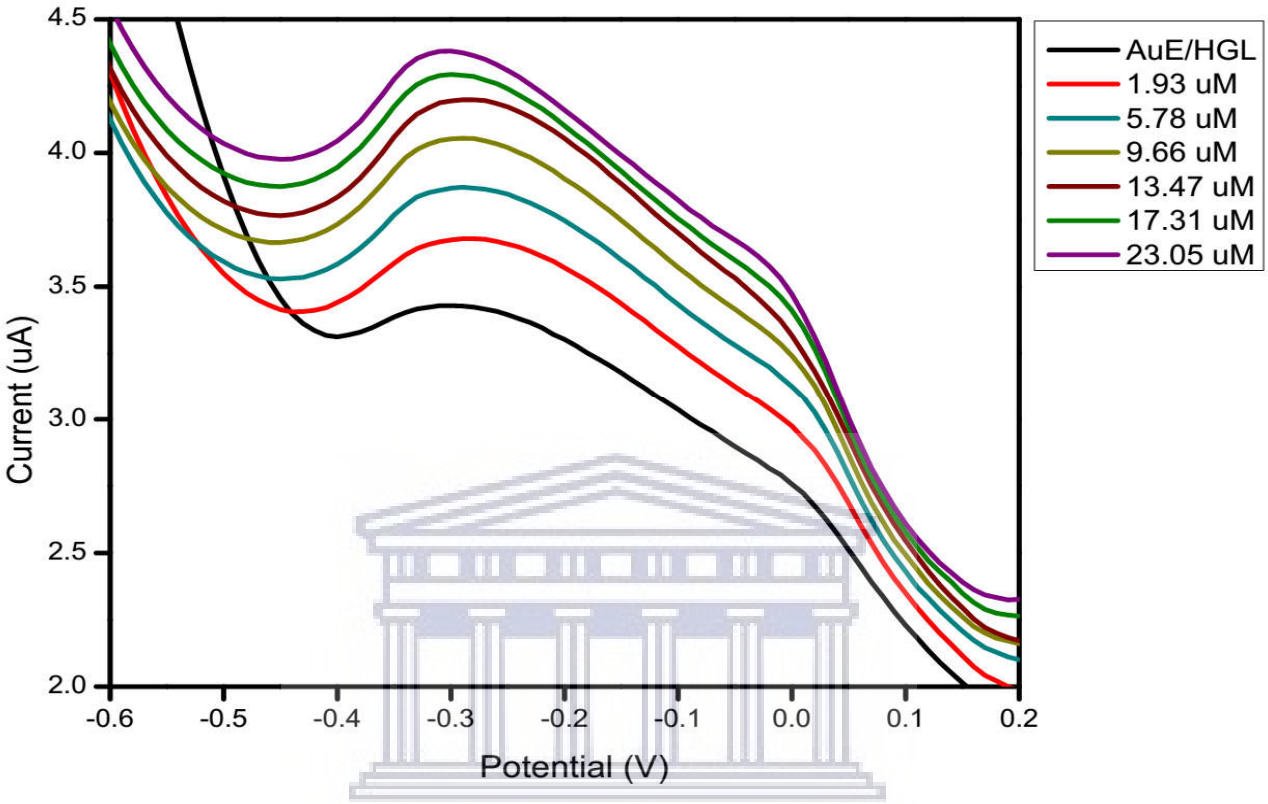

Figure 41: Square wave voltammetry of lead in phosphate buffer solution at the PSF hydrogel-modified gold electrode in the potential range from -0.8 V to 0.2 V. Scan rate 100 mV/s

Figure 42 shows the calibration curves for replicate measurements of Pb(II) at the Au/HGL electrode and since there is always some error associated with the measurement of any signal (due to material differences during preparation as well as human error), this figure shows the differences between measurements. The detections were performed in triplicates and the average current response measured as a function of concentration for the oxidation of Pb to Pb(II) at the Au/HGL electrode was used for the construction of the calibration curve in figure 43 for determination of more parameters. The standard deviations of current response were used to determine error bars. As the concentration increases, error bars increase. The observed change in slope in figure 43 was attributed to near-saturation of the polysulfone hydrogel with Pb. Supposing that there is a direct correlation between the linear section and the binding capacity of PSF hydrogel for Pb, this binding ability is of the order of ~ 13.5 µM Pb for ~ 8.64 $\times 10^{-10}$ mol.cm^{-2} PSF hydrogel. The related

coefficients are in table 11, which also presents the values of sensitivity, LOD, LOQ and R^2. The sensitivities attained from three detections are a little different from each other and hence high RSD.

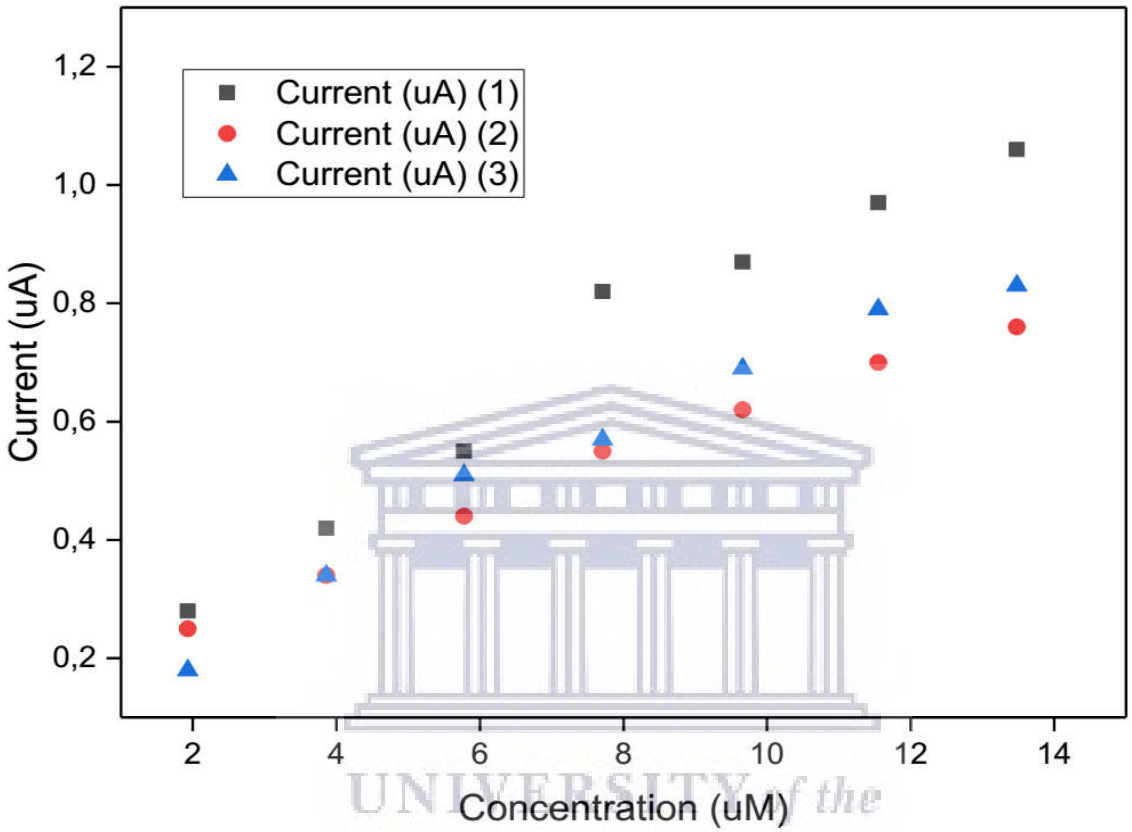

Figure 42: Calibration plot for the triplicate detections of lead at the PSF hydrogel-modified gold electrode

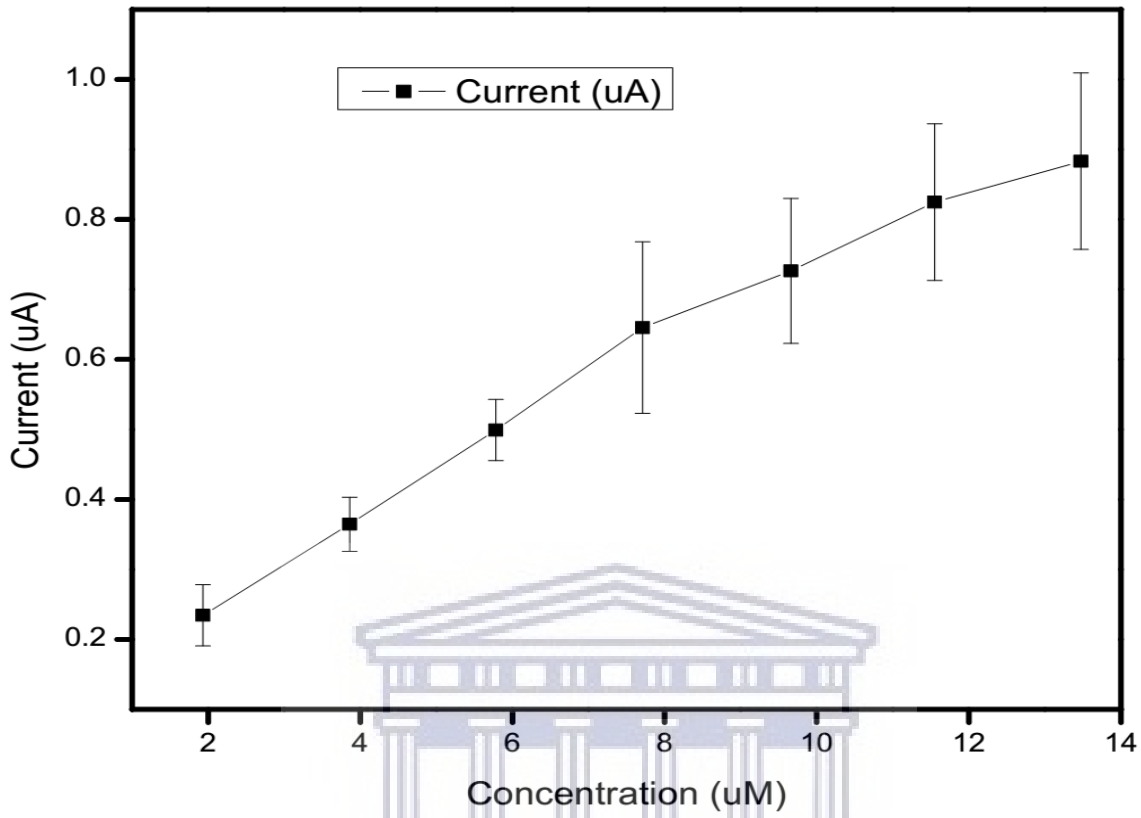

Figure 43: Calibration plot for the detection of lead at the PSF hydrogel-modified gold electrode. The error bars represent the standard deviation of measurements from 3 times repetitions

Table 11: Data for lead detection with PSF hydrogel-modified gold electrode

Electrode Number	Sensitivity (µA/µM)	LOD (µM)	LOQ (µM)	R-square	RSD% (Sensitivity)
AuE/HGL 1	0.0697	6.1893	18.7556	0.96073	17.04%
AuE/HGL 2	0.0458	2.8798	8.7266	0.99127	
AuE/HGL 3	0.0568	6.0149	18.2271	0.96285	

5.5.3. Electrochemical study of lead at the PSF hydrogel/humic acid-modified gold electrode (AuE)

The hydrogel thin film was functionalized with humic acid to develop a sensor for lead detection. No peak was observed in the absence of lead ions as shown in figure 44. The forward potential scan produced two oxidation peaks immediately after the addition of lead and the current responses

increased with the concentration of lead. The wider and uniform peak separation around both -0.3 V and 0 V could be associated with the complexes formed between humic acid and lead ions. In figure 44 a noticeable decrease in current response was observed and that could be due to complexation of free Pb ions with humic acid, whose incorporation seems to have increased the complexation capacity of the sensor. It is known that complexation capacity is determined by pH and the concentration of both metal ions and humic substances. The pH was kept constant throughout the measurement and the same concentration increments were made as in the detection with the hydrogel sensor, so the only difference is the presence of humic acid and hence the observed increase in adsorption is ascribed to the many ionizable functional groups on humic acid.

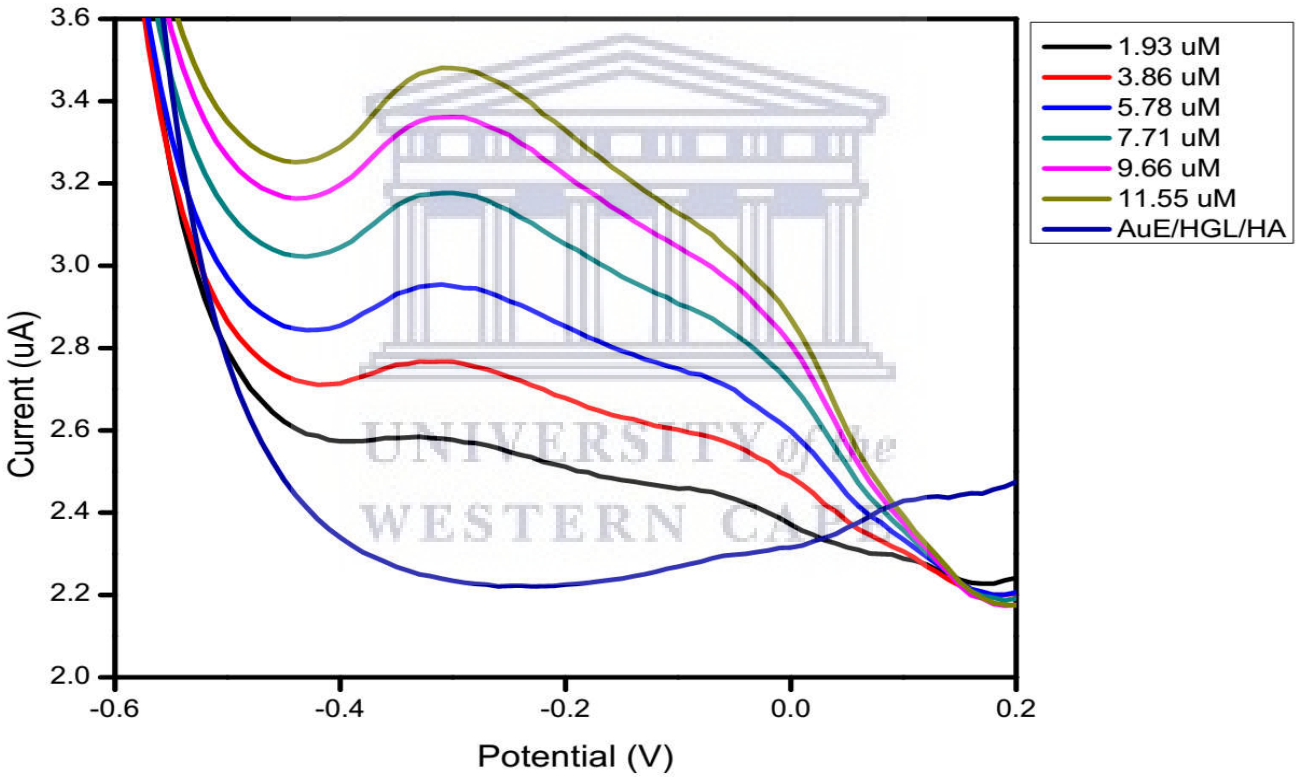

Figure 44: Square wave voltammetry of lead in phosphate buffer solution at the PSF hydrogel/humic acid-modified gold electrode in the potential range from -0.8 V to 0.2 V. Scan rate 100 mV/s

Figure 45 shows the calibration curves for replicate measurements of Pb(II) at the Au/HGL/HA electrode and since there is always some error associated with the measurement of any signal (due to material differences during preparation as well as human error), this figure shows the differences

between measurements. The detections were performed in triplicates and the average current response measured as a function of concentration for the oxidation of Pb to Pb(II) at the Au/HGL/HA electrode was used for the construction of the calibration curve in figure 46 for determination of more parameters. The standard deviations of current response were used to determine error bars. As the concentration increases, error bars increase. The observed change in slope in figure 46 was accredited to near-saturation of the HA with Pb. Presuming that the linear section is directly proportional to the binding ability of the HA for Pb, this binding ability is of the order of ~ 13.5 µM Pb for 0.25 ml of HA. The corresponding coefficients in table 12, in which the values of limits of detection (LOD) and quantitation (LOQ), the coefficient of determination (R^2), sensitivity, RSD and are presented. The values of sensitivity attained from the three detections are different and hence high RSD. That is also the case with LOD values.

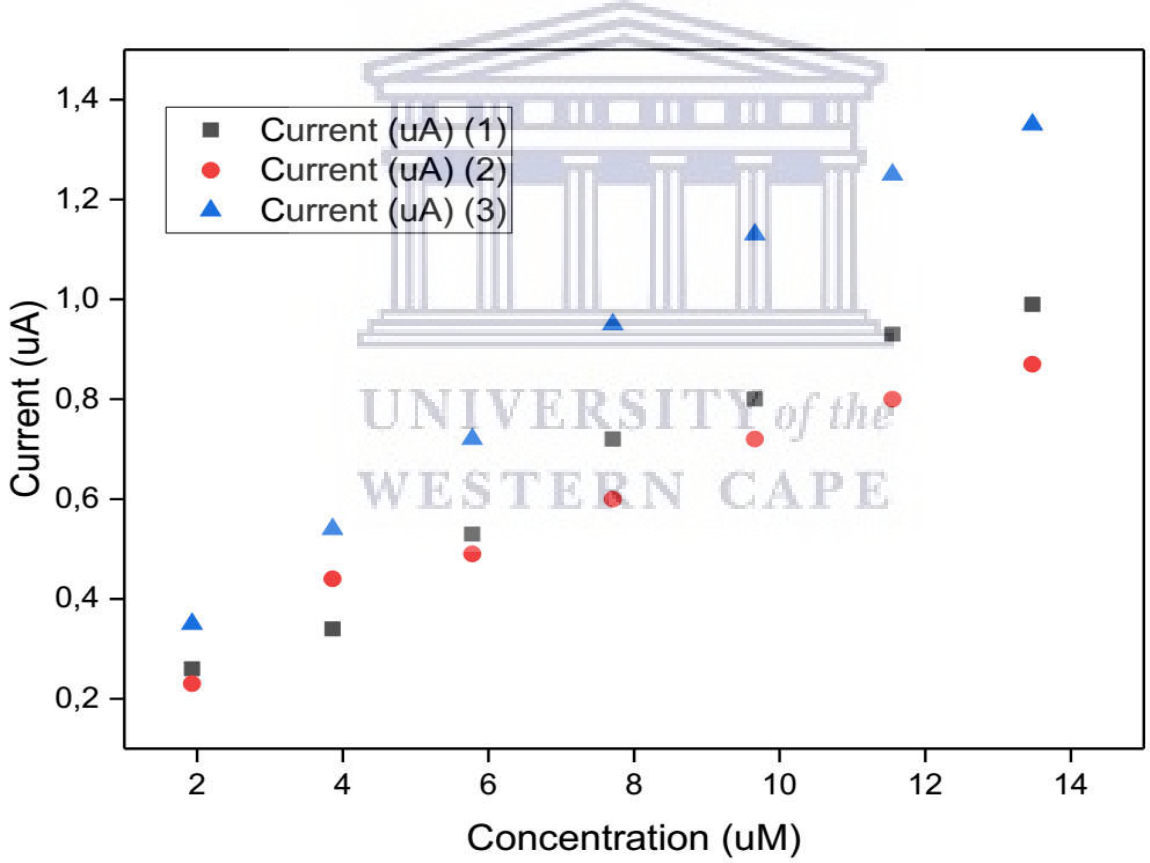

Figure 45: Calibration plot for the triplicate detections of lead at the PSF hydrogel/humic acid-modified gold electrode

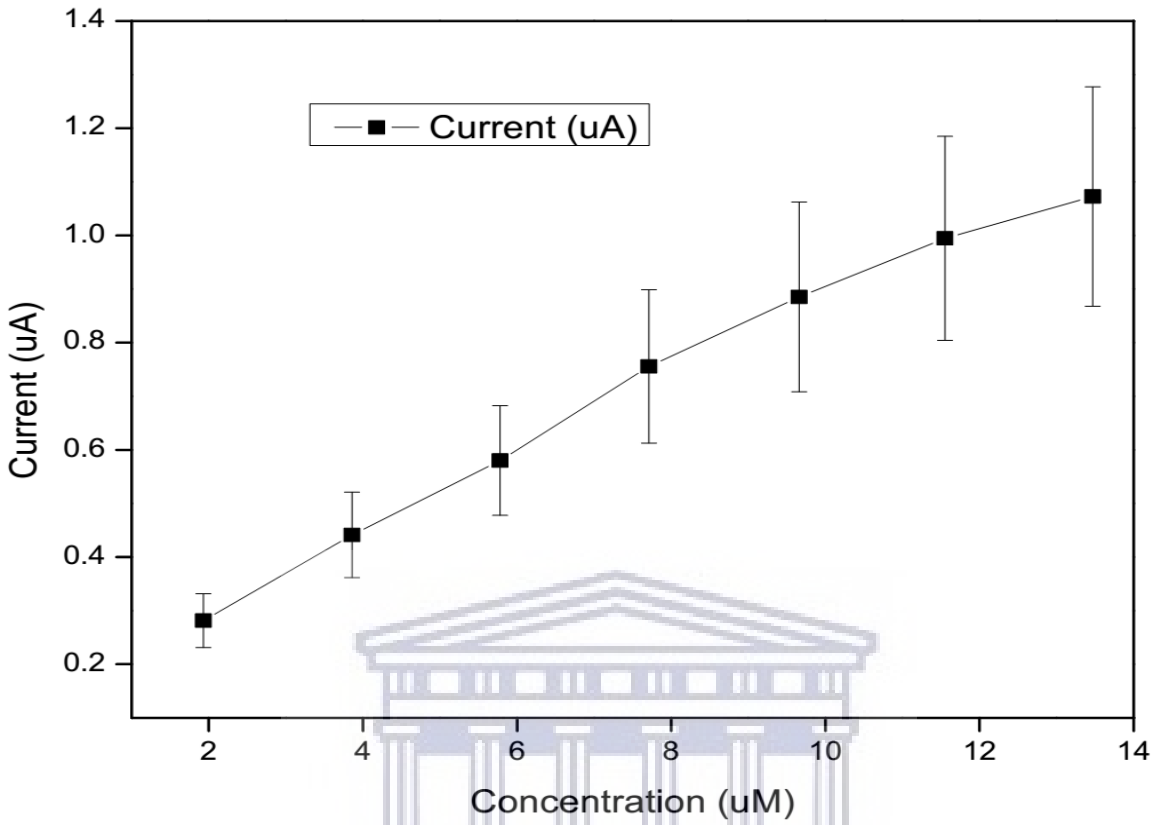

Figure 46: Calibration plot for the detection of lead at the PSF hydrogel/humic acid-modified gold electrode. The error bars represent the standard deviation of measurements from 3 times repetitions

Table 12: Data for lead detection with the PSF hydrogel/humic acid-modified gold electrode

Electrode number	Sensitivity (µA/µM)	LOD (µM)	LOQ (µM)	R-square	RSD% (Sensitivity)
AuE/HGL/HA 1	0.0639	5.7689	17.4817	0.97239	22.34%
AuE/HGL/HA 2	0.0532	5.0285	15.2379	0.97377	
AuE/HGL/HA 3	0.0899	3.7531	11.3729	0.98525	

5.5.4. Conclusions on the electrochemical study of lead

An electrochemical sensor based on gold electrode/ hydrogel/ humic acid for complexation of lead (II) ions has been constructed. The redox chemistry of lead showed the same number, i.e. two, of analytical peaks even after interface modification. The sensitivity values achieved at the bare electrode and at the modified interface show no considerable difference, which is indicative of the

weak complexation ability of the hydrogel and humic acid for lead ions. The measurements were performed in triplicates and the AuE/HGL sensor in the current work achieved an average LOD of 5.03 x 10 µM, which makes it more sensitive than the two sensors from previous works, first, chitosan-coated SPCE treated by SWASV by Hwang et al [153]; where the LOD of 2.82×10^{-5} M was achieved and second, sensor by Chen et al; where Bi/Nafion/thiolatedpolyaniline/GCE treated with SWASV offered a lower LOD value of 2.41×10^{-4}M [148]. One of the factors that could be attributed to the better sensitivity of our AuE/HGL sensor might be higher surface concentration of the be hydrogel which makes more binding sites available. The sensitivity of AuE/HGL Pb (II) sensor was also compared with some LOD values obtained by other researchers, e.g.: a polycyclodextrin-modified carbon paste electrode treated with SWASV by Roa et al where the LOD was found to be 7.14×10^{-7} M [149], a graphene/polyaniline/polystyrene (G/PANI/PS) nanoporous fiber modified screen-printed carbon electrode (SPCE) by Promphet et al offered the LOD of 3.94×10^{-8} M [150], and a nafion modified electrode treated with DPASV by Lu et al [142], whose LOD was found to be 00.049 µM. The humic acid sensor, Au/HGL/HA, in the current work achieved an average LOD of 4.85 µM, which makes it less sensitive than the sensor constructed by Jeong et al [144], where humic acid was incorporated into graphite powder on a carbon paste electrode and achieved an LOD of 5×10^{-10} M. The lower sensitivity of our sensor could be ascribed to different molecular weights of the humic acids. Another explanation could be that the pH was, by any chance, less than 6.6 which leads to repulsive electrostatic interactions between the hydrogel and lead ions. Although the electrostatic interactions between humic acid and Pb ions is attractive for pH values between 1.6 to 9 [154], the fact that humic acid was encapsulated in the hydrogel matrix might have made it difficult for Pb ions to access it due to repulsive interactions between the hydrogel and Pb ions. Our hydrogel-humic acid sensor offered LOD higher than the WHO's guideline value of 0.01 mg/L. Both the linear range and LOD are above the guideline value and hence the detection of concentrations at and below the guideline value is not possible. The concentrations of Pb in air, water and food is way lower than the LOD and linear range achieved by our sensor and hence our sensor needs further modification to achieve higher sensitivity. As far as toxicity of the sensor is concerned, the modification layer, the hydrogel, does no harm to the environment since it is a derivative of two organic polymers, PSF and PVA, which are environmentally friendly due to their biodegradability. The hydrogel was further modified with a naturally occurring organic substance, humic acid, which actually reduces

toxicity. Therefore, the modification layer which would be sensor waste material after detection would not increase toxicity in the environment. The reduction potential for free Pb(II) ions is -0.13 V [145], whereas in complexed form, Pb(II)-HGL, it reduced to -0.272 V. After modification of the hydrogel thin film with humic acid, the reduction potential of the complexed state, Pb(II)-HGL-HA, further decreased to -0.322 V. Overall, a decline in reduction potential has been observed after complexation, which means that the oxidized form, Pb(II), becomes more stable after complexation. This is attributed to higher complexing agent, HGL and HA, stabilization of Pb(II) than Pb and as a result, it reduces the reduction potential of Pb(II)-Pb redox couple. A Pb (II)- bis-(hydrazone) complex was studied by Giraldo et al. [155]; where a shifted formal potential of -1.11 V was obtained.

Chapter 6

6.1. Conclusions

In this current study we have supplied evidence to confirm the formation of polysulfone hydrogels through the incorporation of polyvinyl alcohol (PVA) into polysulfone (PSF) employing glutaraldehyde as a cross-linking agent. The synthesized hydrogels were characterized by electrochemical, spectroscopic and microscopic techniques. Scan rate studies attested the crosslinking of PSF and PVA polymers. The scanning electron microscopy (SEM) analysis exhibits how PSF and the produced hydrogels differ in terms of membrane porosity and morphology. Unaltered PSF exhibits spherical shape good-sized distribution and uniformity of morphology. The integration of PVA into PSF was observed as groups of smaller particles scattered on the PSF template. The synthesized hydrogels exhibited nanometer size distribution and the homogeneous integration of PVA morphology into PSF template was taken as proof of crosslinking between these starting materials to make entirely new hydrogels. Atomic force microscopy was utilized to investigate the surface topography as surface roughness variable, which is connected to the height distribution at the surface. The height distribution attested the properties of the polymers exhibited in SEM images. An increased hydrophilicity of the hydrogel material was inferred from higher roughness. Cyclic voltammetry was used to investigate the redox behavior of the produced hydrogel thin films and the charge transport characteristics of the hydrogel were found to be corresponding to that of an extremely conductive polymer. Square wave voltammetry (SWV) was used to study the redox behavior of heavy metals (Cu, Cd and Pb) at the bare gold electrode, hydrogel-modified and hydrogel/humic acid-modified electrode. For Cu studies, the AuE/HGL/HA sensor was found to be more sensitive than the AuE/HGL sensor. For cadmium (II) studies, the AuE/HGL/HA sensor showed higher sensitivity than the AuE/HGL sensor. The AuE/HGL/HA sensor also achieved better sensitivity than the AuE/HGL sensor. The same number of analytical peaks were observed for the study of all the three metals even after surface modification with the hydrogel and humic acid.

6.2. Recommendations

The investigation attested the successful synthesis of the hydrogel material via crosslinking. Nevertheless, several physical characteristics of the hydrogel are yet to be studied such as temperature degradation profiles by thermogravimetric analysis and swellability. The research to date confirmed the successful use of the hydrogels and humic acid as complexing agents for removal of heavy metals from aqueous solutions. The motivation of the research was to present the hydrogel material as an enhanced metal-complexing agent by functionalization with humic acid ligand. The small-scale tests may be extended to cover more heavy metals and matrices. These hydrogels and humic acid may be evaluated for their complexing ability for other organic pollutants. The achieved results confirm that the functionalization of the hydrogel by humic acid increases the sensitivity of the sensor but it would be interesting in the next studies to find out using different methods which of the possibilities of humic acid complexing metal ions happens, whether it is: 1) chelation between two carboxylic groups, 2) between carboxylic and phenolic groups, 3) binding with phenols or phenolic ethers or 4) complexation with carboxyl group.

We will also work on the implementation of innovative chemical sensors to real sample evaluation and produce a mobile in-site tracking set-up for the assessment of heavy metals and other ecological pollutants. Mobile potentiostats that are cooperative with constructed sensors could be used along with screen printed gold electrodes modified with PSF hydrogel /humic acid to determine chosen heavy metals in particular samples in industrial wastewater. It therefore unveils the potentiality to carry the research facility to the site of pollution to carry out the assessment of a chemical makeup of multi-element samples utilizing uncomplicated sensor devices.

The future work will include the study of sensor efficiency in multi-metal solution since most heavy metal-contaminated waters contain more than one heavy metal, so it would be necessary to determine the binding abilities of the humic acid-functionalized hydrogel with multi-metal solutions. The spectroscopic analysis, by ICP-OES, will also be considered in the future work since the focus of the current work was the electrochemical behaviour of metals.

6.3. References

[1] L. Coetzee, H.H. Du Preez, J.H.J. Van Vuren, Metal concentrations in Clarias gariepinus and Labeo umbratus from the Olifants and Klein Olifants River, Mpumalanga, South Africa: Zinc, copper, manganese, lead, chromium, nickel, aluminium and iron, Water SA. 28 (2002) 433–448. https://doi.org/10.4314/wsa.v28i4.4917.

[2] P.S. Fasinu, O.E. Orisakwe, Heavy metal pollution in sub-Saharan Africa and possible implications in cancer epidemiology, Asian Pacific J. Cancer Prev. 14 (2013) 3393–3402. https://doi.org/10.7314/APJCP.2013.14.6.3393.

[3] J. Yabe, M. Ishizuka, T. Umemura, Current levels of heavy metal pollution in Africa, J. Vet. Med. Sci. 72 (2010) 1257–1263. https://doi.org/10.1292/jvms.10-0058.

[4] J.R. Fianko, S. Osae, D. Adomako, D.K. Adotey, Y. Serfor-Armah, Assessment of heavy metal pollution of the Iture Estuary in the central region of Ghana, Environ. Monit. Assess. 131 (2007) 467–473. https://doi.org/10.1007/s10661-006-9492-2.

[5] M. Snoussi, L. Awosika, Marine capacity building in North and West Africa, Mar. Policy. 22 (1998) 209–215. https://doi.org/10.1016/S0308-597X(98)00007-4.

[6] A.A.K. Abou-Arab, Heavy metal contents in Egyptian meat and the role of detergent washing on their levels, Food Chem. Toxicol. 39 (2001) 593–599. https://doi.org/10.1016/S0278-6915(00)00176-9.

[7] M.A. Barakat, New trends in removing heavy metals from industrial wastewater, Arab. J. Chem. 4 (2011) 361–377. https://doi.org/10.1016/j.arabjc.2010.07.019.

[8] G. March, T.D. Nguyen, B. Piro, Modified electrodes used for electrochemical detection of metal ions in environmental analysis, Biosensors. 5 (2015) 241–275. https://doi.org/10.3390/bios5020241.

[9] Z. Wang, C. Yan, H. Kong, D. Wu, Mechanisms of cadmium toxicity to various trophic saltwater organisms, 2010.

[10] G. Zhao, H. Wang, G. Liu, Electrochemical determination of trace cadmium in soil by a bismuth film/graphene-β-cyclodextrin-nafion composite modified electrode, Int. J. Electrochem. Sci. 11 (2016) 1840–1851.

[11] I. Üstündağ, Z. Üstündağ, O.M. Kalfa, Y.K. Kadioğlu, Geochemical compositions of trona samples by PEDXRF and their identification under confocal Raman spectroscopy: Beypazari{dotless}-Ankara, Turkey, Nucl. Instruments Methods Phys. Res. Sect. B Beam

Interact. with Mater. Atoms. 254 (2007) 153–159. https://doi.org/10.1016/j.nimb.2006.09.018.

[12] Z. Üstündağ, I. Üstündağ, Y. Kağan Kadioğlu, Multi-element analysis of pyrite ores using polarized energy-dispersive X-ray fluorescence spectrometry, Appl. Radiat. Isot. 65 (2007) 809–813. https://doi.org/10.1016/j.apradiso.2007.03.004.

[13] O.M. Kalfa, Z. Üstündağ, I. Özkirim, Y. Kagan Kadioğlu, Analysis of tincal ore waste by energy dispersive X-ray fluorescence (EDXRF) Technique, J. Quant. Spectrosc. Radiat. Transf. 103 (2007) 424–427. https://doi.org/10.1016/j.jqsrt.2006.02.059.

[14] P.E. Paus, Determination of some heavy metals in sea water by atomic absorption spectrophotometry, Fresenius' Zeitschrift Für Anal. Chemie. 264 (1973) 118–122. https://doi.org/10.1007/BF00424622.

[15] C. Martinez-Lopez, M. Sakayanagi, J.R. Almirall, Elemental analysis of packaging tapes by LA-ICP-MS and LIBS, Forensic Chem. 8 (2018) 40–48. https://doi.org/10.1016/j.forc.2018.01.004.

[16] J. Xia, Y. Fang, Y. Chen, Y. Pan, P. Li, M. Xue, Q. Hu, Lead speciation analysis in rice by reversed phase chromatography with inductively coupled plasma mass spectrometry, J. Food Compos. Anal. 60 (2017) 74–80. https://doi.org/10.1016/j.jfca.2017.03.002.

[17] A. Erkal, I. Üstündaı, S. Yavuz, Z. Üstündaı, An Electrochemical application of MnO2 decorated graphene supported glassy carbon ultrasensitive electrode: Pb2+ and Cd2+ analysis of seawater samples, J. Electrochem. Soc. 162 (2015) H213–H219. https://doi.org/10.1149/2.0571504jes.

[18] İ. Üstündağ, A. Erkal, T. Koralay, Y.K. Kadıoğlu, S. Jeon, Gold nanoparticle included graphene oxide modified electrode: Picomole detection of metal ions in seawater by stripping voltammetry, J. Anal. Chem. 71 (2016) 685–695. https://doi.org/10.1134/S1061934816070108.

[19] I. Üstündağ, A. Erkal, Determination of dopamine in the presence of ascorbic acid on digitonin-doped coal tar pitch carbonaceous electrode, Sensors Mater. 29 (2017) 85–94. https://doi.org/10.18494/SAM.2017.1416.

[20] S. Yavuz, A. Erkal, İ.A. Kariper, A.O. Solak, S. Jeon, İ.E. Mülazımoğlu, Z. Üstündağ, Oxide-based carbon electrode: Preparation, characterization, and heavy metal analysis in food samples, Food Anal. Methods. 9 (2016) 322–331. https://doi.org/10.1007/s12161-015-

0198-3.

[21] A. Erkal, M.S. Erdoğan, I. Aşik, H. Ekşi, S. Jeon, A.O. Solak, Z. Üstuũdağ, Electrografting and surface properties of some substituted nitrophenols on glassy carbon electrode and simultaneous Pb2+ - Cd2+ analysis via assist of graphene oxide terminated surface, J. Electrochem. Soc. 161 (2014) 696–704. https://doi.org/10.1149/2.1081410jes.

[22] I. Üstündağ, A. Erkal, Z. Üstündağ, A.O. Solak., Electrochemical detection of cadmium and lead in rice on manganese dioxide reinforced carboxylated graphene oxide nanofilm, MANAS J. Eng. 6 (2018) 96–109.

[23] H.G. Gorchev, G. Ozolins, Guidelines for drinking-water quality, 3rd ed., World Health Organization, 2004. https://doi.org/10.1016/S1462-0758(00)00006-6.

[24] M. Šćiban, M. Klašnja, B. Škrbić, Adsorption of copper ions from water by modified agricultural by-products, Desalination. 229 (2008) 170–180. https://doi.org/10.1016/j.desal.2007.08.017.

[25] K. Feng, G. Wen, Absorbed Pb 2+ and Cd 2+ ions in water by cross-linked starch xanthate, Int. J. Polym. Sci. 2017 (2017). https://doi.org/10.1155/2017/6470306.

[26] M.R. Awual, M. Ismael, T. Yaita, S.A. El-Safty, H. Shiwaku, Y. Okamoto, S. Suzuki, Trace copper(II) ions detection and removal from water using novel ligand modified composite adsorbent, Chem. Eng. J. 222 (2013) 67–76. https://doi.org/10.1016/j.cej.2013.02.042.

[27] F.S. Teodoro, S.N. do C. Ramos, M.M.C. Elias, A.B. Mageste, G.M.D. Ferreira, L.H.M. da Silva, L.F. Gil, L.V.A. Gurgel, Synthesis and application of a new carboxylated cellulose derivative. Part I: Removal of Co2+, Cu2+ and Ni2+ from monocomponent spiked aqueous solution, J. Colloid Interface Sci. 483 (2016) 185–200. https://doi.org/10.1016/j.jcis.2016.08.004.

[28] I. Sierra, D. Pérez-Quintanilla, Heavy metal complexation on hybrid mesoporous silicas: An approach to analytical applications, Chem. Soc. Rev. 42 (2013) 3792–3807. https://doi.org/10.1039/c2cs35221d.

[29] V.C.G. Dos Santos, J.V.T.M. De Souza, C.R.T. Tarley, J. Caetano, D.C. Dragunski, Copper ions adsorption from aqueous medium using the biosorbent sugarcane bagasse in natura and chemically modified, Water, Air, Soil Pollut. 216 (2011) 351–359. https://doi.org/10.1007/s11270-010-0537-3.

[30] E.M. Ahmed, Hydrogel : Preparation, characterization, and applications: A review, J. Adv.

Res. 6 (2015) 105–121. https://doi.org/10.1016/j.jare.2013.07.006.

[31] H.S. Mansur, R.L. Oréfice, A.A.P. Mansur, Characterization of poly(vinyl alcohol)/poly(ethylene glycol) hydrogels and PVA-derived hybrids by small-angle X-ray scattering and FTIR spectroscopy, Polymer (Guildf). 45 (2004) 7193–7202. https://doi.org/10.1016/j.polymer.2004.08.036.

[32] M.F. Akhtar, M. Hanif, N.M. Ranjha, Methods of synthesis of hydrogels . . . A review, Saudi Pharm. J. 24 (2016) 554–559. https://doi.org/10.1016/j.jsps.2015.03.022.

[33] Q. Li, D. Yang, G. Ma, Q. Xu, X. Chen, F. Lu, J. Nie, Synthesis and characterization of chitosan-based hydrogels, Int. J. Biol. Macromol. 44 (2009) 121–127. https://doi.org/10.1016/j.ijbiomac.2008.11.001.

[34] S. Shetye, A. Godbole, S. Bhilegaokar, P. Gajare, Hydrogels: Introduction , preparation , characterization and applications, Int. J. Res. Methodol. 1 (2015) 47–71.

[35] B. Zunic, S. Peter, Hydrogels: Methods of preparation, characterisation and applications, Intech. (2018) 267–322.

[36] P. Hammond, Synthesis and properties of hydrogels of acrylamide and bisacrylamide in water, Massachusetts Inst. Technol. (2006).

[37] M.F. Akhtar, M. Hanif, N.M. Ranjha, Methods of synthesis of hydrogels … A review, Saudi Pharm. J. 24 (2016) 554–559. https://doi.org/10.1016/j.jsps.2015.03.022.

[38] A.S. Hoffman, Hydrogels for biomedical applications, Adv. Drug Deliv. Rev. 64 (2012) 18–23. https://doi.org/10.1016/j.addr.2012.09.010.

[39] S.M.H. Bukhari, S. Khan, M. Rehanullah, N.M. Ranjha, Synthesis and characterization of chemically cross-linked acrylic acid/gelatin hydrogels: Effect of pH and composition on swelling and drug release, Int. J. Polym. Sci. 2015 (2015). https://doi.org/10.1155/2015/187961.

[40] Y. Zhang, L. Tao, S. Li, Y. Wei, Synthesis of multiresponsive and dynamic chitosan-based hydrogels for controlled release of bioactive molecules, Biomacromolecules. 12 (2011) 2894–2901. https://doi.org/10.1021/bm200423f.

[41] W. Hu, Z. Wang, Y. Xiao, S. Zhang, J. Wang, Advances in crosslinking strategies of biomedical hydrogels, Biomater. Sci. 7 (2019) 843–855. https://doi.org/10.1039/c8bm01246f.

[42] O. Akakuru, B. Isiuku, Chitosan hydrogels and their glutaraldehyde-crosslinked

counterparts as potential drug release and tissue engineering systems - synthesis, characterization, swelling kinetics and mechanism, J. Phys. Chem. Biophys. 07 (2017). https://doi.org/10.4172/2161-0398.1000256.

[43] N.E. Valderruten, J.D. Valverde, F. Zuluaga, E. Ruiz-Durántez, Synthesis and characterization of chitosan hydrogels cross-linked with dicarboxylic acids, React. Funct. Polym. 84 (2014) 21–28. https://doi.org/10.1016/j.reactfunctpolym.2014.08.006.

[44] M.R. Islam, Z. Lu, X. Li, A.K. Sarker, L. Hu, P. Choi, X. Li, N. Hakobyan, M.J. Serpe, Responsive polymers for analytical applications: A review, Anal. Chim. Acta. 789 (2013) 17–32. https://doi.org/10.1016/j.aca.2013.05.009.

[45] A.S. Hoffman, Hydrogels for biomedical applications, Adv. Drug Deliv. Rev. 64 (2012) 18–23. https://doi.org/10.1016/j.addr.2012.09.010.

[46] H. Mittal, S.S. Ray, M. Okamoto, Recent Progress on the Design and Applications of Polysaccharide-Based Graft Copolymer Hydrogels as Adsorbents for Wastewater Purification, Macromol. Mater. Eng. 301 (2016) 496–522. https://doi.org/10.1002/mame.201500399.

[47] Y. Zhou, S. Fu, L. Zhang, H. Zhan, M. V. Levit, Use of carboxylated cellulose nanofibrils-filled magnetic chitosan hydrogel beads as adsorbents for Pb(II), Carbohydr. Polym. 101 (2014) 75–82. https://doi.org/10.1016/j.carbpol.2013.08.055.

[48] M.A. Barakat, New trends in removing heavy metals from industrial wastewater, Arab. J. Chem. 4 (2011) 361–377. https://doi.org/10.1016/j.arabjc.2010.07.019.

[49] B. Xiang, W. Fan, X. Yi, Z. Wang, F. Gao, Y. Li, H. Gu, Dithiocarbamate-modified starch derivatives with high heavy metal adsorption performance, Carbohydr. Polym. 136 (2016) 30–37. https://doi.org/10.1016/j.carbpol.2015.08.065.

[50] G.R. Mahdavinia, S. Hasanpour, L. Behrouzi, H. Sheykhloie, Study on adsorption of Cu(II) on magnetic starch-g-polyamidoxime/montmorillonite/Fe3O4 nanocomposites as novel chelating ligands, Starch/Staerke. 68 (2016) 188–199. https://doi.org/10.1002/star.201400255.

[51] A. Buléon, P. Colonna, V. Planchot, S. Ball, Starch granules: Structure and biosynthesis, Int. J. Biol. Macromol. 23 (1998) 85–112. https://doi.org/10.1016/S0141-8130(98)00040-3.

[52] R. Cheng, S. Ou, Application of modified starches in wastewater treatment, Polym. Sci.

(2009) 52–61.

[53] C. Wan, J. Li, Facile synthesis of well-dispersed superparamagnetic γ-Fe2O3 nanoparticles encapsulated in three-dimensional architectures of cellulose aerogels and their applications for Cr(VI) removal from contaminated Water, ACS Sustain. Chem. Eng. 3 (2015) 2142–2152. https://doi.org/10.1021/acssuschemeng.5b00384.

[54] S. Kalidhasan, A. Santhana KrishnaKumar, V. Rajesh, N. Rajesh, Ultrasound-assisted preparation and characterization of crystalline cellulose-ionic liquid blend polymeric material: A prelude to the study of its application toward the effective adsorption of chromium, J. Colloid Interface Sci. 367 (2012) 398–408. https://doi.org/10.1016/j.jcis.2011.09.062.

[55] J. Wang, X. Lu, P.F. Ng, K.I. Lee, B. Fei, J.H. Xin, J. yong Wu, Polyethylenimine coated bacterial cellulose nanofiber membrane and application as adsorbent and catalyst, J. Colloid Interface Sci. 440 (2015) 32–38. https://doi.org/10.1016/j.jcis.2014.10.035.

[56] G. Jing, L. Wang, H. Yu, W.A. Amer, L. Zhang, Recent progress on study of hybrid hydrogels for water treatment, Colloids Surfaces A Physicochem. Eng. Asp. 416 (2013) 86–94. https://doi.org/10.1016/j.colsurfa.2012.09.043.

[57] P.J. Flory, Principles of polymer chemistry, Cornell University Press, 1953.

[58] G.A. Mahmoud, S.F. Mohamed, H.M. Hassan, Removal of methylene blue dye using biodegradable hydrogel and reusing in a secondary adsorption process, Desalin. Water Treat. 54 (2015) 2765–2776. https://doi.org/10.1080/19443994.2014.905978.

[59] P. Souda, L. Sreejith, Environmental sensitive hydrogel for purification of waste water: Part 1: Synthesis and characterization, Polym. Bull. 71 (2014) 839–854. https://doi.org/10.1007/s00289-014-1097-2.

[60] J. Diani, K. Gall, Removal of methylene blue dyes from wastewater using cellulose-based superadsorbent hydrogels, Polym. Eng. Sci. (2006). https://doi.org/10.1002/pen.22020.

[61] T. Trakulsujaritchok, N. Noiphom, N. Tangtreamjitmun, R. Saeeng, Adsorptive features of poly(glycidyl methacrylate-co-hydroxyethyl methacrylate): Effect of porogen formulation on heavy metal ion adsorption, J. Mater. Sci. 46 (2011) 5350–5362. https://doi.org/10.1007/s10853-011-5473-0.

[62] L. Jiang, P. Liu, Design of magnetic attapulgite/fly ash/poly(acrylic acid) ternary nanocomposite hydrogels and performance evaluation as selective adsorbent for Pb2+ Ion,

ACS Sustain. Chem. Eng. 2 (2014) 1785–1794. https://doi.org/10.1021/sc500031z.

[63] D. Buenger, F. Topuz, J. Groll, Hydrogels in sensing applications, Prog. Polym. Sci. 37 (2012) 1678–1719. https://doi.org/10.1016/j.progpolymsci.2012.09.001.

[64] H.J. Van Der Linden, S. Herber, W. Olthuis, P. Bergveld, Stimulus-sensitive hydrogels and their applications in chemical (micro)analysis, Analyst. 128 (2003) 325–331. https://doi.org/10.1039/b210140h.

[65] D. Buenger, F. Topuz, J. Groll, Progress in Polymer Science Hydrogels in sensing applications, Prog. Polym. Sci. 37 (2012) 1678–1719. https://doi.org/10.1016/j.progpolymsci.2012.09.001.

[66] M.A. Cimpean, I. Craciunescu, D. Gligor, Amperometric sensor based on HEMA hydrogels modified with Toluidine Blue for nitrite detection in water samples, Mater. Chem. Phys. 200 (2017) 233–240. https://doi.org/10.1016/j.matchemphys.2017.07.057.

[67] Y.Y. Li, B. Wang, M.G. Ma, B. Wang, Review of Recent Development on Preparation, Properties, and Applications of Cellulose-Based Functional Materials, Int. J. Polym. Sci. 2018 (2018). https://doi.org/10.1155/2018/8973643.

[68] J. Deng, W. Liang, J. Fang, Liquid Crystal Droplet-Embedded Biopolymer Hydrogel Sheets for Biosensor Applications, ACS Appl. Mater. Interfaces. 8 (2016) 3928–3932. https://doi.org/10.1021/acsami.5b11076.

[69] L. Li, Y. Wang, L. Pan, Y. Shi, W. Cheng, Y. Shi, G. Yu, A nanostructured conductive hydrogels-based biosensor platform for human metabolite detection, Nano Lett. 15 (2015) 1146–1151. https://doi.org/10.1021/nl504217p.

[70] L.T. Hoa, K.G. Sun, S.H. Hur, Highly sensitive non-enzymatic glucose sensor based on Pt nanoparticle decorated graphene oxide hydrogel, Sensors Actuators B Chem. 210 (2015) 618–623. https://doi.org/10.1016/j.snb.2015.01.020.

[71] D. Zhai, B. Liu, Y. Shi, L. Pan, Y. Wang, W. Li, R. Zhang, G. Yu, Highly sensitive glucose sensor based on Pt nanoparticle/polyaniline hydrogel heterostructures, Am. Chem. Soc. (2013). https://doi.org/10.1021/nn400482d.

[72] G. Mistlberger, M. Pawlak, E. Bakker, I. Klimant, Photodynamic optical sensor for buffer capacity and pH based on hydrogel-incorporated spiropyran, Chem. Commun. 51 (2015) 4172–4175. https://doi.org/10.1039/c4cc07821g.

[73] Y. Zheng, S. Hua, A. Wang, Adsorption behavior of Cu2+ from aqueous solutions onto

starch-g-poly (acrylic acid)/sodium humate hydrogels, Desalination. 263 (2010) 170–175. https://doi.org/10.1016/j.desal.2010.06.054.

[74] M. Klučáková, Complexation of Copper(II) with Humic Acids Studied by Ultrasound Spectrometry, Org. Chem. Int. 2012 (2012) 1–6. https://doi.org/10.1155/2012/206025.

[75] E.M. Logan, I.D. Pulford, G.T. Cook, A.B. Mackenzie, Complexation of Cu2+ and Pb2+ by peat and humic acid, Eur. J. Soil Sci. 48 (2008) 685–696. https://doi.org/10.1111/j.1365-2389.1997.tb00568.x.

[76] M. Klučáková, M. Pavlíková, Lignitic humic acids as environmentally-friendly adsorbent for heavy metals, J. Chem. 2017 (2017) 14–16. https://doi.org/10.1155/2017/7169019.

[77] T. Bartelme, E. Borneman, C. Braithwaite, A. Calfo, Organic compounds in the reef aquarium, Reef Cent. 8 (2009).

[78] N. Saha, A. Saarai, N. Roy, T. Kitano, P. Saha, Polymeric Biomaterial Based Hydrogels for Biomedical Applications, J. Biomater. Nanobiotechnol. 02 (2011) 85–90. https://doi.org/10.4236/jbnb.2011.21011.

[79] H.P. Merkle, Drug delivery's quest for polymers: Where are the frontiers?, Eur. J. Pharm. Biopharm. 97 (2015) 293–303. https://doi.org/10.1016/j.ejpb.2015.04.038.

[80] D. Schmaljohann, Thermo- and pH-responsive polymers in drug delivery, Adv. Drug Deliv. Rev. 58 (2006) 1655–1670. https://doi.org/10.1016/j.addr.2006.09.020.

[81] O. Okay, Macroporous copolymer networks, Prog. Polym. Sci. 25 (2000) 711–779. https://doi.org/10.1016/S0079-6700(00)00015-0.

[82] W. Kim, J. Jung, Polymer brush: A promising grafting approach to scaffolds for tissue engineering, BMB Rep. 49 (2016) 655–661. https://doi.org/10.5483/BMBRep.2016.49.12.166.

[83] R. Sunasee, R. Narain, Covalent and noncovalent bioconjugation strategies, Chem. Bioconjugates. 9781118359 (2014) 1–75. https://doi.org/10.1002/9781118775882.ch1.

[84] Y. Laor, C. Zolkov, R. Armon, Immobilizing humic acid in a sol-gel matrix: A new tool to study humic-contaminants sorption interactions, Environ. Sci. Technol. 36 (2002) 1054–1060. https://doi.org/10.1021/es010761h.

[85] D.G. Barceloux, Copper, Clin. Toxicol. 37 (1999) 217–230. https://doi.org/10.1081/CLT-100102421.

[86] H. Küpper, E. Andresen, Mechanisms of metal toxicity in plants, 8 (2016) 269–285.

https://doi.org/10.1039/c5mt00244c.

[87] F. Haque, M. Rahman, E. Ahmed, P. Bakshi, A. Shaikh, A cyclic voltammetric study of the redox reaction of Cu(II) in presence of ascorbic acid in different pH media, Dhaka Univ. J. Sci. 61 (2013) 161–166. https://doi.org/10.3329/dujs.v61i2.17064.

[88] B. Feier, I. Bajan, I. Fizeşan, D. Floner, C. Cristea, F. Geneste, R. Săndulescu, Highly selective electrochemical detection of copper (II) using N, N'-bis(acetylacetone)ethylenediimine as a receptor, Int. J. Electrochem. Sci. 10 (2015) 121–139.

[89] J. Taylor, R. DeWoskin, F. Ennever, Toxicological profile for cadmium, ATSDR's Toxicol. Profiles. (2002). https://doi.org/10.1201/9781420061888_ch151.

[90] T.S. Nawrot, J.A. Staessen, H.A. Roels, E. Munters, A. Cuypers, T. Richart, A. Ruttens, K. Smeets, H. Clijsters, J. Vangronsveld, Cadmium exposure in the population: From health risks to strategies of prevention, BioMetals. 23 (2010) 769–782. https://doi.org/10.1007/s10534-010-9343-z.

[91] F. Gay, V. Laforgia, I. Caputo, C. Esposito, M. Lepretti, A. Capaldo, Chronic exposure to cadmium disrupts the adrenal gland activity of the newt triturus carnifex (Amphibia, Urodela), Biomed Res. Int. 2013 (2013). https://doi.org/10.1155/2013/424358.

[92] R.A. Bernhoft, Cadmium toxicity and treatment, Sci. World J. 2013 (2013). https://doi.org/10.1155/2013/394652.

[93] H. Abadin, F. Llandos, Toxicological profile for lead, ATSDR's Toxicol. Profiles. (2002). https://doi.org/10.1201/9781420061888_ch151.

[94] G. Flora, D. Gupta, A. Tiwari, Toxicity of lead: A review with recent updates, Interdiscip. Toxicol. 5 (2012) 47–58. https://doi.org/10.2478/v10102-012-0009-2.

[95] S.H. Kim, S.H. Shin, Y.Y. Go, S.W. Chae, J.J. Song, Effect of lead on human middle ear epithelial cells, Biomed Res. Int. 2018 (2018). https://doi.org/10.1155/2018/5058729.

[96] H.L. Richards, P.G.L. Baker, E. Iwuoha, Metal nanoparticle modified polysulfone membranes for use in wastewater treatment: A critical review, J. Surf. Eng. Mater. Adv. Technol. 02 (2012) 183–193. https://doi.org/10.4236/jsemat.2012.223029.

[97] K. Jamroziak, W. Jargulinski, The analysis of the electrode potential shift in the examination of plastic-covered metal fatigue strength, Int. Sci. J. 41 (2010) 21–27.

[98] A. Morrin, R.M. Moutloali, A.J. Killard, M.R. Smyth, J. Darkwa, E.I. Iwuoha,

Electrocatalytic sensor devices: (I) cyclopentadienylnickel(II) thiolato Schiff base monolayer self-assembled on gold, Talanta. 64 (2004) 30–38. https://doi.org/10.1016/j.talanta.2003.11.046.

[99] F. Peng, X. Huang, A. Jawor, E.M.V. Hoek, Transport, structural, and interfacial properties of poly(vinyl alcohol)-polysulfone composite nanofiltration membranes, J. Memb. Sci. 353 (2010) 169–176. https://doi.org/10.1016/j.memsci.2010.02.044.

[100] A.H.M. El-Aassar, Polysulfone/Polyvinyl alcohol thin film nano-composite membranes: Synthesis, characterization and application for desalination of saline groundwater, J. Appl. Sci. Res. 8 (2012) 3811–3822.

[101] F.N. Muya, L. Phelane, P.G.L. Baker, E.I. Iwuoha, Synthesis and characterization of polysulfone hydrogels, J. Surf. Eng. Mater. Adv. Technol. 04 (2014) 227–236. https://doi.org/10.4236/jsemat.2014.44025.

[102] P.Y. Bruice, Organic chemistry, 6th ed., Pearson Education Inc., 2011.

[103] G. Inzelt, Conducting polymers. A new era in electrochemistry, Springer-Verlag, 2010. https://doi.org/10.1007/s10008-009-0857-7.

[104] S. Thomas, R. Thomas, A.K. Zachariah, R.K. Mishra, Spectroscopic methods for nanomaterials characterization, Elsevier, 2017.

[105] T. Fernández-Abedul, Laboratory methods in dynamic electroanalysis, Elsevier, 2019. https://doi.org/10.1016/c2017-0-03525-5.

[106] S.A. Ozkan, M. Kauffmann, P. Zuman, Electroanalysis in pharmaceutical biomedical and pharmaceutical sciences, Springer, 2015. https://doi.org/10.1007/978-3-662-47138-8_1.

[107] Y Saito, T. Kikuchi, Voltammetry theory, types and applications: Chemical engineering methods and technology., Nova Science Publishers, Inc., 2014.

[108] R.G. Compton, C.E. Banks, Understanding voltammetry, 3rd ed., World Scientific, 2007. https://doi.org/10.1142/9789812779809_0004.

[109] A.A. Zemlianaia, T.A. Fedotcheva, A.I. Fedotchev, Modern approaches to human cognitive activity enhancement, Usp. Fiziol. Nauk. 41 (2010) 45–62.

[110] B.C. Smith, Fundamentals of fourier transform infrared spectroscopy, 2nd ed., Taylor & Francis Group, 2011. https://doi.org/10.1201/b10777.

[111] R. Jones, Infrared technology, Kirk-Othmer Encycl. Chem. Technol. 14 (2005) 379–416. https://doi.org/10.1002/0471238961.0914061810151405.

[112] A. Christy, Y. Ozaki, V. Gregoriou, Modern Fourier transform infrared spectroscopy, Illustrate, Elsevier, 2001. http://www.amazon.com/dp/0444500448.

[113] R.F. Egerton, Physical principles of electron microscopy, Springer, 2005. https://doi.org/10.1016/s1369-7021(05)71290-6.

[114] G. Michler, Electron microscopy of polymers, Springer, 2008. https://doi.org/10.1007/978-3-540-36352-1.

[115] N. Yao, Z.L. Wang, Microscopy for nanotechnology, Kluwer Academic Publishers, 2005. http://medcontent.metapress.com/index/A65RM03P4874243N.pdf.

[116] G.K. Bar, G.F. Meyers, The application of atomic force microscopy to the characterization of industrial polymer materials, MRS Bull. 29 (2004) 464–470. https://doi.org/10.1557/mrs2004.140.

[117] D. Ricci, P.C. Braga, Methods in molecular biology: Atomic force microscopy :Biomedical methods and applications, Humana Press, 2004. https://doi.org/10.1385/1-59259-077-2:199.

[118] A. Wahl, K. Dawson, N. Sassiat, A.J. Quinn, A. O'Riordan, Nanomolar trace metal analysis of copper at gold microband arrays, J. Phys. Conf. Ser. 307 (2011) 1–7. https://doi.org/10.1088/1742-6596/307/1/012061.

[119] P.Y. Bruice, Organic chemistry, 8th ed., Pearson Education, 2016.

[120] J.S. Taurozzi, H. Arul, V.Z. Bosak, A.F. Burban, T.C. Voice, M.L. Bruening, V. V. Tarabara, Effect of filler incorporation route on the properties of polysulfone-silver nanocomposite membranes of different porosities, J. Memb. Sci. 325 (2008) 58–68. https://doi.org/10.1016/j.memsci.2008.07.010.

[121] F. Denisa, A. Ficai, G. Voicu, B.S. Vasile, C. Guran, E. Andronescu, Polysulfone based membranes with desired pores characteristics, Mater. Plast. 47 (2010) 24–27.

[122] J. Pretorius, International protocols regarding global climate change and the impact on water resources, Encycl. Life Support Syst. II (n.d.).

[123] R. Naim, F. Ismail, H. Saidi, E. Saion, Development of sulfonated polysulfone membranes as a material for Proton Exchange Membrane (PEM), Mater. Sci. (2004) 1–17. http://eprints.utm.my/1037/.

[124] K.S. Kim, K.H. Lee, K. Cho, C.E. Park, Surface modification of polysulfone ultrafiltration membrane by oxygen plasma treatment, J. Memb. Sci. 199 (2002) 135–145.

https://doi.org/10.1016/S0376-7388(01)00686-X.

[125] S.H. Baxamusa, L. Montero, J.M. Dubach, H.A. Clark, S. Borros, K.K. Gleason, Protection of sensors for biological applications by photoinitiated chemical vapor deposition of hydrogel thin films, Biomacromolecules. 9 (2008) 2857–2862. https://doi.org/10.1021/bm800632d.

[126] R. Wu, S. Zhang, J. Lyu, F. Lu, X. Yue, J. Lv, A visual volumetric hydrogel sensor enables quantitative and sensitive detection of copper ions, Chem. Commun. 51 (2015) 8078–8081. https://doi.org/10.1039/c5cc00744e.

[127] J.D. Miller, S. Veeramasuneni, J. Drelich, M.R. Yalamanchili, G. Yamauchi, Effect of roughness as determined by atomic force microscopy on the wetting properties of PTFE thin films, Polym. Eng. Sci. 36 (1996) 1849–1855. https://doi.org/10.1002/pen.10580.

[128] S.M. Moosavi, S. Ghassabian, Linearity of calibration curves for analytical methods: A Review of criteria for assessment of method meliability, IntechOpen. (2018). https://doi.org/10.5772/intechopen.72932.

[129] G. Mehmet, The role of and the place of method validation in drug analysis using electroanalytical techniques, Open Anal. Chem. J. 5 (2011) 1–21. https://doi.org/10.2174/187406500115010001.

[130] M. Heitzmann, C. Bucher, J.C. Moutet, E. Pereira, B.L. Rivas, G. Royal, E. Saint-Aman, Complexation of poly(pyrrole-EDTA like) film modified electrodes: Application to metal cations electroanalysis, Electrochim. Acta. 52 (2007) 3082–3087. https://doi.org/10.1016/j.electacta.2006.09.041.

[131] W. Yang, E. Chow, G.D. Willett, D.B. Hibbert, J.J. Gooding, Exploring the use of the tripeptide Gly-Gly-His as a selective recognition element for the fabrication of electrochemical copper sensors, Analyst. 128 (2003) 712–718. https://doi.org/10.1039/b212881k.

[132] A.C. Liu, D.C. Chen, C.C. Lin, H.H. Chou, C.H. Chen, Application of cysteine monolayers for electrochemical determination of sub-ppb copper(II), Anal. Chem. 71 (1999) 1549–1552. https://doi.org/10.1021/ac980956g.

[133] B. Shi, H.E. Allen, M.T. Grassi, H. Ma, Modeling copper partitioning in surface waters, Water Res. 32 (1998) 3756–3764. https://doi.org/10.1016/S0043-1354(98)00162-6.

[134] F.J. Stevenson, Humic substances in the environment, Soil Sci. Soc. Am. J. 39 (1975) vi–

vi. https://doi.org/10.2136/sssaj1975.03615995003900030006x.

[135] J. Gabriel Alonso, A. José Luis Rivera, M. Ana María Mendoza, H. Maria Leonor Mendez, Effect of temperature and pH on swelling behavior of hydroxyethyl cellullose-acrylamide hydrogel, E-Polymers. (2007) 150. https://doi.org/10.1515/epoly.2007.7.1.1744.

[136] Z.X. Sun, R.O. Sköld, A multi-parameter titration method for the determination of formation pH for metal hydroxides, Miner. Eng. 14 (2001) 1429–1443. https://doi.org/10.1016/S0892-6875(01)00157-1.

[137] Q. Rong, K. Zhong, H. Huang, C. Li, C. Zhang, Humic acid reduces the available cadmium, copper, lead, and zinc in soil and their uptake by tobacco, Appl. Sci. (2020). https://doi.org/10.3390/app10031077.

[138] Z.R. Komy, A.M. Shaker, S.E.M. Heggy, M.E.A. El-Sayed, Kinetic study for copper adsorption onto soil minerals in the absence and presence of humic acid, Chemosphere. 99 (2014) 117–124. https://doi.org/10.1016/j.chemosphere.2013.10.048.

[139] L. Mao, S.D. Young, E.H. Bailey, Lability of copper bound to humic acid, Chemosphere. 131 (2015) 201–208. https://doi.org/10.1016/j.chemosphere.2015.03.035.

[140] H. Whitby, C.M.G. van den Berg, Evidence for copper-binding humic substances in seawater, Mar. Chem. 173 (2015) 282–290. https://doi.org/10.1016/j.marchem.2014.09.011.

[141] Y. Oztekin, A. Ramanaviciene, A. Ramanavicius, Electrochemical determination of cu(ii) ions by 4-formylphenylboronic acid modified gold electrode, Electroanalysis. 23 (2011) 1645–1653. https://doi.org/10.1002/elan.201100121.

[142] Y. Lu, X. Liang, C. Niyungeko, J. Zhou, J. Xu, G. Tian, A review of the identification and detection of heavy metal ions in the environment by voltammetry, Talanta. 178 (2018) 324–338. https://doi.org/10.1016/j.talanta.2017.08.033.

[143] M. Radaelli, E. Scalabrin, G. Toscano, G. Capodaglio, High performance size exclusion chromatography-inductively coupled plasma-mass spectrometry to study the copper and cadmium complexation with humic acids, Molecules. 24 (2019). https://doi.org/10.3390/molecules24173201.

[144] E. Jeong, M. Won, Y. Shim, Simultaneous determination of lead, copper, and mercury at a modified carbon paste eletrode containing humic acid, Electroanalysis. 6 (1994) 887–893. https://doi.org/10.1002/elan.1140061014.

[145] S.S. Zumdahl, S.A. Zumdahl, Chemistry, 7th ed., Houghton Mifflin Company, 2007.

[146] G. Tabbì, A. Giuffrida, R.P. Bonomo, Determination of formal redox potentials in aqueous solution of copper(II) complexes with ligands having nitrogen and oxygen donor atoms and comparison with their EPR and UV-Vis spectral features, J. Inorg. Biochem. 128 (2013) 137–145. https://doi.org/10.1016/j.jinorgbio.2013.07.035.

[147] T. Andelković, R. Nikolić, A. Bojić, D. Andelković, G. Nikolić, Binding of cadmium to soil humic acid as a function of carboxyl group content., Maced. J. Chem. Chem. Eng. 29 (2010) 215–224. https://doi.org/10.20450/mjcce.2010.168.

[148] L. Chen, Z. Su, X. He, Y. Liu, C. Qin, Y. Zhou, Z. Li, L. Wang, Q. Xie, S. Yao, Square wave anodic stripping voltammetric determination of Cd and Pb ions at a Bi/Nafion/thiolated polyaniline/glassy carbon electrode, Electrochem. Commun. 15 (2012) 34–37. https://doi.org/10.1016/j.elecom.2011.11.021.

[149] G. Roa, M.T. Ramírez-Silva, M.A. Romero-Romo, L. Galicia, Determination of lead and cadmium using a polycyclodextrin-modified carbon paste electrode with anodic stripping voltammetry, Anal. Bioanal. Chem. 377 (2003) 763–769. https://doi.org/10.1007/s00216-003-2126-4.

[150] N. Promphet, P. Rattanarat, R. Rangkupan, O. Chailapakul, N. Rodthongkum, An electrochemical sensor based on graphene/polyaniline/polystyrene nanoporous fibers modified electrode for simultaneous determination of lead and cadmium, Sensors Actuators, B Chem. 207 (2015) 526–534. https://doi.org/10.1016/j.snb.2014.10.126.

[151] M. Grabarczyk, A. Koper, Direct determination of cadmium traces in natural water by adsorptive stripping voltammetry in the presence of cupferron as a chelating agent, Electroanalysis. 24 (2012) 33–36. https://doi.org/10.1002/elan.201100357.

[152] J. Rangarajan, R. Sundaresan, B.I. Nemade, A polarographic study of methionine complexes of cadmium in mixed solvents, Proc. Indian Acad. Sci. 86 (1977) 333–340. https://doi.org/10.1007/BF03046848.

[153] J.H. Hwang, P. Pathak, X. Wang, K.L. Rodriguez, H.J. Cho, W.H. Lee, A novel bismuth-chitosan nanocomposite sensor for simultaneous detection of Pb(II), Cd(II) and Zn(II) in wastewater, Micromachines. 10 (2019). https://doi.org/10.3390/mi10080511.

[154] W.L. Yan, R. Bai, Adsorption of lead and humic acid on chitosan hydrogel beads, Water Res. 39 (2005) 688–698. https://doi.org/10.1016/j.watres.2004.11.007.

[155] W. Giraldo, E. Romero, M. Chaur, Electrochemical studies of grid and linear type M^2+ (M=Zn, Cd and Pb) complexes of a bis-(hydrazone) bearing two symmetric carboxylic groups, Rev. Ciencias. 21 (2018) 113. https://doi.org/10.25100/rc.v21i1.6347.